REGULATION OF THE TUBULIN CODE IN CARDIAC HYPERTROPHY AND FAILURE

Sai Aung Phyo

A DISSERTATION

in

Cell and Molecular Biology

Presented to the Faculties of the University of Pennsylvania

in

Partial Fulfillment of the Requirements for the

Degree of Doctor of Philosophy

2022

Supervisor of Dissertation

Benjamin L. Prosser, PhD

Associate Professor of Physiology

Graduate Group Chairperson

Daniel S. Kessler, PhD

Associate Professor of Cell and Developmental Biology

Dissertation Committee

Mark L. Kahn, MD, Edward S. Cooper, MD/Norman Roosevelt and Elizabeth Meriwether McLure Professor

Edward E. Morrisey, PhD, Robinette Foundation Professor of Cardiovascular Medicine

Eric F. Joyce, PhD, Assistant Professor of Genetics

Joel D. Boerckel, PhD, Assistant Professor of Orthopaedic Surgery

To my mom and my aunt without whom I would not be writing this

ACKNOWLEDGMENT

To my advisor and mentor, Ben: Over the past four years, it has been a great pleasure learning with you and working for you through the thick and thins of life and science. During my time in your lab, you constantly challenged me to think critically of my science and aspired me to be a better scientist who is not daunted by any question. At the same time, you give me time and space to find my identity which has allowed me to grow into an individual, and for all of those, I am eternally grateful. Thank you so much for not only being my scientific mentor, but also for being a genuine person who is always willing to lend me an ear through tough times.

To my mom and my aunt: I am sure you will not probably see this unless I show you, but this section would not be complete without you two. Although we have been away from each other so long, your constant unwavering supports make me feel as if we live right next to each other. Thank you and love you both so much.

To former and current Prosser Lab members: From providing me with great camaraderie to helping me with experiments and helping make sense biology, you all made my time in lab the best possible. Special shoutouts to Keita for always willing to mentor, talk, laugh, and help me in any way you possible could, and to Emily and Alex for making my days in lab more joyful.

To my thesis committee members: I could not have done this without your input and your desires to push me to be a better scientist. Thank you very much for always keeping my best interest at heart and for always nudging me in the right direction to get my PhD.

To Dr. Carter and Dr. Vancurova: Without whom, I would not even be in science. Thank you, Dr. Carter, for seeing potential in me, for being my first mentor in the US, and for continue believing in me during the dark times of my training; I am very lucky to still be a part of your life and I am always looking forward to seeing you again soon. Thank you, Dr. Vancurova, for taking a chance in me and for letting me work in your lab during my undergraduate years; you showed me the joy of doing amazing science with a great team and it is the experiences in your lab that you fostered that made me chose the path I am on.

Finally, to my friends, family, and past teachers: I miss you all dearly and even though we might not be in constant contact, you are always on my mind, and I will always treasure all my shared moments. It is cliché to say but I am who I am right now because of you, and you will always be a part of me. I hope one day I will get to see and spend time with each and every one of you. In the meantime, I wish all of you all a joyous journey.

ABSTRACT

REGULATION OF THE TUBULIN CODE IN CARDIAC HYPERTROPHY AND FAILURE

Sai Aung Phyo

Benjamin L. Prosser

A proliferated and post-translationally modified microtubule network underlies cellular growth in cardiac hypertrophy and contributes to contractile dysfunction in heart failure. Yet how the heart achieves this modified network is poorly understood. Determining how the “tubulin code” – the permutations of tubulin isoforms and post-translational modifications – is rewritten upon cardiac stress may provide new targets to modulate cardiac remodeling. Further, while tubulin can autoregulate its own expression, it is unknown if autoregulation is operant in the heart or tuned in response to stress. Here I use heart failure patient samples and murine models of cardiac remodeling to interrogate transcriptional, autoregulatory, and post-translational mechanisms that contribute to microtubule network remodeling at different stages of heart disease. I find that autoregulation is operant across tubulin isoforms in the heart and leads to an apparent disconnect in tubulin mRNA and protein levels in heart failure. I also find that within 4 hours of a hypertrophic stimulus and prior to cardiac growth, microtubule detyrosination is rapidly induced to help stabilize the network. This occurs concomitant with rapid transcriptional and autoregulatory activation of specific tubulin isoforms and microtubule motors. Upon continued hypertrophic stimulation, there is an increase in post-translationally modified microtubule tracks and anterograde motors to support cardiac growth, while total tubulin content increases through progressive transcriptional and autoregulatory induction of tubulin isoforms. My work provides a new model for how

the tubulin code is rapidly rewritten to establish a proliferated, stable microtubule network that drives cardiac remodeling, and provides the first evidence of tunable tubulin autoregulation during pathological progression.

TABLE OF CONTENTS

PREFACE

The following chapters has been adapted from:

Phyo, S.A., Uchida, K., Chen, C.Y., Caporizzo, M.A., Bedi, K., Griffin, J., Margulies, K., and Prosser, B.L. (2022). Transcriptional, Post-Transcriptional, and Post-Translational Mechanisms Rewrite the Tubulin Code During Cardiac Hypertrophy and Failure. Frontiers Cell Dev Biology *10*, 837486. https://doi.org/10.3389/fcell.2022.837486.

CHAPTER 1: INTRODUCTION

A. The heart and its functional subunit, the cardiomyocytes

The heart, a muscular organ that resides in the thorax of vertebrates, sits at the core of the circulatory system and is responsible for the circulation of blood throughout an organism. In human, the heart is divided into 4 chambers, namely: 1) right-atrium, 2) right-ventricle, 3) left-atrium, and 4) left-ventricle. The right and left atria receive blood from the systemic or the pulmonary circulation, whereas the right and left ventricles pump blood into the pulmonary or the systemic circulation, respectively. Since the left-ventricle is responsible for pumping blood throughout the body, it is this chamber that encounters the highest resistance (afterload) and produces the strongest force to overcome the resistance.

The pumping action of the heart is achieved by the collective and synchronized contraction of the cardiomyocytes, the functional subunit of the heart. In addition to the cardiomyocytes, which accounts for ~56% of the cells (Banerjee et al., 2007) or ~70-85% of the volume (Zhou and Pu, 2016) in the heart, the heart also consists of other cell types such as cardiac fibroblast, vascular smooth muscles, and immune cells such as macrophages(Pinto et al., 2016). All these cells are indispensable for the structure and function of the heart, but cardiomyocytes are the main source of force generation. Within a cardiomyocyte, the basic contractile unit known as a sarcomere, which is mainly composed of actin and myosin proteins, is responsible for force generation through shortening from its normal resting length of ~2.2μm in cardiomyocytes(Pollack and Huntsman, 1974).

Cardiomyocytes are terminally differentiated cells and are responsive to electrical stimulation. At the molecular level, the contraction of cardiomyocyte is initiated by the

depolarization of the sarcolemma that travels down the T-tubules and leads to an influx of extracellular calcium through the L-type calcium channels(Tanabe et al., 1990). This influx of calcium triggers rapid release of sarcoplasmic-reticulum (SR) -stored calcium into the cytosol via the type 2 ryanodine receptor (RyR2) at the junctional-SR through a process commonly known as calcium-induced calcium release (CIRC)(Ferrier and Howlett, 2001). This rise in cytosolic calcium concentration enables myosin binding to actin that leads to the shortening of sarcomeres and thus produces a contractile force.

Following the calcium-induced contraction, the cardiomyocyte must also relax adequately to allow the chambers to be filled with blood properly for subsequent ejection. Additionally, the cardiomyocyte stretch induced by the forces of the filling blood (preload) allows proper contraction through the Frank-Starling mechanism(Frank, 1959). During the relaxation phase, SR rapidly reuptake calcium through the sarco/endoplasmic reticulum calcium-ATPase (SERCA)(Brini and Carafoli, 2009), leading to a fall in cytosolic calcium concentration and subsequent dissociation of myosin from actin. This leads to lengthening of the cardiomyocyte back to its resting length, primed for a subsequent contraction.

Given the central importance of calcium signaling in the heart, it is through this modulation of calcium signaling by which the heart achieves short-term variations in the strength of contraction (reviewed in:(Eisner et al., 2017). However, when the heart needs to produce stronger force of contraction for an extended period due to physiological or pathological increases in afterload or preload, regulation solely through calcium signaling becomes unsustainable. To overcome this problem, the heart needs to increase the total number of sarcomeres that can ultimately increase the ability of the heart to generate greater force. This could be accomplished by either increasing the number of cardiomyocytes through cell division and thus effectively increases the number of

sarcomeres, or by the addition of new sarcomeres to those preexisting in cardiomyocytes. Since cardiomyocytes are terminally differentiated and are no longer capable of cellular division, the only way feasible is for the cardiomyocytes to grow larger through the process of cardiac hypertrophy.

B. Pathological cardiac hypertrophy and heart failure

The initial onset of hypertrophy is an adaptive response to increase contractility to match the increased demand. The newly synthesized sarcomeres are added to the pre-existing sarcomeres either in parallel leading to thicker walls and a smaller chamber known as concentric hypertrophy, or in series leading to thinner walls and a bigger chamber known as eccentric hypertrophy. The precise molecular determinants that control concentric versus eccentric hypertrophy are yet to be identified. However, it has been established that the heart undergoes concentric or eccentric hypertrophy in response to increased afterload such as pressure-overload or to increased preload such as fluid-overload, respectively(Gaasch, 1979). Although most causes of pathological cardiac hypertrophy are in response to increased afterload or preload, there are also genetic causes that leads to cardiac hypertrophy, such as a frameshift mutation of MYBPC3 gene that encodes for cardiac myosin binding protein C (cMyBP-C)(Carrier et al., 1997).

Regardless of the etiology of pathological remodeling, as long as the heart with its increased sarcomere numbers can meet the increased demand of an organism, the hypertrophy is said to be compensated. However, since pathological hypertrophy is associated with the activation of natriuretic peptides (Rockman et al., 1991) and reactivation of many fetal genes such as the expression of myosin heavy chain 7 (MYH7)(Morkin, 1993) as well as fibrosis and some cardiac dysfunctions (Weeks et al.,

2017) overtime this compensated hypertrophy can become decompensated which is when the heart can no longer supply the necessary demand; this decompensation is accompanied by further processes such as cardiomyocyte apoptosis, calcium dysregulation, and metabolic reprogramming (reviewed in:(Nakamura and Sadoshima, 2018). Moreover symptoms of heart failure first emerge during this maladaptive decompensation.

Heart Failure is a complex condition in which the patient presents with symptoms such as fatigue and shortness of breath, as a sequela of mismatched supply and demand of cardiac output. The mismatch can stem from diastolic dysfunction, in which the thickened walls fail to relax adequately during the filling of blood, or systolic dysfunction, in which the thinned walls fail to contract adequately to force blood out. Current heart failure therapies include the use of inotropes to increase contractility for systolic dysfunction(Tariq and Aronow, 2015) or diuretics to decrease fluid overload for diastolic dysfunction(Ha and Oh, 2009). These therapies can decelerate the progression of heart failure, but it would better if we can prevent decompensation in the first place.

Although the progression of cardiac hypertrophy to heart failure seems like a one-way direction, reversal of cardiac hypertrophy is feasible and has been observed. For example, using dilated cardiomyopathy (DCM) mice model, McMullen et al. showed that DCM mice subjected to swim training live longer than the untrained controls and showed lower levels of fetal gene transcription (McMullen et al., 2007). Likewise, obese and sedentary patients with left-ventricular hypertrophy can reverse and induce favorable changes in their left-ventricular structure, assessed through echocardiography, by weight management and aerobic exercise(Hinderliter et al., 2002). Hence, if we were to fully understand the temporal progression of the pathological changes during cardiac

hypertrophy, we could find points of intervention to reverse cardiac hypertrophy and thus prevents its progression to heart failure.

With regards to future interventions for heart failure, recent research into the pathophysiology of heart failure has yielded great insights that could one day translate into even more effective therapies and treatments. For example, metabolomic study using blood from artery, coronary sinus, and femoral vein from normal and heart failure patients shows that failing heart preferentially uses ketones and lactate instead of fatty acids(Murashige et al., 2020). Though the complete mechanism of such switch in metabolite remains to be elucidated, thorough characterizations of the different pathological changes associated with cardiac hypertrophy and failure would inevitably open new avenues for treatment of heart diseases.

A rapidly evolving area of cardiac research is studying the role of microtubules in heart diseases such as hypertrophy and heart failure. Microtubules have been shown to be essential for the development of cardiac hypertrophy(Fassett et al., 2019, 2009; Scarborough et al., 2021), and contribute to contractile dysfunction in heart failure(Caporizzo et al., 2018, 2020; Chen et al., 2018; Tsutsui et al., 1999). I will expand on the role of microtubules in heart disease in more details below.

C. The biology of microtubules and the tubulin code

Microtubules are hollow tubular structures found inside all eukaryotic cells. They are about 25nm in diameter, consisting of 13 laterally associated protofilaments(Sui and Downing, 2010), and are formed through the guanosine-5'-triphosphate (GTP) dependent polymerization of obligate heterodimers of α- and β- tubulin(Weisenberg et al., 1976). They play essential roles in the structural support of cells, intracellular transport, cell motility, and mitosis(Inoué and Sato, 1967; Nogales, 2001). Unlike other

cytoskeletal elements, microtubules exist in a dynamic state whereby they exhibit periods of stochastic growth and shrinkage(Mitchison and Kirschner, 1984). In addition to growth and shrinkage, microtubules undergo catastrophe, during which a microtubule quickly depolymerizes from the “plus-end” to form free tubulin dimers, and rescue, during which the catastrophic event is halted to resume growth. Despite the dynamicity of the microtubules, during normal physiological conditions, the free and polymerized tubulin pools exist in a state of equilibrium and the total mass of both α- and β- tubulin is kept relatively constant.

In addition to transcriptional regulation of tubulin genes to keep a constant level of tubulin transcripts in a cell at a given time(Havercroft and Cleveland, 1984), the abundance of tubulin transcript is also controlled through a tubulin-specific mRNA regulatory mechanism known as autoregulation(Ben-Ze’ev et al., 1979; Cleveland et al., 1983). Autoregulation is controlled by the relative free : polymerized tubulin concentration in the cell(Ben-Ze’ev et al., 1979; Cleveland et al., 1981). When free tubulin level increases, such as during the depolymerization of microtubules by depolymerizing agents such as colchicine, the free tubulin dimers activate a ribosomal RNase to degrade nascent tubulin transcripts (autoinhibition) that have been docked on ribosome for translation; conversely, when free tubulin level decreases, autoregulation is released (autoactivation) allowing the nascent transcripts to be to restore a homeostatic concentration of free tubulin with respect to the total microtubules. The complete mechanism by which the free tubulin triggers the activation of ribosomal RNase is unknown but through mutagenesis of the β-tubulin, it is known that the Met-Arg-Glu-Ile (MREI) motif that resides close to the N-terminus is necessary and sufficient for autoregulation(Yen et al., 1988).

Since the discovery of autoregulation in 1979 by Ben-Ze'ev & colleagues, the field of autoregulation has been static despite its importance in tubulin biology. In the past two years, increasing number of research has been undertaken to further my understanding of autoregulation. Lin et al. in 2020 showed that the protein Tetratricopeptide repeat domain 5 (TTC5) plays an indispensable role in autoregulation by allowing the MREI motif on the nascent tubulin peptide to be recognized by the ribosome to activate RNase for transcript degradation(Lin et al., 2020). Additionally, autoregulation was generally thought of as a degradation mechanism that degrades mRNA in the presence of excess free tubulin; then in 2019, Gasic et al. showed that autoregulation can also increase the level of mature tubulin RNA without a corresponding increase in nascent tubulin transcript (Gasic et al., 2019). These research opens an interesting line of questioning on the interplays of transcription and autoregulation in the temporal control of tubulin transcripts and proteins in different physiological and pathological conditions.

Autoregulation becomes more intriguing when given the fact that there are a multitude of α and β -tubulin isoforms that arise not from alternative gene splicing but from different tubulin genes and serve different purposes (reviewed in:(Janke and Magiera, 2020). In humans, there are nine α- and nine β- tubulin isoforms, whereas in mice, there are seven α- and eight β- tubulin isoforms. Despite some homologies between the tubulin isoforms, study using *Drosophila melanogaster* β- tubulin isoforms shows that the tubulin isoforms are non-redundant and that they have different intrinsic functional capacity(Hoyle and Raff, 1990). Interestingly, using in vitro cancer cell lines, autoregulation was observed to regulate tubulin on an isoform-specific level (Gasic et al., 2019). Despite its relevance in tubulin biology, tubulin isoforms and autoregulation of

cardiac microtubules remains underappreciated, and their roles in cardiac physiology and pathological remains unexplored.

In addition to the diverse array of tubulin isoforms, the tubulin subunits are also subjected to diverse post-translational modifications (PTMs) such as detyrosination and acetylation. Microtubule PTMs have been shown to influence microtubule stability and dynamics as well as their biochemical properties. The permutation of the $\alpha\beta$-tubulin isoforms and their PTMs is known as the “tubulin code” (Figure 1) and this cell-type and context-dependent tubulin code results in microtubule networks with distinct biochemical and mechanical properties.

Finally, in addition to the tubulin code, the property and complexity of microtubules are further diversified by microtubule-associated proteins (MAPs) and motors, whose interactions with microtubules are also regulated by the tubulin code. MAPs themselves can be post-translationally modified, are expressed in a cell-type and context-dependent fashion and can impart further biophysical properties when associated with microtubules (Janke and Magiera, 2020).

D. Microtubules in the heart and heart diseases

While cardiac microtubules are indispensable for cardiomyocyte’s cellular processes such as intracellular transport, microtubules serve additional functions in the heart. Microtubules, which were conventionally thought of as stiff cytoskeletal rods that runs the length of the cardiomyocyte(McGrath, 2006), were shown to be indeed flexible structures that contribute dynamically during both contraction and relaxation of the cardiomyocyte(Brangwynne et al., 2006; Robison et al., 2016). Through its interactions with an intermediate filament in the cardiac Z-disk structure, desmin, microtubules were directly observed to buckle during cardiac contraction. Owing to the viscoelastic

properties of the microtubule network, subsequent study shows the buckling and unbuckling of microtubules add resistance during both the contractile and relaxation phases(Caporizzo et al., 2018).

In addition, microtubules are also involved in the structural integrity of the nucleus inside the cardiomyocyte(Heffler et al., 2020). In addition to the pulling force exerted on the nucleus by desmin intermediate filaments, microtubules exert a pushing force on the nucleus, keeping a balance of forces to maintain a homeostatic nuclear shape. The interaction between desmin and microtubules to the nuclear membrane is mediated by KASH-domain containing nesprin proteins in the outer nuclear membrane and SUN-domain containing inner nuclear membrane proteins(Tapley and Starr, 2013). Thus, through microtubules and desmin, the nucleus is physically coupled to the cell membrane and allows the transduction of mechanical stimuli from the cell periphery to the nucleus.

During cardiac hypertrophy and heart failure, the microtubule network is significantly remodeled and acts as a double-edged sword. On one hand, a proliferated, stable microtubule network is essential for the development of cardiac hypertrophy in response to stressors such as adrenergic stimulation and hemodynamic overload(Fassett et al., 2019, 2009; Sato et al., 1997; Scarborough et al., 2021). Upon such hypertrophic stimuli, a dense microtubule network and the anterograde motor protein kinesin-1 coordinates the trafficking of mRNA and the translational machinery to control local synthesis and integration of nascent proteins(Scarborough et al., 2021). In the absence of microtubules, increased protein translation is decoupled from protein integration and the heart fails to grow(Scarborough et al., 2021), identifying an essential role of microtubule-based transport in adaptive cardiac growth.

On the other hand, a collective body of research has also established a causal link between aberrant microtubule remodeling, the tubulin code, and impaired cardiac mechanics in heart failure(Caporizzo et al., 2019; Magiera et al., 2018; Tsutsui et al., 1999). In the hearts of heart failure patients(Chen et al., 2018) and pressure-overloaded animals(Fassett et al., 2019; Sato et al., 1997), microtubule density is consistently increased, and its pharmacological dedensification partially restores dysfunctional cardiac contractility(Caporizzo et al., 2018; Tsutsui et al., 1999).

Moreover, detyrosination, a PTM of α-tubulin, is increased in the myocardium of pressure-overload animals(Fassett et al., 2019; Sato et al., 1997), and in the cardiomyocytes(Chen et al., 2018) and myocardium(Schuldt et al., 2020) of heart failure patients. Detyrosination is the removal of the penultimate tyrosine residue on the C-terminal tail of polymerized α-tubulin by vasohibins 1 & 2 (VASH1/2)(Aillaud et al., 2017; Nieuwenhuis et al., 2017); tubulin tyrosine ligase (TTL) mediates the reverse reaction(Szyk et al., 2011). Mechanistic studies into microtubule detyrosination identified it as a critical determinant of myocyte mechanics(Robison et al., 2016), whereby detyrosinated microtubules impart a viscoelastic drag that limits cardiomyocyte motion during the cardiac cycle(Caporizzo et al., 2020). Suppressing detyrosination in failing cardiomyocytes using parthenolide (Chen et al., 2018), TTL overexpression(Chen et al., 2018), or VASH1 depletion(Chen et al., 2020) lowers cardiomyocyte stiffness and ameliorates the dysfunctional contractility.

A recent study reported a novel axis involving rapid microtubule detyrosination and microtubule-affinity regulating kinase 4 (MARK4) during cardiac ischemia(Yu et al., 2021). The authors demonstrated that MARK4-induced MAP4 phosphorylation dissociates MAP4 from polymerized microtubule, giving VASH2 access to detyrosinated microtubules(Yu et al., 2021). Despite these advances, the temporal progression of

detyrosination, particularly in the context of non-ischemic cardiac remodeling, remains unclear.

Acetylation of α-tubulin has also been recently examined in the heart. Acetylation is an addition of an acetyl group on K40 of polymerized α-tubulin by α-Tubulin acetyltransferase 1 (αTAT1)(Kalebic et al., 2013); deacetylation is mediated by histone deacetylase 6 (HDAC6)(Hubbert et al., 2002). Acetylated microtubules are resilient against repeated mechanical stresses(Portran et al., 2017) and resistant to mechanical breakage(Xu et al., 2017). Acetylation is induced in hypertrophic cardiomyopathy(Dorsch et al., 2019); however, the mechanical consequences of this induction remain unclear, as different studies in various contexts have seen both softening(Swiatlowska et al., 2020) and stiffening(Coleman et al., 2021) effects of acetylation on the cardiomyocyte. While more work is needed, these studies add to a growing body of literature indicating diverse regulation and functional consequences of αβ-tubulin PTMs in cardiac physiology and pathology.

In addition to the tubulin code, several MAPs are also implicated in cardiac remodeling. MAP4, the most abundant cardiac MAP, binds and stabilizes microtubules in a phosphorylation-dependent manner. MAP4 is increased in human heart failure(Chen et al., 2018) and in feline pressure-overload induced cardiac hypertrophy(Sato et al., 1997), and MAP4 dephosphorylation at S924 and S1056 has been causally linked to microtubule network stabilization and densification(Chinnakkannu et al., 2010). Conversely, Li et al. demonstrated that MAP4 hyperphosphorylation at S737 and S760 is also sufficient to drive eccentric remodeling in mice(Li et al., 2018).

Similar to MAP4, phosphorylation of CLIP170 (CAP-Gly Domain Containing Linker Protein 1/170), a microtubule plus-end tracking protein, by AMP-activated protein kinase (AMPK) leads to its dissociation from microtubule plus-ends and de-stabilizes

microtubules(Nakano et al., 2010). Yashirogi et al. recently demonstrated that in the absence of mechanical-stress dependent localization of AMPK to the cardiac intercalated disks to phosphorylates and dissociates CLIP170 from microtubules, microtubules accumulate at the intercalated disk causing eccentric hypertrophy with reduced ejection fraction(Yashirogi et al., 2021). Hence, through such changes in the tubulin code and the associated MAPs, microtubules play an indispensable role in heart disease.

While the state of the microtubule network in advanced heart failure has been well-defined by recent studies(Chen et al., 2018; Schuldt et al., 2020), we know little about the drivers and temporal progression of changes to the microtubule network that occur during the early phases of cardiac remodeling such as during cardiac hypertrophy. There are a multitude of mechanisms to achieve a dense, heavily post-translationally modified microtubule network as observed in cardiac hypertrophy and heart failure. A seemingly obvious mechanism to increase tubulin mass is through transcriptional upregulation; yet when I examine published transcriptomic and proteomic data from heart failure samples, we observe a consistent inverse correlation between tubulin mRNA and protein levels across different causes of heart failure in multiple studies (Fig. 2A-B). This motivates a deeper examination between transcriptional and translation coupling of $\alpha\beta$-tubulin isoforms and other factors that could contribute to microtubule proliferation.

In this study, I aimed to comprehensively characterize the time-dependent changes to the tubulin code and MAPs during the early stages of cardiac microtubule remodeling at the network, protein, and transcript levels. Additionally, given the central importance of autoregulation in tubulin biology, and as no studies have been undertaken to determine its role in cardiac pathophysiology, I sought to elucidate how tubulin

autoregulation affects microtubule synthesis during cardiac hypertrophy. To this end, I combined two acute models of adrenergic stress-induced cardiac hypertrophy with echocardiographic, histologic, transcriptomic, and proteomic assessments to gain insight into cytoskeletal remodeling during the transition from a non-pathological state to cardiac hypertrophy. my goal is to provide a comprehensive assessment of this process to open novel lines of inquiry into cardiac hypertrophy and provide new targets for the reversal or prevention of hypertrophy and its progression into heart failure.

CHAPTER 2: METHODS AND MATERIALS

A. Human myocardial tissue

Procurement of human myocardial tissue was performed under protocols and ethical regulations approved by Institutional Review Boards at the University of Pennsylvania and the Gift-of-Life Donor Program (Pennsylvania, USA) and as described(Chen et al., 2018). In summary, failing human hearts were procured at the time of orthotropic heart transplantation at the Hospital of the University of Pennsylvania following informed consent from all participants. Non-failing hearts were obtained at the time of organ donation from cadaveric donors. In all cases, hearts were arrested in situ using ice-cold cardioplegia solution and transported on wet ice. Transmural myocardial samples were dissected from the mid left ventricular free wall below the papillary muscle and the samples were kept frozen at 80°C. Contractile parameters, including left ventricle ejection fraction, were determined by echocardiography in subjects. In this study, a total of 35 donor hearts were used. 12 donors were classified as near-normal non-failing (NF) without left-ventricular hypertrophy, and 23 donors were classified as heart failure with 12 hearts from hypertrophic cardiomyopathy patients and 11 hearts from dilated cardiomyopathy patients.

B. Animal care

Animal care and procedures were approved and performed in accordance with the standards set forth by the University of Pennsylvania Institutional Animal Care and Use Committee (IACUC) and the Guide for the Care and Use of Laboratory Animals published by the US National Institutes of Health (NIH).

C. Drug injection

Eight to twelve weeks old male C57/Bl6 mice were used throughout the study. On days 0 and 2, based on their body weights, mice were subcutaneously injected with either ascorbic acid (Ctrl, Sigma-Aldrich: A92902), 10mg/kg phenylephrine (PE, Sigma-Aldrich: P6126) prepared in Ctrl, or 5mg/kg isoproterenol (Iso, Sigma-Aldrich: I6504) prepared in Ctrl.

D. Cardiac Tissue Harvest

Mice were put under general anesthesia using isoflurane and the hearts were surgically removed. Excised hearts were thoroughly washed in ice-cooled PBS and extra-cardiac tissues were removed. To properly measure heart weight (HW), residual blood from the chambers was removed by sandwiching the heart between Kimwipes and gently squeezing it. After HW measurement, atrial and right ventricular tissues were removed, the remaining septal and left-ventricular tissues were cut into five pieces of similar size and from similar locations of the heart. The weights of the individual pieces were recorded, frozen in liquid nitrogen, and stored at -80°C until further processing. Concurrent with tissue harvest, the tibia length (TL) of respective mouse was measured to calculate HW-over-TL (HW/TL).

E. Exclusion criteria

During the study: for the 4-hour time point, there were 6 mice per treatment group for a total of 18 mice, and for the 4-day time point, there were 8 mice per treatment group for a total of 24 mice. As I aimed to study mice who underwent consistent cardiac hypertrophy, for the 4-day time point, I set exclusion criteria as the

followings: (1) hearts whose HW/TL were beyond 2 standard-deviations (SD) of the population mean, and (2) experimental hearts whose classical hypertrophy response genes were not changed relative to that of the control hearts. After the removal of outliers, in the final study: for the 4-hour time point, there are 6 mice per treatment group for a total of 18 mice, and for the 4-day time point, there are 7 mice in Ctrl, 7 mice in PE, and 6 mice in Iso, for a total of 20 mice.

F. Mouse cardiomyocyte isolation, culture, and drug treatment

Primary adult ventricular myocytes were isolated from 8- to 12-week-old C57/Bl6 mice using the protocol previously described(Prosser et al., 2011). Briefly, mice were put under general anesthesia using isoflurane and were injected peritoneally with heparin (~1000 units/kg). The heart was excised and cannulated to a Langendorff apparatus for retrograde perfusion with enzymatic digestion solution at 37°C. Once digested, the heart was minced and triturated with glass pipettes. The isolated cardiomyocytes were centrifuged at 300 revolution per minute for 2 minutes. The supernatant containing debris was discarded and the isolated cells were resuspended in cardiomyocyte media containing Medium 199 (GIBCO: 11150-59) supplemented with 1x insulin-transferrin-selenium-X (GIBCO: 51500-56), 20mM HEPES pH 7.4, 0.1 mg/mL Primocin, and 25 mmol/L of cytochalasin D. Immediately following cell isolation, the cardiomyocytes were treated with either DMSO, 10mM colchicine, or 10mM taxol, and incubated at 37°C and 5% CO_2 for 6 hours.

G. Echocardiography

On day 4, transthoracic echocardiography was performed on mice, which were anesthetized using intraperitoneal injection of 0.01mL/gram body weight of 2.5% Avertin, using Vevo2100 Ultrasound System (VisualSonics Inc., Toronto, Ontario, Canada). Fractional shortening, chamber dimensions, and ventricular wall-thickness were measured from short axis M-mode images at the mid-level view of the papillary muscle.

H. Total protein lysate preparation

Frozen aliquoted cardiac tissue obtained from similar locations of the heart was pulverized finely using a liquid nitrogen-cooled mortar and pestle. 1x Radioimmunoprecipitation assay (RIPA) buffer (Cayman Chemical Company: 10010263) supplemented with 1x protease inhibitor cocktail (Cell Signaling Technology: 5872S) and 1:200 diluted endonuclease (Lucigen: OC7850K) was immediately added to the pulverized tissue at a constant ratio of 15μL/mg of tissue. The sample was then mechanically homogenized using a handheld homogenizer until visible chunks of tissues were dissociated. The sample was incubated for 10 minutes on ice to allow endonuclease to cleave DNA. After processing of all samples, the samples underwent two freeze-thaw cycles, after which, equal-volume of 5% SDS-10% glycerol boiling (SGB) buffer was added to each sample. The samples were vortexed thoroughly then heated to 100°C for 8 minutes. Residual undissolved cell debris were removed from the resulting samples by centrifugation at 8000g for 5 minutes at room temperature (22°C). The concentrations of the total protein were determined using Bicinchoninic acid (BCA) assay; all samples were diluted to 4μg/μL using RIPA:SGB buffer. The diluted total protein lysates were aliquoted and stored at -80°C until further processing.

I. Microtubule Fractionation

100mM PIPES-KOH pH 6.8, 1mM $MgCl_2$, 1mM EGTA-KOH pH 7.7 (PME) buffer was prepared fresh and was supplemented with 1mM DTT, 1mM GTP (Sigma-Aldrich: G8877), and 1x protease inhibitor cocktail. 7 parts supplemented PME buffer was mixed with 3 parts glycerol; the final PME-30G buffer was kept incubated in a 37°C water bath. Frozen aliquoted cardiac tissue obtained from similar locations of the heart was pulverized crudely using a liquid nitrogen-cooled mortar and pestle. Immediately following pulverization, warmed PME-30G buffer was added at a constant ratio of 20μL/mg of tissue. The sample was then mechanically homogenized using the handheld homogenizer until visible chunks of tissues were dissociated and was set aside at 22°C until all samples were processed.

All processed samples were then centrifuged at 16000g for 15 minutes at 30°C; the supernatants were transferred into fresh tubes and were saved as free tubulin (Free) fractions. 10μL of 1 part RIPA and 1 part SGB (RIPA:SGB) buffer was added to the pellet obtained from 1mg of tissue and the sample was homogenized using the handheld homogenizer. After processing of all samples, the samples were heated to 100°C for 8 minutes, cooled on ice, and centrifuged at 8000g for 5 minutes at 22°C; the supernatants were transferred into fresh tubes and were saved as polymerized tubulin (Poly) fractions. The concentrations of the Poly fractions were determined using BCA assay. The Poly fractions were diluted to 4μg/μL using RIPA:SGB buffer; the respective Free fraction was diluted with PME-30G buffer using twice the volume needed to dilute the Poly fraction. The final diluted Free and Poly fractions were aliquoted and stored at -80°C until further processing.

J. Sample preparations and Western blot (WB) analysis

To quantify the relative abundance of specific proteins of interest in the total protein lysate, aliquoted diluted total protein lysate samples were thawed at 22°C. 1 part 4x loading buffer (125mM Tris-HCl pH 6.8, 35% v/v glycerol, 0.2% w/v Orange G) freshly supplemented with 10% v/v β-mercepthoethanol (BME) was mixed with 3 parts total protein lysate to get final concentrations of 1x loading buffer with 2.5% BME, and 3μg/μL of total protein. The final samples were heated to 100°C for 8 minutes. The heated samples were cooled to 22°C, centrifuged briefly, vortexed thoroughly, and loaded 5μL/sample onto precast protein gels (Bio-Rad: 5671085).

To quantify the relative abundances of the Free and Poly fractions, aliquoted diluted Free and Poly fractions were thawed at 22°C. For the Free fractions, 2x loading buffer (62.5mM Tris-HCL pH 6.8, 5% v/v SDS, 0% glycerol, 0.1% w/v Orange G) freshly supplemented with 5% v/v BME was used, whereas, for the Poly fractions, 4x loading buffer freshly supplemented with 10% v/v BME was used; to prepare the final samples, the respective loading buffers were diluted to 1x using the Free and Poly fractions. The final samples were heated to 100°C for 8 minutes. The heated samples were cooled to 22°C, centrifuged briefly, vortexed thoroughly, and loaded 5μL/Poly fraction and 10μL/Free fraction onto precast protein gels.

Protein gel electrophoresis was carried out under constant voltage of 135V for the Midi gels for 1 hour. The resolved proteins were transferred onto a nitrocellulose membrane using the Turbo Transfer System (Bio-Rad) under recommended conditions. The post-transferred membrane was blocked in blocking buffer (LI-COR Biosciences: 927-60003) for at least 1 hour at 22°C (or overnight at 4°C). The blocked membrane was incubated overnight at 4°C with primary antibodies diluted in 1x Tris buffered saline with Tween-20 (TBST, Cell Signaling Technology: 9997S). The membrane was washed twice

using TBST and incubated for 1 hour at 22°C with secondary antibodies diluted in blocking buffer. The final immunoblotted membrane was washed twice using TBST and was imaged using the Odyssey Western Blot Imaging System (LI-COR Biosciences).

K. WB data analysis

The WB data was analyzed using Image Studio Lite (LI-COR Biosciences). The signal intensity of an individual band was obtained by drawing a rectangular block encompassing the entire band. The background was thresholded using the parameters: median, border width = 3, Top/Bottom. 2 technical replicates (n) per sample, and 6 biological replicates (N) per treatment for 4-hour time point and 8 biological replicates per treatment for 5-day time point were used in the analysis. GAPDH intensity was used as a loading control. A mean value of the Ctrls that were run on the same blot was used to normalize the data and to calculate the relative fold-changes over the Ctrl. Statistical analyses were performed as described below.

L. Mass spectrometry (MS) sample preparation

To quantify the relative changes of multiple proteins of interest in the total protein lysate, aliquoted diluted total protein lysate samples were thawed at 22°C. 1 part 4x loading buffer freshly supplemented with 10% v/v BME was mixed with 3 parts total protein lysate. The final samples were heated to 100°C for 8 minutes. The heated samples were cooled to 22°C, centrifuged briefly, vortexed thoroughly, and loaded 50μL/sample onto precast protein gels (Bio-Rad: 4561034). Protein gel electrophoresis was carried out under constant voltage of 110V for the Mini gels for 1.5 hours. The resolved protein gel was stained with Coomassie blue (Bio-Rad: 1610435) using the

provided protocol. After the destaining of the gel, the 50kDa bands were carefully excised and stored in deionized water at 4°C until further processing.

The gel bands were destained with 100mM ammonium bicarbonate/acetonitrile (50:50). The bands were reduced in 10mM dithiothreitol/100mM Ammonium bicarbonate for over 60 minutes at 52°C; the bands were then alkylated with 50mM iodoacetamide/100mM ammonium bicarbonate at 22°C for 1 hour in the dark. The proteins in the gel bands were digested with enzymes while incubating overnight at 37°C; different enzymes such as trypsin, Chymotrypsin, and Glu-C were used according to protein sequences. The supernatants were transferred and kept in fresh tubes. Additional peptides were extracted from the gel by adding 50% acetonitrile/1% TFA and incubated for 10 minutes on a shaker. The supernatants were combined and dried. The dried samples were reconstituted using 0.1% formic acid for MS analysis.

M. MS analysis using Nano-LC-MS/MS

Peptides were analyzed on a Q-Exactive HF (Thermo Fisher Scientific) attached to an Ultimate 3000 rslcnano system (Thermo Fisher Scientific) at 400 nL/min. Peptides were eluted with a 55 minutes gradient from 5% to 32% ACN (25 minutes) and 90% ACN over 5 minutes in 0.1% formic acid. Data-dependent acquisition mode with a dynamic exclusion of 45 seconds was enabled. One full MS scan was collected with a scan range of 350 to 1200 *m*/*z*, resolution of 70 K, maximum injection time of 50 milliseconds, and AGC of 1×10^6. Then, a series of MS2 scans were acquired for the most abundant ions from the MS1 scan (top 12). Ions were filtered with charges 2–4. An isolation window of 2 *m*/*z* was used with quadruple isolation mode. Ions were fragmented using higher-energy collisional dissociation (HCD) with a collision energy of

27%. Orbitrap detection was used with a scan range of 140 to 2000 *m*/*z*, resolution of 30 K, maximum injection time of 54 milliseconds, and AGC of 50,000.

N. MS data analysis

Proteome Discoverer (Thermo Fisher Scientific, version 2.4) was used to process the raw spectra. Default search parameters were used, including precursor mass tolerance of 10 ppm, fragment mass tolerance of 0.02 Da, enzymes specific cleavage, and up to 2 mis-cleavage. Carbamidomethyl [C] was set as a fixed modification, while Oxidation [M] and Acetylation [N-terminal and K] were set as variable modifications. The target-decoy approach was used to filter the search results, in which the false discovery rate was less than 1% at the peptide and protein levels. For measuring the relative protein abundances, all the chromatographic data were aligned and normalized to peptide groups and protein abundances, missing values were imputed and scaled. The normalized protein abundance values from 4 Ctrls, 5 PE, and 4 Iso 4-day mice were used in the subsequent analysis. Since the different tubulin isoforms share multiple homologous regions, only unique peptides that are unambiguous to each isoform were used to calculate protein abundance. The unique peptides acquired for the analyzed isoforms ranged from 1-13 peptides and the full suite of peptide and protein groups used in the analysis can be found in the public proteomic repository as outlined in the data availability statement. Statistical analyses were performed on the calculated protein abundances as described below.

O. Total RNA extraction

Frozen aliquoted cardiac tissue obtained from similar locations of the heart was pulverized finely using a liquid nitrogen-cooled mortar and pestle. 500μL of ice cooled RNAzol (Molecular Research Center: RN 190) was added to the pulverized tissue and immediately homogenized using the handheld homogenizer until visible chunks of tissues were dissociated. 200μL of molecular grade water was added to the sample; the sample was vortexed and incubated for 15 minutes at 22°C. After processing of all samples, the samples were then centrifuged at 12000g for 15 minutes at 22°C. 550μL of the clear supernatant was carefully removed and transferred into a fresh tube. 550μL of isopropanol was then added to the supernatant, vortexed, and incubated for 10 minutes at 22°C. The samples were centrifuged at 16000g for 10 minutes at 22°C, and the resulting supernatants were discarded. The visible RNA pellets were washed in 75% ethanol in molecular grade water three times. The undried RNA pellets were resuspended in 30μL of RNase free water. The total RNA concentrations, and 260/230 and 260/280 ratios were determined using NanoDrop ND-1000 Spectrophotometer (NanoDrop Technologies). The RNA samples were stored at -80°C until further analysis.

P. NanoString nCounter analysis

Total RNAs from 37 samples were analyzed. The concentration of the total RNA was reassessed using NanoDrop spectrophotometer. The quality of the total RNA was assessed using the Agilent 4200 TapeStation (Agilent Technologies). Only samples that were pure as defined by OD 260/280 and 260/230 ratios > 1.8, and integrity RIN value > 8.0 were used in the study. 100ng of total RNA per sample for tubulin and hypertrophy panels or 200ng of total RNA per sample for tubulin autoregulation panel was used for

the subsequent step. Hybridization between the target mRNA and reporter-capture probe pairs was performed for 18 hours at 65°C using Mastercycler Pro S Thermal Cycler (Eppendorf) according to the manufacturer's protocol. Post-hybridization processing was carried out on a fully automated nCounter Prep Station (NanoString Technologies) liquid-handling robotic device using the High Sensitivity setting. For image acquisition and data processing, the probe/target complexes were immobilized on the nCounter cartridge that was then placed in the nCounter Digital Analyzer (NanoString Technologies) as per the manufacturer's protocol with FOV set to 555. The expression level of a gene was measured by counting the number of times the probe with a unique barcode, which was targeted against that gene, was detected. The barcode counts were then tabulated in a comma-separated value (.csv) format.

Q. NanoString nCounter data and statistical analysis

The raw digital counts of expressions were exported into nSolver Analysis software (NanoString, version 4.0) for downstream analysis. The data was analyzed in nSolver using the Nanostring Analysis and Advanced Analysis software packages. The background of the data was thresholded using the geometric means after removing negative control values that are three-times higher than the rest. The data was then normalized using the geometric means of the positive controls, after removing "F" if the value is too close to background, and the three housekeeping genes (Gapdh, Rpl4, Tbp). Without removing low count values, the Bonferroni-corrected differentially expressed gene (DEG) analysis of the normalized data was computed using Treatment as covariates. For tubulin autoregulation panel, raw counts were exported, and statistical analyses were carried as outlined below.

R. Proximity Ligation Assay (PLA)

For desmin-EB1 and actinin-EB1 experiments, untreated isolated rat cardiomyocytes were used. For EB-CLIP170 experiments, freshly isolated rat cardiomyocytes were treated for 48 hours with Null, TTL, or E331Q adenoviruses at 37°C with 5% CO_2. Once viral construct expressions were confirmed using the tagged mCherry, the cardiomyocytes were glued to cleaned coverglass (EMS 72222-01) using MyoTak (IonOptix). The cardiomyocytes on coverslips were fixed in 4% paraformaldehyde for 10min at RT, followed by 2 washes in PBS, and then permeabilized using 0.25% Triton in PBS for 10min at RT. The samples were blocked in Sea Block overnight at 4°C and stored until further processing.

The samples were incubated with either desmin and EB1, or α-actinin and EB1, or EB1 and CLIP-170 primary antibodies overnight at 4°C. The coverslips were then washed in PBS with 0.1% Tween (PBST) for 10min at RT. Following immediately, PLA was performed in humidified chambers using the manufacturer's protocol starting with "Duolink PLA Probe Incubation." Briefly, the samples were incubated with Duolink PLA secondary antibodies followed by ligation and amplification. Amplification was performed using Duolink FarRed detection reagents (Sigma DUO92013). Post-amplified samples were washed in PBS and incubated with 1:1000 405-Hoechst plus 1:200 488-WGA for 15min at RT for desmin-EB1 or α-actinin-EB1 experiments, or incubated with α-tubulin antibody (DM1A) conjugated to AF 488 (Cell Signaling #8058S) in Sea Block overnight at RT. The final processed samples were washed with PBST for 10min at RT then twice with PBS, and the coverslips were mounted using ProLong Diamond Antifade Mountant (Thermo Fisher P36961).

S. Image Acquisition and Analysis

Imaging was performed using Zeiss AiryScan microscope. 1x 2μm slice per cell or 6x 0.18μm slices were sampled for each cell in desmin-actinin-EB1 experiments and EB1-CLIP170 experiments, respectively; 10 cells were sampled per group per experiment (N=3, n=30). ImageJ was used to analyze the images. For desmin-actinin-EB1 experiment: an automated threshold image of the WGA channel was used to identify the cell outline. The % Area coverage of the PLA puncta was then determined using the cell outline. An average % Area coverage of all desmin-EB1 cells per experiment was calculated to determine the relative fold-change of actinin-EB1 within experiments. For EB1-CLIP170 experiment: an ROI was drawn to outline the cardiomyocyte border and the microtubule-PLA overlap Raw Integrated Density (RID) normalized to microtubule RID was calculated for each slice. The average microtubule-PLA overlap RID for one cell is determined using information from the 6 slices. Finally, the average value of all control cells in an experiment was used to calculate the relative fold-change for each experiment.

T. Statistical Analysis

Graphing and statistical analyses were performed using OrginPro 2019 software (OriginLabs). First, the normality of the data was determined using the Shapiro-Wilk test. For comparison of data distributions whose normality cannot be rejected at 0.05 level, the calculated probability of the means (p) between the control and the experimental group was calculated using the two-tailed two-sample Welch-corrected student's t-test. For comparison of data distributions whose normality is rejected at 0.05 level, the p-value between the control and the experimental group was calculated using the two-tailed two-sample Kolmogorov-Smirnov test. For significance level, I used the

Bonferroni-corrected significance cut-off of $p < 0.025$ denoted by * ; ** represents $p < 0.01$ and *** represents $p < 0.001$. P-values to two significant figures were reported for $0.05 < p < 0.025$. For all bar graphs, the bar represents mean and the whisker represents + 1 SEM. For all box plots, the bolded line represents mean, and the whiskers represent ± 1 standard error of mean (SEM).

U. Raw Data Availability

The Nanostring data presented in the study have been deposited to the GEO Omnibus repository with the accession number GSE194397. The mass spectrometry proteomics data have been deposited to the ProteomeXchange Consortium via the PRIDE partner repository with the dataset identifier PXD031797.

CHAPTER 3: RESULTS

A. Tubulin autoregulation is operant in the heart and induced in heart failure

Despite the importance of microtubule proliferation in cardiac pathology, any role of tubulin autoregulation has not been examined. I utilized a previously established strategy to test for autoregulation by measuring the relative abundances of pre-spliced (i.e. intron-containing) and spliced (i.e. those without introns) tubulin mRNAs(Gasic et al., 2019). Using this approach, one can detect transcriptional regulation of a target through correlated changes in intronic and exonic mRNA levels (y = x in Fig. 2E, for example), whereas post-transcriptional autoregulation would only affect exonic mRNA (shift along the y-axis of Fig. 2E). To study autoregulation in an isoform-specific fashion, I designed NanoString nCounter probes for direct and unique detection of either intronic or exonic regions of individual tubulin isoforms. To determine if autoregulation is operant in heart muscle cells, I treated isolated mouse cardiomyocytes for 6 hours with colchicine, a microtubule depolymerizing agent predicted to trigger autoinhibition (decrease in only exonic species) by increasing free tubulin, or taxol, a microtubule polymerizing agent predicted to trigger autoactivation (increase in only exonic species) by shifting free tubulin into the polymerized pool. Consistently, depolymerization significantly reduced the amount of exonic but not intronic mRNA across most tubulin isoforms, while polymerization increased the amount of exonic tubulin mRNA (Fig. 2D-E). This data serves as the first demonstration that autoregulation is operant in the cardiomyocyte and that it regulates the majority of tubulin isoforms.

Next, I tested whether tubulin autoregulation can partially explain the discrepancy in mRNA and protein levels observed in heart failure. To this end, I designed a separate Nanostring probe set against introns and exons of human tubulin isoforms and probed RNA extracted from 35 cardiac samples from 12 non-failing donors and 23 patients with

advanced heart failure. Figure 1F-G shows the relative intron and exon abundances for all tubulin isoforms that could be readily detected at the intron, exon and protein level (Chen et al., 2018)(Fig. 2A-B). In failing hearts, the majority of tubulin isoforms showed reduced exonic relative to intronic levels, indicative of active autoinhibition across most isoforms. An exception is *TUBA1A*, the only isoform that demonstrated significant transcriptional induction; consistently *TUBA1A* is also being the only isoform to show both increased and correlated mRNA and protein levels in this heart failure population (Fig. 2A-B). Of additional note, *TUBB4B* is by far the most abundant β-tubulin isoform expressed in the heart, and it exhibits robust autoinhibition in heart failure, yet maintains increased protein abundance. Taken together this data indicates that in heart failure, elevated tubulin protein triggers persistent autoinhibition of tubulin mRNA. The maintained elevation in tubulin protein may be explained by significantly increased tubulin stability/lifetime.

However, there remains no explanation as to how the heart achieved the increased tubulin protein in the first place or whether autoregulation plays any role in the establishment of the increased tubulin mass observed in pathological cardiac remodeling. To better understand this, I employed mice models of cardiac hypertrophy that allows us to explore the early roles of tubulin transcription, autoregulation, and stability.

B. Acute adrenergic agonism induces anatomic and transcriptional cardiac remodeling

To determine how the microtubule network remodels during the development of cardiac hypertrophy, I characterized the myocardial cytoskeleton at two time points in two mouse models of adrenergic agonist-induced hypertrophy(Scarborough et al., 2021)

(Fig. 3A). A 4-hour post-injection time point was chosen to capture a stage when hearts were exposed to hypertrophic stimuli but have not yet hypertrophied, and a 4-day post-injection time point was chosen to capture a stage when hearts had demonstrably hypertrophied. As expected, no change in heart-weight-to-tibia-length (HW/TL) was observed 4 hours after injection of either phenylephrine (PE) or isoproterenol (Iso) compared to vehicle control (Ctrl) (Fig. 3B, left). When mice were given a second injection on day 2 and hearts were collected on day 4, I observed a consistent cardiac hypertrophy with both PE and Iso (Fig. 3B, right).

Concurrently, I observed a similar increase in cardiomyocyte area in myocardial tissue cross-sections (Fig. 4C). There was no mortality nor significant cardiac fibrosis in control and experimental groups (Fig. 4D). To assess left-ventricular remodeling and function, I performed echocardiography on the 4-day hypertrophy animals. I observed consistent evidence of concentric hypertrophy upon both PE and Iso treatment, with elevated left-ventricular (LV) mass and increased wall and septal thickness (Fig. 3C-D). Neither group exhibited evidence of decompensation toward heart failure, with no evidence of ventricular dilation or depressed contractility, indicating a compensated, concentric hypertrophy in response to acute adrenergic agonism.

I further validated my models using NanoString nCounter to assess transcriptional markers of cardiac remodeling in the hearts of PE and Iso treated mice. Using direct RNA counting of 42 transcripts sorted into immediate early genes (IEGs), hypertrophy-related genes, and fibrosis-related genes, I analyzed differentially expressed genes (DEGs) in the septa and LV of my time-matched control and experimental groups. I hypothesized that IEGs would be upregulated after 4-hours of adrenergic stimulation, followed by upregulation of canonical markers of hypertrophic remodeling after 4 days. Consistent with this hypothesis, I observed robust upregulation

of the canonical IEGs – *cMyc* and *cFos* – in both PE and Iso treated mice at 4-hours (Fig. 3E & Fig. 5), followed by induction of stress markers – *Nppa* and *Nppb* – at 4-days, along with markers of fetal reprogramming including myosin isoform switching (reduced *Myh6:Myh7* ratio).

The full complement of DEGs in each experimental group at the 4-hour and 4-day time points are depicted in Fig. 5. At both 4-hours and 4-days after adrenergic agonism, I observed upregulation of hypertrophy-related gene *Fhl1*(Friedrich et al., 2012), and fibrosis-related genes *Ctgf* (Hayata et al., 2008) & *Vcan*(Vistnes et al., 2014). Additional potentially relevant DEGs included the upregulation of *Col4a1*(Steffensen and Rasmussen, 2018) and *Timp1*(Barton et al., 2003), and the downregulation of *Agrn*(Baehr et al., 2020; Bassat et al., 2017), among others (see discussion for further contextualization).

C. The microtubule network is rapidly detyrosinated upon hypertrophic stimulation

Having validated the 4-hour and 4-day models, I examined microtubule network remodeling in these contexts. I first determined whether the total αβ-tubulin content and free vs. polymerized tubulin pools are altered in the pre-hypertrophic (4-hour) state. I observed no significant differences in these metrics of total tubulin content or fractionation at this early time point (Fig. 6A-C).

I next determined whether tubulin is rapidly post-translationally modified upon hypertrophic stimulation. I immunoblotted for the five best-studied PTMs using validated antibodies: acetylation, detyrosination, polyglutamylation, polyglycylation, and Δ2 tubulin. Polyglutamylation, polyglycylation, and Δ2 are well characterized in cilia, flagella, and the

brain(Aillaud et al., 2016; Paturle-Lafanechère et al., 1994), but they have not been studied in the heart. Detyrosination and acetylation, which occur predominantly on polymerized microtubules, are common markers of stable, long-lived microtubules, and of microtubule damage and repair-stabilization processes(Portran et al., 2017; Xu et al., 2017) respectively.

At the 4-hour time point, I did not observe any significant differences in either the absolute (PTM/GAPDH) or the relative (PTM/α-tubulin) amounts of acetylation, polyglutamylation, polyglycylation, or Δ2 tubulin (Fig. 6D, F-H). Surprisingly, I did observe robust induction of the absolute and relative amounts of detyrosination in both PE and Iso treated groups (Fig. 6E). These data suggest that within 4 hours of hypertrophic stimulation, prior to other overt changes in tubulin mass, microtubules are rapidly detyrosinated, which may serve as an early driver of microtubule stabilization.

D. Post-translationally modified microtubules proliferate during the establishment of cardiac hypertrophy

I next characterized microtubule network remodeling at day 4, concurrent with cardiac hypertrophy. I probed the 3 tubulin pools and immunoblotted for α-tubulin, β-tubulin, acetylation, detyrosination, polyglutamylation, polyglycylation, Δ2 as described above.

At this stage I observed increased free, polymerized, and total αβ-tubulin protein in the hearts of PE and Iso-treated mice (Fig. 7A-C). In the PE group, the ratio of free:polymerized α-tubulin decreased (Fig. 8A), consistent with enhanced microtubule stability. In PE-treated mice, I observed increases in the absolute amounts of acetylation, polyglutamylation, and polyglycylation, and in the absolute and relative

amounts of detyrosination. Iso treated mice showed a similar trend for each PTM, but of reduced magnitude and greater variability (Fig. 7C-H). Taken together, these data indicate that during cardiac hypertrophy tubulin content increases, the polymerized network densifies, and there is a proportionally increased abundance of post-translationally modified microtubules with a modest enrichment of detyrosination.

I next sought to determine how specific tubulin isoforms contribute to the increase in tubulin content observed at 4-days. To this end, I utilized mass spectrometric (MS) analysis of the total tubulin pool. I observed that the predominant α- and β-tubulin isoforms of murine LV were Tuba1a and Tubb4b, respectively (Fig. 9A). Each of these predominant isoforms were modestly increased upon PE and Iso treatment. I also determined the relative changes of all detectable tubulin isoforms and observed significant increases in Tuba1a, Tuba1c, Tubb2a, Tubb2b, Tubb3, Tubb5, and Tubb6 (Fig. 9A-B). Of note, Tuba4a – the only tubulin isoform that is synthesized in its detyrosinated form – was clearly not increased upon hypertrophic stimulation. This indicates that the early increases in detyrosination are not due to increased synthesis of Tuba4a, and instead likely due to altered activity of the enzymes of the tyrosination cycle. Tubb6 exhibited the highest degree of upregulation with a ~4-fold increase upon PE treatment; this is notable as Tubb6 induction has been causally implicated in microtubule network reorganization in Duchenne Muscular Dystrophy(Randazzo et al., 2019). Despite significant upregulation of multiple low abundance isoforms, the overall composition of the total tubulin pool is largely conserved at this stage of hypertrophic remodeling (Fig. 9A).

E. Transcriptional analysis of αβ-tubulin isoforms, tubulin modifying enzymes, and MAPs during the induction and establishment of hypertrophy

I next examined the contribution of transcriptional changes to the protein and network level microtubule remodeling at the 4-hour and 4-day timepoints. To this end, I utilized NanoString analysis of total RNA using another set of 47 genes that includes tubulin isoforms, tubulin modifying enzymes, and MAPs.

While tubulin protein content was unchanged 4-hours after adrenergic stimulation, I noted significant upregulation of several tubulin transcripts with both PE and Iso treatment at this stage, including *Tuba1c, Tubb2a and Tubb6*, with additional and more robust upregulation of *Tubb2b and Tubb3* by day 4 (Fig. 9C). Consistent with proteomics assessments, *Tuba4a* and *Tuba8* were either unchanged or even downregulated upon PE and Iso treatment.

Regardless of the directionality of response, specific tubulin isoforms generally responded similarly to either adrenergic stimulus (Fig. 9C). Further, in contrast to what was observed in advanced heart failure, transcript levels were also well-correlated with protein abundance across most isoforms at the 4-day time point (R^2 = 0.38, slope = 0.20, p = 1.4e-4) (Fig. 9D). Consistent with protein expression lagging transcriptional regulation, the four isoforms (Tuba4a, Tuba8, Tubb2b, Tubb3) that displayed the greatest deviation in the change in the mRNA relative to the change in the protein levels (i.e. located furthest away from the y = x line when plotting $\log_2$FC of mRNA vs protein levels) were transcripts that showed delayed regulation; these isoforms were unchanged after 4-hours but differentially expressed by 4-days. Consistent upregulation at the transcript and protein level was seen for Tuba1c, Tubb2a, Tubb2b, Tubb3, and Tubb6. Combined with the early upregulation of tubulin transcripts, this data indicates that increased tubulin mRNA at least partly underlies the isoform-specific increase in tubulin

protein, and therefore tubulin mass, that is necessary for hypertrophic remodeling(Sato et al., 1997; Scarborough et al., 2021; Tsutsui et al., 1999).

I noted several additional transcriptional changes of tubulin modifying enzymes and MAPs that may bear relevance to cardiac remodeling and warrant further investigation (Fig. 9E-F; Fig. 10). These include: (1) *Vash2,* which encodes a tubulin detyrosinase, exhibited the greatest differential expression among the 47 assessed transcripts at the 4-hr PE time point; this may contribute to the robust early induction of detyrosination in this group (2) Early upregulation of *Kif5b* after 4-hours in PE(Tigchelaar et al., 2016), which encodes the primary transport kinesin heavy chain 1 implicated in mRNA transport during myocyte growth(Scarborough et al., 2021); (3) upregulation of *Mapre1* in both PE and Iso at 4-hours*,* which encodes a member of microtubule associated protein RP/EB family of +TIP tracking protein that guides microtubule growth; (4) Robust upregulation of *Kif15* in both PE and Iso by 4-days, which encodes a kinesin family member implicated in stabilizing parallel growing microtubules; (5) induction of *Map1a* in both PE and Iso at 4-days, which encodes a stabilizing structural MAP.

I next sought to determine whether these mRNA changes were reflected at the protein level for targets for which I could obtain robust signal via western blot from validated antibodies. Generally, transcripts that were upregulated early at the 4-hour time point such as *Kif5b* and *Mapre1* also appeared to be upregulated at the protein level by day 4, whereas transcripts that were unchanged or only upregulated later at 4-days (such as *Vash1* and *Kif15*), did not show protein level changes at day 4 (Fig. 8B-C).

All tubulin-associated transcript volcano plots (Fig. 10) were asymmetric, tending to show a greater degree of upregulated than downregulated genes, implying a generalized induction of a tubulin-associated program at 4-days. This was particularly

evident in the PE groups, and with progressive upregulation from the 4-hour to 4-day time point. There were, however, notable down-regulated transcripts. While kinesin isoforms, which encode plus-end directed anterograde motors, were generally upregulated in treated groups, transcripts encoding subunits of the dynein/dynactin minus-end directed motor (*Dynll2, Dync1h1, Dctn2)* were either downregulated or unchanged (Fig. 9F). This preferential induction of anterograde motors would bias trafficking toward the microtubule plus-end and away from the minus-end, which has implications for directed cardiac growth and for autophagic flux, which requires minus-end directed transport (McLendon et al., 2014). I also noted the early downregulation of enzymes involved in the polyglutamylation cycle, such as cytosolic carboxypeptidase 5 (*Ccp5*) and TTL-like family members 1 and 5 (*Ttll1/5*), which were all reduced in PE and Iso at the 4-hour time point (Fig. 10).

To determine the conservation of these tubulin-associated transcriptional responses across varied hypertrophic stimuli, I compared my data with publicly available RNA sequencing datasets from two separate studies that examined early time-points following pressure-overload and angiotensin II induced hypertrophy. While data is not available for all transcripts, transcripts that were consistently reported across studies demonstrate well-conserved transcriptional signatures at both early (hours) and later (days) timepoints (Fig. 11), including the consistent upregulation of most αβ-tubulin isoforms but with the notable downregulation of *Tuba4a* and *Tuba8*.

F. Transcriptional and autoregulatory mechanisms underlie isoform-specific increases in αβ-tubulin mRNA

The above transcriptional and proteomic profiling indicates that the upregulation of tubulin mRNAs is an early driver of microtubule proliferation during the development

of hypertrophy. This may arise from two non-exclusive mechanisms – (1) increased transcription or (2) decreased autoregulation (i.e., autoactivation). To differentiate between the two, I utilized the tubulin isoform and location -specific approach outlined above to interrogate the mechanism of tubulin upregulation during cardiac hypertrophy.

Overall, I observed that by day 4 the exonic levels of almost all tubulin isoforms increased more than intronic levels, suggesting a generalized autoactivation of tubulin isoforms driven by microtubule stabilization (Fig. 12). The most prominent cases of autoactivation are that of *Tubb2b*, whose increase in transcript level is solely through an increase in exonic species at both 4-hours and 4-days, and *Tuba1a*, whose immediate response at 4-hours was through an increase in exonic level with no change in intronic level (Fig. 12A). Additionally, in a subset of the tubulin isoforms – *Tuba1b*, *Tubb2a*, *Tubb5*, and *Tubb6* – we observed robust increases in intronic levels that indicate direct transcriptional activation by the hypertrophic stimuli (Fig. 12B, Fig. 13).

Interestingly, despite a generalized upregulation and autoactivation of tubulin isoforms in the early stages of hypertrophy, *Tuba4a* and *Tuba8* are downregulated and autoinhibited, respectively. These data collectively show that ab-tubulin mRNA is controlled in an isoform-specific and time-dependent fashion through both transcriptional and autoregulatory mechanisms to rewrite the tubulin code during cardiac remodeling.

CHAPTER 4: DISCUSSIONS & FUTURE DIRECTIONS

In this work, I combined transcriptomic and proteomic assessments of advanced heart failure samples and temporally well-defined murine models of cardiac remodeling to understand how a dense and modified microtubule network is achieved. Among other observations expanded upon below, I arrive at four primary conclusions: 1) tubulin autoregulation is operant in the heart and represses mRNA levels of tubulin isoforms in heart failure, contributing to the observed discrepancy between tubulin RNA and protein in heart failure; 2) the microtubule network is rapidly post-translationally detyrosinated within 4 hours of a hypertrophic stimuli; 3) concomitantly, the abundance of tubulin mRNA is rapidly altered in an isoform-specific fashion through both transcriptional and autoregulatory mechanisms; 4) the time-dependent upregulation of discrete αβ-tubulin transcripts drives an increase in microtubule mass during cardiac hypertrophy.

A. Advantages of the acute adrenergic murine models of cardiac hypertrophy

To date, there is an abundance of animal models for cardiac hypertrophy such as trans-aortic banding(Rockman et al., 1991), high-salt diet(Takeda et al., 2000; Yuan and Leenen, 1991), and use of osmotic pumps to deliver adrenergic(Chang et al., 2018) and angiotensin agonists (Balakumar et al., 2007). The advantages of these pre-existing models are that they mimic the pathophysiology of cardiac hypertrophy and provide us with an invaluable tool to study efficacy of interventions. However, the disadvantages are that they need special technicians and can take variable amounts of time to establish discernable hypertrophy; this unpredictability of how long it takes to observe the hypertrophic phenotype makes it challenging to study the temporal aspects of the pathological process. In the acute adrenergic stress-induced cardiac hypertrophy models presented in this study, I was able to not only study the pathological changes associated

with the microtubule network in the context of cardiac hypertrophy, but also elucidate the time-dependent changes of the microtubules at all levels, i.e., network, protein, and transcripts, as the heart transitions from a normal state to overt hypertrophy.

B. Temporal evaluation of previously identified cardiac hypertrophy-associated factors

In conjunction with the feasible of the models to be temporally controlled, NanoString analyses of my hypothesized transcripts also yielded insightful observations especially in associating transcriptional changes that had been previously described in the cardiac hypertrophy literature but were temporally undetermined. To elaborate, thrombospondin-4 (*Thbs4*)(Frolova et al., 2012; Palao et al., 2018), osteoblast specific factor-2 (*Osf2*)(Lin et al., 2013), and lumican (*Lum*)(Engebretsen et al., 2013; Mohammadzadeh et al., 2019) were all previously described to be upregulated in either cardiac hypertrophy, heart failure, or both. Based on my data, I observed that the upregulations of *Thbs4* and *Osf2* occurs in hypertrophy but not in pre-hypertrophy (Fig. 5). In addition, *Lum* is upregulated only when the heart has hypertrophied; in fact, *Lum* was observed to be downregulated during pre-hypertrophic stage.

C. Evaluation of additional cytoskeletal elements

Beyond the key conclusions, several additional observations on additional cytoskeletal remodeling are of note. The association of the microtubule network with motor proteins such as kinesins alters its mechano-biochemical properties as well as its density. As an example, Kif15 (kinesin-12) has been shown to cross-link nearby parallel microtubules, causing them to bundle, and subsequently decreases the catastrophic

events of dynamic microtubules(Drechsler and McAinsh, 2016). Interestingly, during both PE and Iso -induced hypertrophy, *Kif15* is upregulated, suggesting that *Kif15* could contribute to microtubule network densification.

Kif5b (Kinesin-1), the predominant anterograde motor in the heart, was previously reported to be increased in PE induced-hypertrophy of neonatal rat ventricular cardiomyocytes(Tigchelaar et al., 2016). I observed similar and rapid increase in Kif5b transcript and protein levels in my hypertrophy models (Fig. 9F, Fig. 10). Kinesin-1 was recently identified to be required for the distribution of mRNA and ribosomes that enables cardiomyocyte hypertrophy (Scarborough et al., 2021), and past work indicates that kinesin-1 prefers to transport cargo along detyrosinated microtubule tracks(Kaul et al., 2014). Meanwhile, the dynein/dynactin retrograde motor protein complex (transcriptionally downregulated, Fig. 9F), prefers tyrosinated microtubule tracks(Nirschl et al., 2016). Taking together, these observations suggest that the heart both rapidly induces its primary anterograde transport motor and remodels its preferred tracks in response to a hypertrophic stimulus.

In addition to the suggestive time-dependent transcriptional changes, using my NanoString data in conjunction with the microtubule characterizations, I observed another interesting correlation. I observed an upregulation of *Timp1*(Barton et al., 2003) and downregulation of *Agrn*(Bassat et al., 2017)(Fig. 5). *Timp1* upregulation would lead to an inhibition of extra-cellular matrix (ECM) degradation and a subsequent increase in dystrophin-glycoprotein complex (DGC). Likewise, *Agrn* downregulation would also increase DGC, through decreased association of agrin with α-dystroglycan and subsequent ERK inactivation(Bassat et al., 2017). These two mechanisms could potentially lead to stabilize microtubule network through increased DGC, and so the increase in detyrosination at 4-hour could reflect this stabilization.

D. Differential regulation of tubulin isoforms in muscle pathologies

Insights into tubulin isoforms in muscle biology have pointed towards the potential detrimental effects of specific isoforms in muscle pathologies; for example, TUBB6 is upregulated in dystrophic skeletal muscles, and it contributes to microtubule disorganization and altered muscle regeneration in muscular dystrophy(Randazzo et al., 2019). Elevated TUBA4A in human cardiomyopathy contributes to the increased detyrosination that impedes myocyte function(Chen et al., 2018; Schuldt et al., 2020).

Strikingly, when I examine publicly available transcriptomic and proteomic data from chronically hypertrophied or failing human hearts (Fig. 1A), I observe an inverse relationship between the transcript and protein levels of almost all $\alpha\beta$-tubulin isoforms. It is worth noting that TUBA8 is the lone tubulin transcript that is consistently *increased* in heart failure while the protein level is consistently *decreased*. Intriguingly, *Tuba8* was also the sole isoform to clearly escape autoactivation (and appear seemingly autoinhibited) during early hypertrophic remodeling (Fig. 12A). I have no current explanation for how or why Tuba8 shows unique regulation in both settings. In contrast to this inverse relationship in heart failure, I observed that during the establishment of hypertrophy, transcript and protein levels are highly correlated, suggesting an uncoupling of transcript and protein levels that occurs later in the course of cardiac remodeling. Chronic, robust microtubule stabilization and increased tubulin lifetime could account for the stably elevated tubulin protein content despite persistent autoinhibition that I observe in heart failure.

E. Potential pathophysiological role of Tubb6 in cardiac hypertrophy

Moreover, given the fact that TUBB6 upregulation in dystrophic skeletal muscles is causally linked to microtubule disorganization and altered muscle regeneration in muscular dystrophy(Randazzo et al., 2019), it would fair to assume that the increase in Tubb6 protein level during cardiac hypertrophy may also have a detrimental effect as well. In line with this enquiry, studying the function of Tubb6 in cardiac biology using in vitro and in vivo approaches is warranted. Furthermore, since I observed that the increase transcription of Tubb6 gene underlies Tubb6 protein level increase, it would be interesting to study the effects of Tubb6 knock-down during cardiac hypertrophy on microtubules such as its dynamicity and viscoelasticity, and on cardiomyocyte such as its contractility.

F. Tubulin isoform specificity of transcription and autoregulation

Although I have a good albeit incomplete understanding of how transcription regulates total tubulin levels, I still lack knowledge of how it effects tubulin on an isoform-specific level. In line with this thinking, it would be interesting to unravel the transcription factors involved in transcription of tubulin isoforms and to understand how changes to the transcriptional programs can influence the isoform composition of microtubules and hence its biomechanical properties. Preliminary analysis of the tubulin isoforms that are deemed to be transcriptionally regulated at 4-hours post-hypertrophic stimuli showed that Kruppel-like factor 4 (KLF4) binding motif is present in the promoter regions (data not shown). It would be interesting to perform chromatin immunoprecipitation (ChIP) experiment followed by NanoString nCounter analysis or RNA-sequencing to test the hypothesis that KLF4 controls transcription of certain tubulin isoforms and that during pathological conditions, this transcriptional regulation would change.

Since only recently tubulin autoregulation was observed to regulate tubulin on an isoform-specific level, it would be tremendously beneficial for the field of tubulin biology to understand the molecular and genetic determinants of isoform-specificity. Although the former would be harder to study, the latter could be accomplished by careful mutagenesis experiments using model in vitro systems. Further interesting avenues such as the crosstalk between tubulin isoforms, or the crosstalk between transcription and autoregulation programs would serve well to have a complete understanding of tubulin biology and to come up with unique treatment modalities for heart failure.

G. Subcellular localization of tubulin isoforms in cardiomyocyte

Since different tubulin isoforms are shown to have differing biochemical properties and expression patterns, it would also be interesting to determine the sub-cellular localization of the tubulin isoforms before and after pathological stimulation using RNA-FISH (fluorescent in situ hybridization). These experiments could potentially uncover further regulations of tubulin isoforms not only at the level of expression through transcription and autoregulation, but also at how the tubulin isoforms are utilized through differences in its cellular location.

H. Role of intermediate filament, desmin, in cardiac hypertrophy

A recent *in vitro* study using optical traps to examine the biochemical interactions between vimentin, an intermediate filament akin to muscle-specific desmin, and microtubules, observed a direct interaction of vimentin and microtubules through hydrophobic and electrostatic forces(Schaedel et al., 2021). I can hypothesize that a

similar interaction between desmin and microtubule would be present in cardiomyocytes. Indeed, recent work from my lab has shown that desmin and microtubules do interact, and that their interaction decreases microtubule catastrophe and increases growth(Salomon et al., 2021). From my current hypertrophy study in conjunction with previous observations, an increase in detyrosination at 4-hour post-hypertrophic stimulations suggests a possible mechanism in which the increased exposure of charged amino-acid, glutamic acid, on tubulin C-terminal end through detyrosination could reinforce the desmin-microtubule interaction to increase microtubule stability.

CHAPTER 5: UNPUBLISHED DATA & CONCLUSIONS

A. Unpublished Data 1 – Desmin and tubulin tyrosination influences microtubule stability

Recent unpublished data from the Prosser lab have shown that (1) loss of desmin promotes microtubule catastrophes and prevents pausing of growing microtubules on the sarcomere Z-disk, while (2) tubulin tyrosination promotes growth and catastrophe frequencies (Salomon et al., 2021). However, two unanswered questions remained: (1) is desmin directly interacting with microtubules and thus stabilizing them or does it stabilize microtubules merely by being present at the Z-disk, and (2) how does tubulin tyrosination promotes catastrophe?

To answer these two questions, I utilized an imaging approach known as proximity-ligation assay (PLA) in which the proximity of two target proteins (baits) are determined using target-specific antibodies; if two baits reside within 40nm, a PLA signal will be observed whereas if the targets reside further than 40nm, no signal will be observed. Using this approach, I first tested whether desmin and not the other sarcomeric Z-disk protein, such as alpha-actinin, interacts with the microtubule. To specifically test for desmin or alpha-actinin's interaction with the growing microtubules, I used desmin or α-actinin as the first bait and End-Binding Protein 1 (EB1) as the second bait because EB1 is associated with the plus-end or the growing end of the microtubules (Vitre et al., 2008). Indeed, EB1 interacts with both α-actinin and desmin at the Z-disk. However, it was evident that EB1 preferentially interacts with desmin over α-actinin since I observed a ~20-fold increase of PLA puncta in desmin-EB1 compared to α-actinin-EB1 (Fig. 15A).

Next, I attempted to determine how tyrosinated microtubules exhibit increased growth and catastrophe frequencies. It is unlikely that changes in the PTM alone would lead to the observed phenotype (Khawaja et al., 1988; Webster et al., 1990). However, the addition of hydrophobic tyrosine residue and the subsequent blocking of glutamic residue will alter the hydrophobic and electrostatic interactions between the outer surface of the polymerized microtubule and MAPs, enabling tyrosination to alter microtubule dynamics through association with destabilizing MAPs or changes in MAP composition on microtubules(Chen et al., 2021; Peris et al., 2009).

Recent in vitro microtubule reconstitution study suggests that synergistic binding of EB1 and CLIP-170 on microtubules increases frequency of growth and catastrophe in a tyrosination-dependent manner(Chen et al., 2021). Hence, I hypothesized that EB1 and CLIP-170 association will increase with tyrosination and this association is independent of tubulin sequestration. To test this hypothesis, I performed PLA using EB1 and CLIP-170 as baits in a three-group experiment in which I treated adult rat cardiomyocytes with adenoviruses containing Null, TTL, or catalytically dead TTL (TTL-E331Q), which sequesters tubulin like TTL but does not tyrosinate. To control for TTL or E331Q induced microtubule network changes and to analyze only those EB1-CLIP-170 interactions on microtubules, I used total microtubule staining as a fiduciary marker. Using image analysis, I determined the Raw Integrated Density (RID) of EB-CLIP170 PLA and microtubule overlap normalized to total microtubule (see methods for more details). I observed that relative to the Null, TTL cardiomyocytes exhibited increased EB1 and CLIP-170 association on microtubules; this increase is independent of tubulin sequestration since EB1-CLIP-170 association remains unchanged in E331Q cardiomyocytes compared to control (Fig. 15B). Collectively, the data suggest that the increased growth and catastrophe frequencies of tyrosinated microtubules is partly

mediated through tyrosination-dependent association of EB1 and CLIP-170 in cardiomyocytes.

B. Unpublished Data 2 – Tubulin tyrosination improves cardiac function during hypertrophy

Given my observation that detyrosination of cardiac microtubules increased within 4 hours following a pathological stimulus, I wondered whether detyrosination of microtubules could be causal in the development of early adaptive hypertrophy. I therefore hypothesized that microtubule detyrosination is required for the induction of cardiac hypertrophy.

To test this hypothesis, I initiated a pilot experiment in which I attempt to rescue the phenylephrine-induced hypertrophy using adenovirus (Adv) mediated overexpression of tubulin tyrosine ligase (TTL) prior to administration of phenylephrine. In collaboration with a post-doctoral fellow in the Prosser Lab, I retro-orbitally injected five 6-weeks old C57/Bl6 mice with saline or four 6-weeks old C57/Bl6 mice with Adv-TTL and let the virus to be transduced for 2 weeks. After 2 weeks when the mice reached 8 weeks of age, I challenged all nine animals with phenylephrine on day 0 and day 2 and collected the heart tissues on day 4. I then measured the HW/TL and performed western blot to discern the amount of TTL overexpression.

As shown in Fig. 16, TTL was overexpressed robustly in the cardiac tissues of Adv-TTL 8-weeks old mice. Although I observed a slight decrease in the HW/TL in Adv-TTL group, I did not observe any significant differences in the heart-weight-to-body weight or HW/TL ratios (Fig. 16). I wondered whether this insignificant reduction of HW/TL in the Adv-TTL group compared to saline group could be made significant by

increasing the extent of phenylephrine-induced hypertrophy so that there is more room to observe the rescue effect by TTL overexpression.

To this end, I attempted to induce a greater degree of cardiac hypertrophy than what was previously observed by increasing the number of phenylephrine or isoproterenol injections from two to nine. I again utilized C57/Bl6 wild-type mice (5 mice per experiment) and injected with either 10mg/kg phenylephrine or 5mg/kg isoproterenol or ascorbic acid control every other day starting at day 1 for a total of 9 injections. To test the rescue effect of TTL overexpression, I also included a group of five additional mice, in which I injected Adv-TTL retro-orbitally at 6 weeks of age and injected them with phenylephrine after two weeks at 8 weeks of age, for a total of 9 injections (Fig. 17A).

In addition to harvesting heart tissues at the end of the experiment on day 19 to determine the HW/TL (Fig. 17B) and microtubule post-translational modifications (Fig. 18) using western blot analysis, I ascertained the cardiac functions of the control, phenylephrine, and phenylephrine + TTL mice using extensive echocardiography analysis on days 5, 12, and 19. During the experiment, there was only two mortalities in the long-term isoproterenol injected group (data not shown). The full suite of echocardiography data for day 19 is presented in Figure 17C. Interestingly, as shown in figure 17A, I no longer observed the phenylephrine and isoproterenol induced hypertrophy phenotypes on day 19. This null observation could be attributable to β-adrenergic signal desensitization of the experimental animals due to chronic phenylephrine exposure(Dewenter et al., 2022; Najafi et al., 2016).

Despite the null observation in the HW/TL metric in the control and TTL overexpressed groups, I did observe significant changes in multiple echocardiographic parameters of the experimental animals on day 19. Experimental animals in the phenylephrine alone group did show increases in Left-Ventricular Mass Index (LVMI)

and Isovolumic Relaxation Time (IVRT), suggesting that the heart did undergo phenylephrine-induced hypertrophy and that this hypertrophy is accompanied by slower rates of isovolumic relaxation and diastolic strain (Fig. 17C). Interestingly, TTL overexpression seems to block phenylephrine-induced hypertrophy as well as the aberrant isovolumic relaxation and diastolic strain phenotypes.

Finally, western blot analyses of the tubulin PTMs (Fig. 18) showed a decrease of detyrosination in TTL overexpressed group along with a decrease in $\Delta 2$ tubulin formation and an increase in polyglutamylation. The decreased in detyrosinated and $\Delta 2$ tubulin in the TTL overexpressed group is expected given that TTL catalyzes tyrosination and detyrosinated tubulin is the substrate for $\Delta 2$ formation. All in all, my preliminary data on the effects of TTL overexpression before phenylephrine-induced hypertrophy shows promising results in which TTL overexpression blocks hypertrophic phenotype while improving aberrant cardiac functions that are associated with cardiac hypertrophy. This study could be of interest in future studies to elucidate and ascertain the role of microtubule detyrosination in mediating cardiac hypertrophy and its associated functional declines.

C. Conclusions

The data I have presented thus far in my thesis support the conclusions that (1) in addition to tubulin post-translational modifications, tubulin isoforms remodel rapidly during cardiac pathology through concerted mechanisms of transcription and post-transcriptional autoregulation, and (2) through understanding the regulations of the tubulin code, we can modulate the properties of the microtubule network and one day

discover novel microtubule-centric therapies that can stop the progression of hypertrophy into heart failure.

Some limitations of this study include the use of animal models for hypertrophy to study tubulin isoforms, and the lack of tubulin isoform data from animal models of heart failure. Given the differences in the expressed tubulin isoforms between human and mice, the findings on which tubulin isoforms are controlled transcriptionally or autoregulationally presented above should be interpreted in appropriate context of murine models. Another limitation is the use of total cardiac tissue that comprises of different cell types; however, it is important to note that cardiomyocytes make up ~56% of all cells or 70-80% by mass, which means that the changes observed in total cardiac tissue can be attributed mostly due to changes in the cardiomyocytes.

Combining this work with past literature, I propose the following sequential model for the formation of a proliferated and stabilized microtubule network in the remodeled heart (Fig. 14). Within hours of a hypertrophic stimuli and prior to detectable growth, the microtubule network is detyrosinated (Fig. 7E). my data indicate that this increase in detyrosination is likely due to transcriptional (Fig. 9E) or post-translational(Yu et al., 2021) upregulation of the recently identified detyrosinating enzyme complex, as my data argues against alternative mechanisms such as increased Tuba4a expression (Fig. 9C), increased polymerized or long-lasting microtubule substrate (Fig. 6C-D), or decreased TTL expression (Fig. 8B-C). Detyrosination serves as a network stabilizer to protect microtubules from breaking down by regulating EB1-CLIP170 association on microtubules (Fig. 15B) or through its interaction with the desmin intermediate filament (Fig. 15A); reduction of detyrosination by overexpressing TTL can prevent adrenergic-induced cardiac hypertrophy (Fig. 17). Microtubule stabilization, in turn, shuttles free

tubulin into the polymerized microtubule pool, triggering autoactivation that increases tubulin mRNA stability and translation.

How autoregulation may achieve isoform-specificity is not understood, although indicated by my data (see *Tubb2b* vs. *Tuba8*, Fig. 12). In concert with post-transcriptional upregulation of tubulin mRNA, increased transcription of several isoforms concomitantly increases tubulin mRNA. Independent of the mode of upregulation, tubulin mRNAs appear to be efficiently translated, as mRNA levels are well correlated with peptide abundance across tubulin isoforms (Fig. 9D). As the stimuli persists and the heart enlarges, the newly translated tubulin is integrated into the microtubule network, resulting in increased microtubule mass and additional substrate for post-translational modifications (Fig. 7). Finally, I showed that by preventing microtubule detyrosination, we can prevent the onset of cardiac hypertrophy following pathological stimulation.

BIBLIOGRAPHY

Aillaud, C., Bosc, C., Saoudi, Y., Denarier, E., Peris, L., Sago, L., Taulet, N., Cieren, A., Tort, O., Magiera, M.M., et al. (2016). Evidence for new C-terminally truncated variants of α- and β-tubulins. Mol Biol Cell *27*, 640–653. https://doi.org/10.1091/mbc.e15-03-0137.

Aillaud, C., Bosc, C., Peris, L., Bosson, A., Heemeryck, P., Dijk, J.V., Friec, J.L., Boulan, B., Vossier, F., Sanman, L.E., et al. (2017). Vasohibins/SVBP are tubulin carboxypeptidases (TCPs) that regulate neuron differentiation. Science *358*, 1448–1453. https://doi.org/10.1126/science.aao4165.

Baehr, A., Umansky, K.B., Bassat, E., Jurisch, V., Klett, K., Bozoglu, T., Hornaschewitz, N., Solyanik, O., Kain, D., Ferraro, B., et al. (2020). Agrin Promotes Coordinated Therapeutic Processes Leading to Improved Cardiac Repair in Pigs. Circulation *142*, 868–881. https://doi.org/10.1161/circulationaha.119.045116.

Balakumar, P., Singh, A.P., and Singh, M. (2007). Rodent models of heart failure. J Pharmacol Toxicol *56*, 1–10. https://doi.org/10.1016/j.vascn.2007.01.003.

Banerjee, I., Fuseler, J.W., Price, R.L., Borg, T.K., and Baudino, T.A. (2007). Determination of cell types and numbers during cardiac development in the neonatal and adult rat and mouse. Am J Physiol-Heart C *293*, H1883–H1891. https://doi.org/10.1152/ajpheart.00514.2007.

Barton, P.J.R., Birks, E.J., Felkin, L.E., Cullen, M.E., Koban, M.U., and Yacoub, M.H. (2003). Increased expression of extracellular matrix regulators TIMP1 and MMP1 in deteriorating heart failure. J Hear Lung Transplant *22*, 738–744. https://doi.org/10.1016/s1053-2498(02)00557-0.

Bassat, E., Mutlak, Y.E., Genzelinakh, A., Shadrin, I.Y., Umansky, K.B., Yifa, O., Kain, D., Rajchman, D., Leach, J., Bassat, D.R., et al. (2017). The extracellular matrix protein agrin promotes heart regeneration in mice. Nature *547*, 179–184. https://doi.org/10.1038/nature22978.

Ben-Ze'ev, A., Farmer, S.R., and Penman, S. (1979). Mechanisms of regulating tubulin synthesis in cultured mammalian cells. Cell *17*, 319–325. https://doi.org/10.1016/0092-8674(79)90157-0.

Brangwynne, C.P., MacKintosh, F.C., Kumar, S., Geisse, N.A., Talbot, J., Mahadevan, L., Parker, K.K., Ingber, D.E., and Weitz, D.A. (2006). Microtubules can bear enhanced compressive loads in living cells because of lateral reinforcement. J Cell Biology *173*, 733–741. https://doi.org/10.1083/jcb.200601060.

Brini, M., and Carafoli, E. (2009). Calcium Pumps in Health and Disease. Physiol Rev *89*, 1341–1378. https://doi.org/10.1152/physrev.00032.2008.

Caporizzo, M.A., Chen, C.Y., Salomon, A.K., Margulies, K.B., and Prosser, B.L. (2018). Microtubules Provide a Viscoelastic Resistance to Myocyte Motion. Biophys J *115*, 1796–1807. https://doi.org/10.1016/j.bpj.2018.09.019.

Caporizzo, M.A., Chen, C.Y., and Prosser, B.L. (2019). Cardiac microtubules in health and heart disease. Exp Biol Med *244*, 1255–1272. https://doi.org/10.1177/1535370219868960.

Caporizzo, M.A., Chen, C.Y., Bedi, K., Margulies, K.B., and Prosser, B.L. (2020). Microtubules Increase Diastolic Stiffness in Failing Human Cardiomyocytes and Myocardium. Circulation *141*, 902–915. https://doi.org/10.1161/circulationaha.119.043930.

Carrier, L., Bonne, G., Bahrend, E., Yu, B., Richard, P., Niel, F., Hainque, B., Cruaud, C., Gary, F., Labeit, S., et al. (1997). Organization and Sequence of Human Cardiac Myosin Binding Protein C Gene (MYBPC3) and Identification of Mutations Predicted to Produce Truncated Proteins in Familial Hypertrophic Cardiomyopathy. Circ Res *80*, 427–434. https://doi.org/10.1161/01.res.0000435859.24609.b3.

Chang, S.C., Ren, S., Rau, C.D., and Wang, J.J. (2018). Isoproterenol-Induced Heart Failure Mouse Model Using Osmotic Pump Implantation. Methods Mol Biology Clifton N J *1816*, 207–220. https://doi.org/10.1007/978-1-4939-8597-5_16.

Chen, C.Y., Caporizzo, M.A., Bedi, K., Vite, A., Bogush, A.I., Robison, P., Heffler, J.G., Salomon, A.K., Kelly, N.A., Babu, A., et al. (2018). Suppression of detyrosinated microtubules improves cardiomyocyte function in human heart failure. Nat Med *24*, 1225–1233. https://doi.org/10.1038/s41591-018-0046-2.

Chen, C.Y., Salomon, A.K., Caporizzo, M.A., Curry, S., Kelly, N.A., Bedi, K.C., Bogush, A.I., Krämer, E., Schlossarek, S., Janiak, P., et al. (2020). Depletion of Vasohibin 1 Speeds Contraction and Relaxation in Failing Human Cardiomyocytes. Circ Res https://doi.org/10.1161/circresaha.119.315947.

Chen, J., Kholina, E., Szyk, A., Fedorov, V.A., Kovalenko, I., Gudimchuk, N., and Roll-Mecak, A. (2021). α-tubulin tail modifications regulate microtubule stability through selective effector recruitment, not changes in intrinsic polymer dynamics. Dev Cell https://doi.org/10.1016/j.devcel.2021.05.005.

Chinnakkannu, P., Samanna, V., Cheng, G., Ablonczy, Z., Baicu, C.F., Bethard, J.R., Menick, D.R., Kuppuswamy, D., and Cooper, G. (2010). Site-specific Microtubule-associated Protein 4 Dephosphorylation Causes Microtubule Network Densification in Pressure Overload Cardiac Hypertrophy*. J Biol Chem *285*, 21837–21848. https://doi.org/10.1074/jbc.m110.120709.

Cleveland, D.W., Lopata, M.A., Sherline, P., and Kirschner, M.W. (1981). Unpolymerized tubulin modulates the level of tubulin mRNAs. Cell *25*, 537–546. https://doi.org/10.1016/0092-8674(81)90072-6.

Cleveland, D.W., Pittenger, M.F., and Feramisco, J.R. (1983). Elevation of tubulin levels by microinjection suppresses new tubulin synthesis. Nature *305*, 738–740. https://doi.org/10.1038/305738a0.

Coleman, A.K., Joca, H.C., Shi, G., Lederer, W.J., and Ward, C.W. (2021). Tubulin acetylation increases cytoskeletal stiffness to regulate mechanotransduction in striated muscle. J Gen Physiol *153*, e202012743. https://doi.org/10.1085/jgp.202012743.

Dewenter, M., Pan, J., Knödler, L., Tzschöckel, N., Henrich, J., Cordero, J., Dobreva, G., Lutz, S., Backs, J., Wieland, T., et al. (2022). Chronic isoprenaline/phenylephrine vs. exclusive isoprenaline stimulation in mice: critical contribution of alpha1-adrenoceptors to early cardiac stress responses. Basic Res Cardiol *117*, 15. https://doi.org/10.1007/s00395-022-00920-z.

Dorsch, L.M., Schuldt, M., Remedios, C.G. dos, Schinkel, A.F.L., Jong, P.L. de, Michels, M., Kuster, D.W.D., Brundel, B.J.J.M., and Velden, J. van der (2019). Protein Quality Control Activation and Microtubule Remodeling in Hypertrophic Cardiomyopathy. Cells *8*, 741. https://doi.org/10.3390/cells8070741.

Drechsler, H., and McAinsh, A.D. (2016). Kinesin-12 motors cooperate to suppress microtubule catastrophes and drive the formation of parallel microtubule bundles. Proc National Acad Sci *113*, E1635–E1644. https://doi.org/10.1073/pnas.1516370113.

Eisner, D.A., Caldwell, J.L., Kistamás, K., and Trafford, A.W. (2017). Calcium and Excitation-Contraction Coupling in the Heart. Circ Res *121*, 181–195. https://doi.org/10.1161/circresaha.117.310230.

Engebretsen, K.V.T., Lunde, I.G., Strand, M.E., Waehre, A., Sjaastad, I., Marstein, H.S., Skrbic, B., Dahl, C.P., Askevold, E.T., Christensen, G., et al. (2013). Lumican is increased in experimental and clinical heart failure, and its production by cardiac fibroblasts is induced by mechanical and proinflammatory stimuli. Febs J *280*, 2382–2398. https://doi.org/10.1111/febs.12235.

Fassett, J., Xu, X., Kwak, D., Zhu, G., Fassett, E.K., Zhang, P., Wang, H., Mayer, B., Bache, R.J., and Chen, Y. (2019). Adenosine kinase attenuates cardiomyocyte microtubule stabilization and protects against pressure overload-induced hypertrophy and LV dysfunction. J Mol Cell Cardiol *130*, 49–58. https://doi.org/10.1016/j.yjmcc.2019.03.015.

Fassett, J.T., Xu, X., Hu, X., Zhu, G., French, J., Chen, Y., and Bache, R.J. (2009). Adenosine regulation of microtubule dynamics in cardiac hypertrophy. Am J Physiol-Heart C *297*, H523–H532. https://doi.org/10.1152/ajpheart.00462.2009.

Ferrier, G.R., and Howlett, S.E. (2001). Cardiac excitation-contraction coupling: role of membrane potential in regulation of contraction. Am J Physiol-Heart C *280*, H1928–H1944. https://doi.org/10.1152/ajpheart.2001.280.5.h1928.

Frank, O. (1959). On the dynamics of cardiac muscle. Am Heart J *58*, 282–317. https://doi.org/10.1016/0002-8703(59)90345-x.

Friedrich, F.W., Wilding, B.R., Reischmann, S., Crocini, C., Lang, P., Charron, P., Müller, O.J., McGrath, M.J., Vollert, I., Hansen, A., et al. (2012). Evidence for FHL1 as a novel disease gene for isolated hypertrophic cardiomyopathy. Hum Mol Genet *21*, 3237–3254. https://doi.org/10.1093/hmg/dds157.

Gaasch, W.H. (1979). Left ventricular radius to wall thickness ratio. Am J Cardiol *43*, 1189–1194. https://doi.org/10.1016/0002-9149(79)90152-8.

Gasic, I., Boswell, S.A., and Mitchison, T.J. (2019). Tubulin mRNA stability is sensitive to change in microtubule dynamics caused by multiple physiological and toxic cues. Plos Biol *17*, e3000225. https://doi.org/10.1371/journal.pbio.3000225.

Ha, J.-W., and Oh, J.K. (2009). Therapeutic Strategies for Diastolic Dysfunction: A Clinical Perspective. J Cardiovasc Ultrasound *17*, 86–95. https://doi.org/10.4250/jcu.2009.17.3.86.

Havercroft, J.C., and Cleveland, D.W. (1984). Programmed expression of beta-tubulin genes during development and differentiation of the chicken. J Cell Biology *99*, 1927–1935. https://doi.org/10.1083/jcb.99.6.1927.

Hayata, N., Fujio, Y., Yamamoto, Y., Iwakura, T., Obana, M., Takai, M., Mohri, T., Nonen, S., Maeda, M., and Azuma, J. (2008). Connective tissue growth factor induces cardiac hypertrophy through Akt signaling. Biochem Bioph Res Co *370*, 274–278. https://doi.org/10.1016/j.bbrc.2008.03.100.

Heffler, J., Shah, P.P., Robison, P., Phyo, S., Veliz, K., Uchida, K., Bogush, A., Rhoades, J., Jain, R., and Prosser, B.L. (2020). A Balance Between Intermediate Filaments and Microtubules Maintains Nuclear Architecture in the Cardiomyocyte. Circ Res *126*, e10–e26. https://doi.org/10.1161/circresaha.119.315582.

Hinderliter, A., Sherwood, A., Gullette, E.C.D., Babyak, M., Waugh, R., Georgiades, A., and Blumenthal, J.A. (2002). Reduction of Left Ventricular Hypertrophy After Exercise and Weight Loss in Overweight Patients With Mild Hypertension. Arch Intern Med *162*, 1333–1339. https://doi.org/10.1001/archinte.162.12.1333.

Hoyle, H.D., and Raff, E.C. (1990). Two Drosophila beta tubulin isoforms are not functionally equivalent. J Cell Biology *111*, 1009–1026. https://doi.org/10.1083/jcb.111.3.1009.

Hubbert, C., Guardiola, A., Shao, R., Kawaguchi, Y., Ito, A., Nixon, A., Yoshida, M., Wang, X.-F., and Yao, T.-P. (2002). HDAC6 is a microtubule-associated deacetylase. Nature *417*, 455–458. https://doi.org/10.1038/417455a.

Inoué, S., and Sato, H. (1967). Cell Motility by Labile Association of Molecules. J Gen Physiology *50*, 259–292. https://doi.org/10.1085/jgp.50.6.259.

Janke, C., and Magiera, M.M. (2020). The tubulin code and its role in controlling microtubule properties and functions. Nat Rev Mol Cell Bio 1–20. https://doi.org/10.1038/s41580-020-0214-3.

Kalebic, N., Sorrentino, S., Perlas, E., Bolasco, G., Martinez, C., and Heppenstall, P.A. (2013). αTAT1 is the major α-tubulin acetyltransferase in mice. Nat Commun *4*, 1962. https://doi.org/10.1038/ncomms2962.

Kaul, N., Soppina, V., and Verhey, K.J. (2014). Effects of α-Tubulin K40 Acetylation and Detyrosination on Kinesin-1 Motility in a Purified System. Biophys J *106*, 2636–2643. https://doi.org/10.1016/j.bpj.2014.05.008.

Khawaja, S., Gundersen, G.G., and Bulinski, J.C. (1988). Enhanced stability of microtubules enriched in detyrosinated tubulin is not a direct function of detyrosination level. J Cell Biology *106*, 141–149. https://doi.org/10.1083/jcb.106.1.141.

Li, L., Zhang, Q., Zhang, X., Zhang, J., Wang, X., Ren, J., Jia, J., Zhang, D., Jiang, X., Zhang, J., et al. (2018). Microtubule associated protein 4 phosphorylation leads to pathological cardiac remodeling in mice. Ebiomedicine *37*, 221–235. https://doi.org/10.1016/j.ebiom.2018.10.017.

Lin, Q., Huang, Y., Booth, C.J., Haase, V.H., Johnson, R.S., Simon, M.C., Giordano, F.J., and Yun, Z. (2013). Activation of Hypoxia-Inducible Factor-2 in Adipocytes Results in Pathological Cardiac Hypertrophy. J Am Heart Assoc *2*, e000548. https://doi.org/10.1161/jaha.113.000548.

Lin, Z., Gasic, I., Chandrasekaran, V., Peters, N., Shao, S., Mitchison, T.J., and Hegde, R.S. (2020). TTC5 mediates autoregulation of tubulin via mRNA degradation. Science *367*, 100–104. https://doi.org/10.1126/science.aaz4352.

Magiera, M.M., Singh, P., Gadadhar, S., and Janke, C. (2018). Tubulin Posttranslational Modifications and Emerging Links to Human Disease. Cell *173*, 1323–1327. https://doi.org/10.1016/j.cell.2018.05.018.

McGrath, J.L. (2006). Microtubule Mechanics: A Little Flexibility Goes a Long Way. Curr Biol *16*, R800–R802. https://doi.org/10.1016/j.cub.2006.08.043.

McLendon, P.M., Ferguson, B.S., Osinska, H., Bhuiyan, Md.S., James, J., McKinsey, T.A., and Robbins, J. (2014). Tubulin hyperacetylation is adaptive in cardiac proteotoxicity by promoting autophagy. Proc National Acad Sci *111*, E5178–E5186. https://doi.org/10.1073/pnas.1415589111.

McMullen, J.R., Amirahmadi, F., Woodcock, E.A., Schinke-Braun, M., Bouwman, R.D., Hewitt, K.A., Mollica, J.P., Zhang, L., Zhang, Y., Shioi, T., et al. (2007). Protective effects of exercise and phosphoinositide 3-kinase(p110α) signaling in dilated and hypertrophic cardiomyopathy. Proc National Acad Sci *104*, 612–617. https://doi.org/10.1073/pnas.0606663104.

Mitchison, T., and Kirschner, M. (1984). Dynamic instability of microtubule growth. Nature *312*, 237–242. https://doi.org/10.1038/312237a0.

Mohammadzadeh, N., Lunde, I.G., Andenæs, K., Strand, M.E., Aronsen, J.M., Skrbic, B., Marstein, H.S., Bandlien, C., Nygård, S., Gorham, J., et al. (2019). The extracellular matrix proteoglycan lumican improves survival and counteracts cardiac dilatation and failure in mice subjected to pressure overload. Sci Rep-Uk *9*, 9206. https://doi.org/10.1038/s41598-019-45651-9.

Morkin, E. (1993). Regulation of myosin heavy chain genes in the heart. Circulation *87*, 1451–1460. https://doi.org/10.1161/01.cir.87.5.1451.

Murashige, D., Jang, C., Neinast, M., Edwards, J.J., Cowan, A., Hyman, M.C., Rabinowitz, J.D., Frankel, D.S., and Arany, Z. (2020). Comprehensive quantification of fuel use by the failing and nonfailing human heart. Science *370*, 364–368. https://doi.org/10.1126/science.abc8861.

Najafi, A., Sequeira, V., Kuster, D.W.D., and Velden, J. (2016). β-adrenergic receptor signalling and its functional consequences in the diseased heart. Eur J Clin Invest *46*, 362–374. https://doi.org/10.1111/eci.12598.

Nakamura, M., and Sadoshima, J. (2018). Mechanisms of physiological and pathological cardiac hypertrophy. Nat Rev Cardiol *15*, 387–407. https://doi.org/10.1038/s41569-018-0007-y.

Nakano, A., Kato, H., Watanabe, T., Min, K.-D., Yamazaki, S., Asano, Y., Seguchi, O., Higo, S., Shintani, Y., Asanuma, H., et al. (2010). AMPK controls the speed of microtubule polymerization and directional cell migration through CLIP-170 phosphorylation. Nat Cell Biol *12*, 583–590. https://doi.org/10.1038/ncb2060.

Nieuwenhuis, J., Adamopoulos, A., Bleijerveld, O.B., Mazouzi, A., Stickel, E., Celie, P., Altelaar, M., Knipscheer, P., Perrakis, A., Blomen, V.A., et al. (2017). Vasohibins encode tubulin detyrosinating activity. Science *358*, 1453–1456. https://doi.org/10.1126/science.aao5676.

Nirschl, J.J., Magiera, M.M., Lazarus, J.E., Janke, C., and Holzbaur, E.L.F. (2016). α-Tubulin Tyrosination and CLIP-170 Phosphorylation Regulate the Initiation of Dynein-Driven Transport in Neurons. Cell Reports *14*, 2637–2652. https://doi.org/10.1016/j.celrep.2016.02.046.

Nogales, E. (2001). STRUCTURAL INSIGHTS INTO MICROTUBULE FUNCTION. Annu Rev Bioph Biom *30*, 397–420. https://doi.org/10.1146/annurev.biophys.30.1.397.

Paturle-Lafanechère, L., Manier, M., Trigault, N., Pirollet, F., Mazarguil, H., and Job, D. (1994). Accumulation of delta 2-tubulin, a major tubulin variant that cannot be tyrosinated, in neuronal tissues and in stable microtubule assemblies. J Cell Sci *107 (Pt 6)*, 1529–1543. .

Peris, L., Wagenbach, M., Lafanechère, L., Brocard, J., Moore, A.T., Kozielski, F., Job, D., Wordeman, L., and Andrieux, A. (2009). Motor-dependent microtubule disassembly driven by tubulin tyrosination. J Cell Biol *185*, 1159–1166. https://doi.org/10.1083/jcb.200902142.

Pinto, A.R., Ilinykh, A., Ivey, M.J., Kuwabara, J.T., D'Antoni, M.L., Debuque, R., Chandran, A., Wang, L., Arora, K., Rosenthal, N.A., et al. (2016). Revisiting Cardiac Cellular Composition. Circ Res *118*, 400–409. https://doi.org/10.1161/circresaha.115.307778.

Pollack, G., and Huntsman, L. (1974). Sarcomere length-active force relations in living mammalian cardiac muscle. Am J Physiology-Legacy Content *227*, 383–389. https://doi.org/10.1152/ajplegacy.1974.227.2.383.

Portran, D., Schaedel, L., Xu, Z., Théry, M., and Nachury, M.V. (2017). Tubulin acetylation protects long-lived microtubules against mechanical ageing. Nat Cell Biol *19*, 391–398. https://doi.org/10.1038/ncb3481.

Prosser, B.L., Ward, C.W., and Lederer, W.J. (2011). X-ROS Signaling: Rapid Mechano-Chemo Transduction in Heart. Science *333*, 1440–1445. https://doi.org/10.1126/science.1202768.

Randazzo, D., Khalique, U., Belanto, J.J., Kenea, A., Talsness, D.M., Olthoff, J.T., Tran, M.D., Zaal, K.J., Pak, K., Pinal-Fernandez, I., et al. (2019). Persistent upregulation of the β-tubulin tubb6, linked to muscle regeneration, is a source of microtubule disorganization in dystrophic muscle. Hum Mol Genet *28*, 1117–1135. https://doi.org/10.1093/hmg/ddy418.

Robison, P., Caporizzo, M.A., Ahmadzadeh, H., Bogush, A.I., Chen, C.Y., Margulies, K.B., Shenoy, V.B., and Prosser, B.L. (2016). Detyrosinated microtubules buckle and bear load in contracting cardiomyocytes. Science *352*, aaf0659. https://doi.org/10.1126/science.aaf0659.

Rockman, H.A., Ross, R.S., Harris, A.N., Knowlton, K.U., Steinhelper, M.E., Field, L.J., Ross, J., and Chien, K.R. (1991). Segregation of atrial-specific and inducible expression of an atrial natriuretic factor transgene in an in vivo murine model of cardiac hypertrophy. Proc National Acad Sci *88*, 8277–8281. https://doi.org/10.1073/pnas.88.18.8277.

Salomon, A.K., Okami, N., Heffler, J., Lee, J.-J., Robison, P., Bogush, A.I., and Prosser, B.L. (2021). Desmin intermediate filaments and tubulin detyrosination stabilize growing microtubules in the cardiomyocyte. Biorxiv 2021.05.26.445641. https://doi.org/10.1101/2021.05.26.445641.

Sato, H., Nagai, T., Kuppuswamy, D., Narishige, T., Koide, M., Menick, D.R., and Cooper, G. (1997). Microtubule Stabilization in Pressure Overload Cardiac Hypertrophy. J Cell Biol *139*, 963–973. https://doi.org/10.1083/jcb.139.4.963.

Scarborough, E.A., Uchida, K., Vogel, M., Erlitzki, N., Iyer, M., Phyo, S.A., Bogush, A., Kehat, I., and Prosser, B.L. (2021). Microtubules orchestrate local translation to enable cardiac growth. Nat Commun *12*, 1547. https://doi.org/10.1038/s41467-021-21685-4.

Schaedel, L., Lorenz, C., Schepers, A.V., Klumpp, S., and Köster, S. (2021). Vimentin Intermediate Filaments Stabilize Dynamic Microtubules by Direct Interactions. Biorxiv 2020.05.20.106179. https://doi.org/10.1101/2020.05.20.106179.

Schuldt, M., Pei, J., Harakalova, M., Dorsch, L.M., Schlossarek, S., Mokry, M., Knol, J.C., Pham, T.V., Schelfhorst, T., Piersma, S.R., et al. (2020). Proteomic and Functional Studies Reveal Detyrosinated Tubulin as Treatment Target in Sarcomere Mutation-Induced Hypertrophic Cardiomyopathy. Circulation Hear Fail *14*, e007022. https://doi.org/10.1161/circheartfailure.120.007022.

Steffensen, L.B., and Rasmussen, L.M. (2018). A role for collagen type IV in cardiovascular disease? Am J Physiol-Heart C *315*, H610–H625. https://doi.org/10.1152/ajpheart.00070.2018.

Sui, H., and Downing, K.H. (2010). Structural Basis of Interprotofilament Interaction and Lateral Deformation of Microtubules. Structure *18*, 1022–1031. https://doi.org/10.1016/j.str.2010.05.010.

Swiatlowska, P., Sanchez-Alonso, J.L., Mansfield, C., Scaini, D., Korchev, Y., Novak, P., and Gorelik, J. (2020). Short-term angiotensin II treatment regulates cardiac nanomechanics via microtubule modifications. Nanoscale *12*, 16315–16329. https://doi.org/10.1039/d0nr02474k.

Szyk, A., Deaconescu, A.M., Piszczek, G., and Roll-Mecak, A. (2011). Tubulin tyrosine ligase structure reveals adaptation of an ancient fold to bind and modify tubulin. Nat Struct Mol Biol *18*, 1250–1258. https://doi.org/10.1038/nsmb.2148.

Takeda, Y., Yoneda, T., Demura, M., Miyamori, I., and Mabuchi, H. (2000). Sodium-Induced Cardiac Aldosterone Synthesis Causes Cardiac Hypertrophy. Endocrinology *141*, 1901–1904. https://doi.org/10.1210/endo.141.5.7529.

Tanabe, T., Mikami, A., Numa, S., and Beam, K.G. (1990). Cardiac-type excitation-contraction coupling in dysgenic skeletal muscle injected with cardiac dihydropyridine receptor cDNA. Nature *344*, 451–453. https://doi.org/10.1038/344451a0.

Tapley, E.C., and Starr, D.A. (2013). Connecting the nucleus to the cytoskeleton by SUN–KASH bridges across the nuclear envelope. Curr Opin Cell Biol *25*, 57–62. https://doi.org/10.1016/j.ceb.2012.10.014.

Tariq, S., and Aronow, W.S. (2015). Use of Inotropic Agents in Treatment of Systolic Heart Failure. Int J Mol Sci *16*, 29060–29068. https://doi.org/10.3390/ijms161226147.

Tigchelaar, W., Jong, A.M. de, Bloks, V.W., Gilst, W.H. van, Boer, R.A. de, and Silljé, H.H.W. (2016). Hypertrophy induced KIF5B controls mitochondrial localization and function in neonatal rat cardiomyocytes. J Mol Cell Cardiol *97*, 70–81. https://doi.org/10.1016/j.yjmcc.2016.04.005.

Tsutsui, H., Tagawa, H., Cooper, G., and Takeshita, A. (1999). Role of Microtubules in the Transition from Compensated Cardiac Hypertrophy to Failure. Heart Fail Rev *4*, 311–318. https://doi.org/10.1023/a:1009847418264.

Vistnes, M., Aronsen, J.M., Lunde, I.G., Sjaastad, I., Carlson, C.R., and Christensen, G. (2014). Pentosan Polysulfate Decreases Myocardial Expression of the Extracellular Matrix Enzyme ADAMTS4 and Improves Cardiac Function In Vivo in Rats Subjected to Pressure Overload by Aortic Banding. Plos One *9*, e89621. https://doi.org/10.1371/journal.pone.0089621.

Vitre, B., Coquelle, F.M., Heichette, C., Garnier, C., Chrétien, D., and Arnal, I. (2008). EB1 regulates microtubule dynamics and tubulin sheet closure in vitro. Nat Cell Biol *10*, 415–421. https://doi.org/10.1038/ncb1703.

Webster, D.R., Wehland, J., Weber, K., and Borisy, G.G. (1990). Detyrosination of alpha tubulin does not stabilize microtubules in vivo. J Cell Biology *111*, 113–122. https://doi.org/10.1083/jcb.111.1.113.

Weeks, K.L., Bernardo, B.C., Ooi, J.Y.Y., Patterson, N.L., and McMullen, J.R. (2017). Exercise for Cardiovascular Disease Prevention and Treatment, From Molecular to Clinical, Part 2. Adv Exp Med Biol *1000*, 187–210. https://doi.org/10.1007/978-981-10-4304-8_12.

Weisenberg, R.C., Deery, W.J., and Dickinson, P.J. (1976). Tubulin-nucleotide interactions during the polymerization and depolymerization of microtubules. Biochemistry-Us *15*, 4248–4254. .

Xu, Z., Schaedel, L., Portran, D., Aguilar, A., Gaillard, J., Marinkovich, M.P., Théry, M., and Nachury, M.V. (2017). Microtubules acquire resistance from mechanical breakage through intralumenal acetylation. Science *356*, 328–332. https://doi.org/10.1126/science.aai8764.

Yashirogi, S., Nagao, T., Nishida, Y., Takahashi, Y., Qaqorh, T., Yazawa, I., Katayama, T., Kioka, H., Matsui, T.S., Saito, S., et al. (2021). AMPK regulates cell shape of cardiomyocytes by modulating turnover of microtubules through CLIP-170. Embo Rep *22*, e50949. https://doi.org/10.15252/embr.202050949.

Yen, T.J., Machlin, P.S., and Cleveland, D.W. (1988). Autoregulated instability of β-tubulin mRNAs by recognition of the nascent amino terminus of βtubulin. Nature *334*, 580–585. https://doi.org/10.1038/334580a0.

Yu, X., Chen, X., Amrute-Nayak, M., Allgeyer, E., Zhao, A., Chenoweth, H., Clement, M., Harrison, J., Doreth, C., Sirinakis, G., et al. (2021). MARK4 controls ischaemic heart failure through microtubule detyrosination. Nature 1–6. https://doi.org/10.1038/s41586-021-03573-5.

Yuan, B.X., and Leenen, F.H. (1991). Dietary sodium intake and left ventricular hypertrophy in normotensive rats. Am J Physiol-Heart C *261*, H1397–H1401. https://doi.org/10.1152/ajpheart.1991.261.5.h1397.

Zhou, P., and Pu, W.T. (2016). Recounting Cardiac Cellular Composition. Circ Res *118*, 368–370. https://doi.org/10.1161/circresaha.116.308139.

APPENDICES

A. Appendix A: Figures

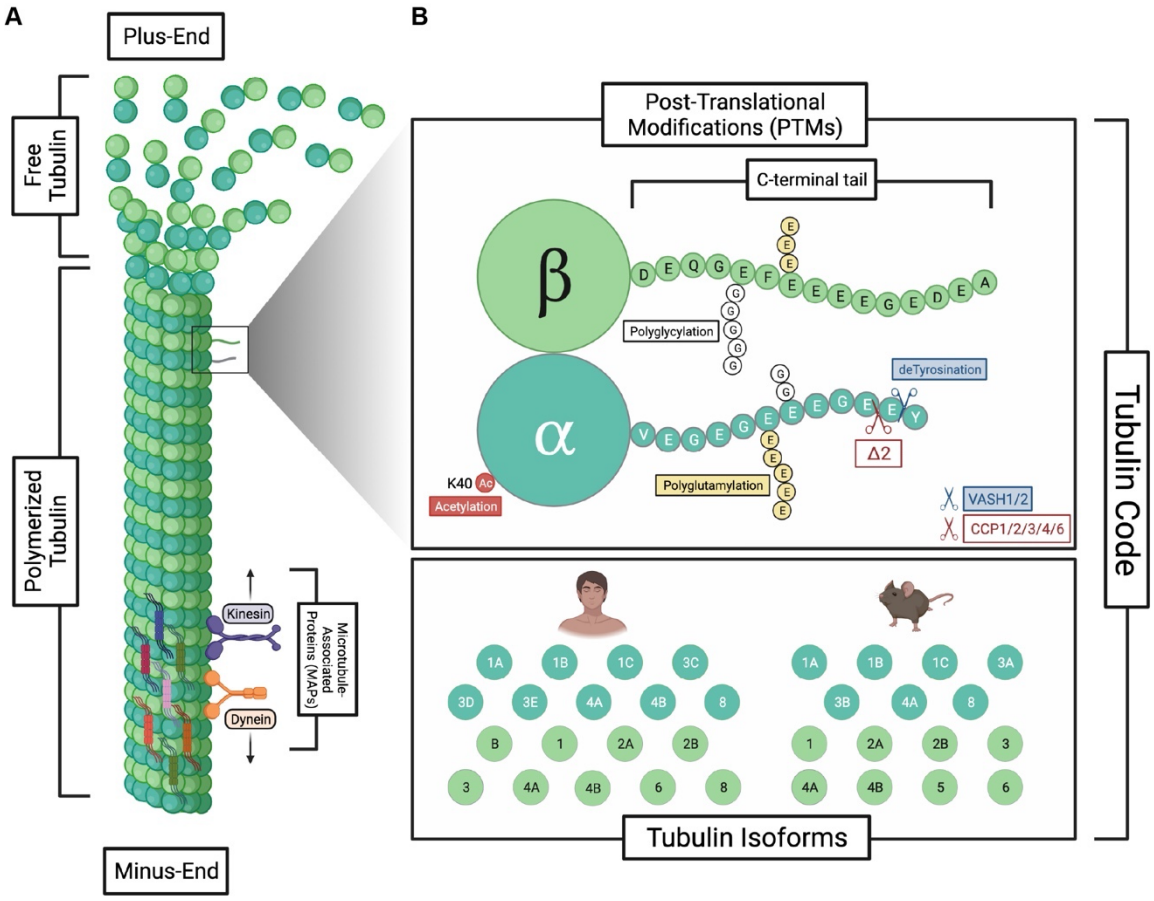

Figure 1. Summary of the tubulin code.

(A) Free & polymerized tubulins are in dynamic equilibrium.

(B) The tubulin code is the permutation of the tubulin post-translational modifications & isoforms.

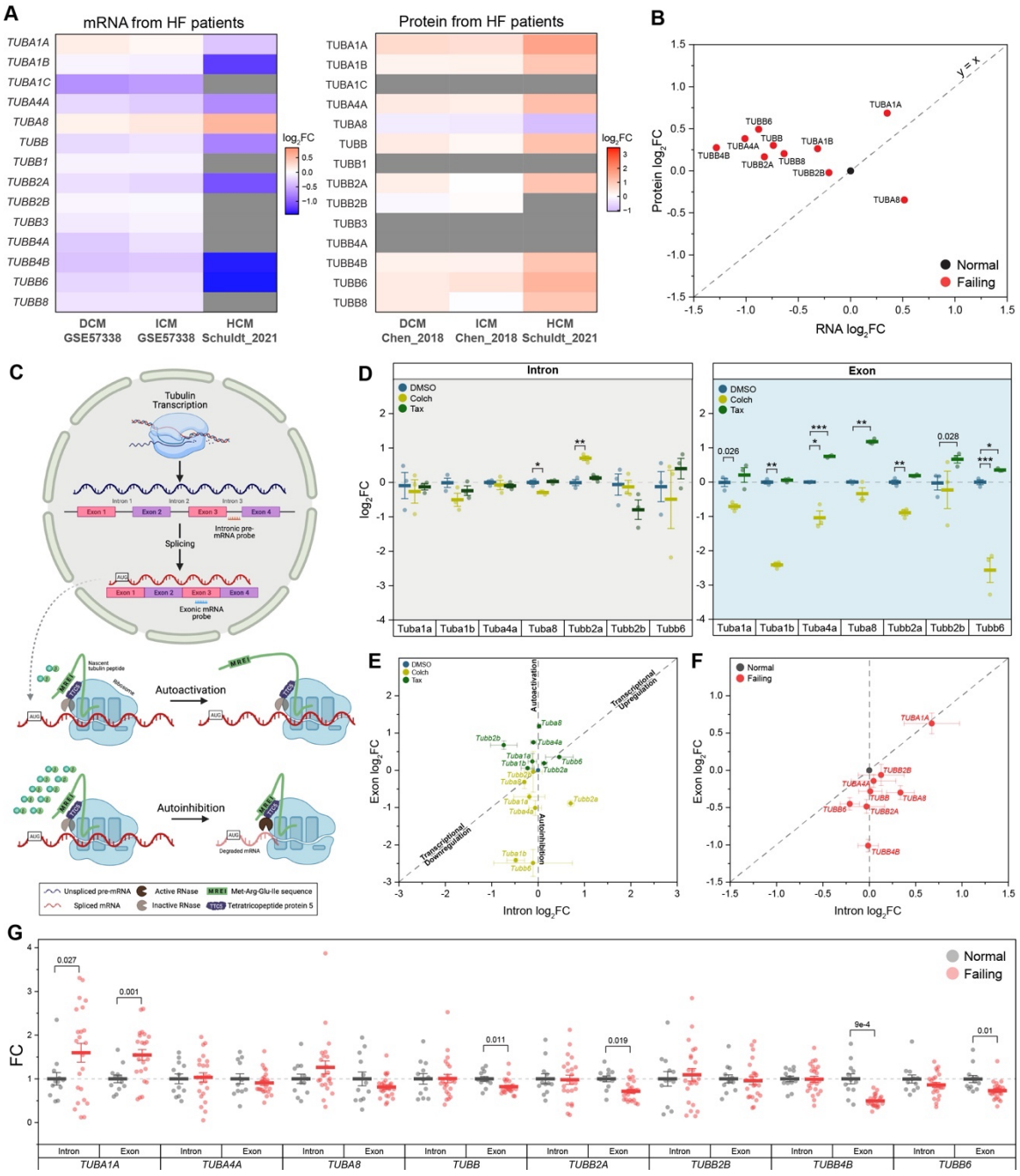

Figure 2. Tubulin autoregulation is operant in the heart and activated in heart failure.

(A) Heatmaps of previously published mRNA (left) & protein (right) data of human αβ-tubulin isoforms during dilated (DCM), ischemic (ICM), & hypertrophic (HCM) cardiomyopathies.

(B) Scatter-plot of $\log_2$fold-change of mRNA on x-axis and $\log_2$fold-change of protein on y-axis in heart failure; each data point represents an average $\log_2$fold-change value from DCM and ICM groups from (A), and y = x represents a proportionate change between mRNA and peptide.

(C) Schematic of tubulin autoregulation: The introns of tubulin pre-mRNA are spliced out and the mRNA is fully translated in the absence of excess free tubulin; in the presence of excess free tubulin, the mRNA, but not the pre-mRNA, is degraded.

(D) Relative $\log_2$fold-change of mRNA counts of intronic (left) and exonic (right) αβ-tubulin isoforms in isolated adult mouse cardiomyocytes after treatment with either depolymerizing (Colch) or polymerizing (Tax) agents (n=3); whiskers represent ± 1SEM, bolded line represents mean, * represents p-value from Welch-corrected two-tailed two-sample t-test on non-log data < 0.025 (Bonferroni-corrected for two comparisons), ** represents $p < 0.01$, and *** represents $p < 0.001$.

(E) Scatter-plot of relative $\log_2$fold-change of intron on x-axis and exon on y-axis after Colch or Tax treatment in adult mouse cardiomyocytes; whiskers represent ± 1SEM.

(F) Scatter-plot of relative $\log_2$fold-change of intron on x-axis and exon on y-axis in near-normal and failing patient heart samples; whiskers represent ± 1SEM.

(G) Relative fold-change of mRNA counts of intronic and exonic αβ-tubulin isoforms in near-normal and failing patient heart samples; whiskers represent ± 1SEM, bolded line represents mean, and p-values are from Welch-corrected two-tailed two-sample t-test.

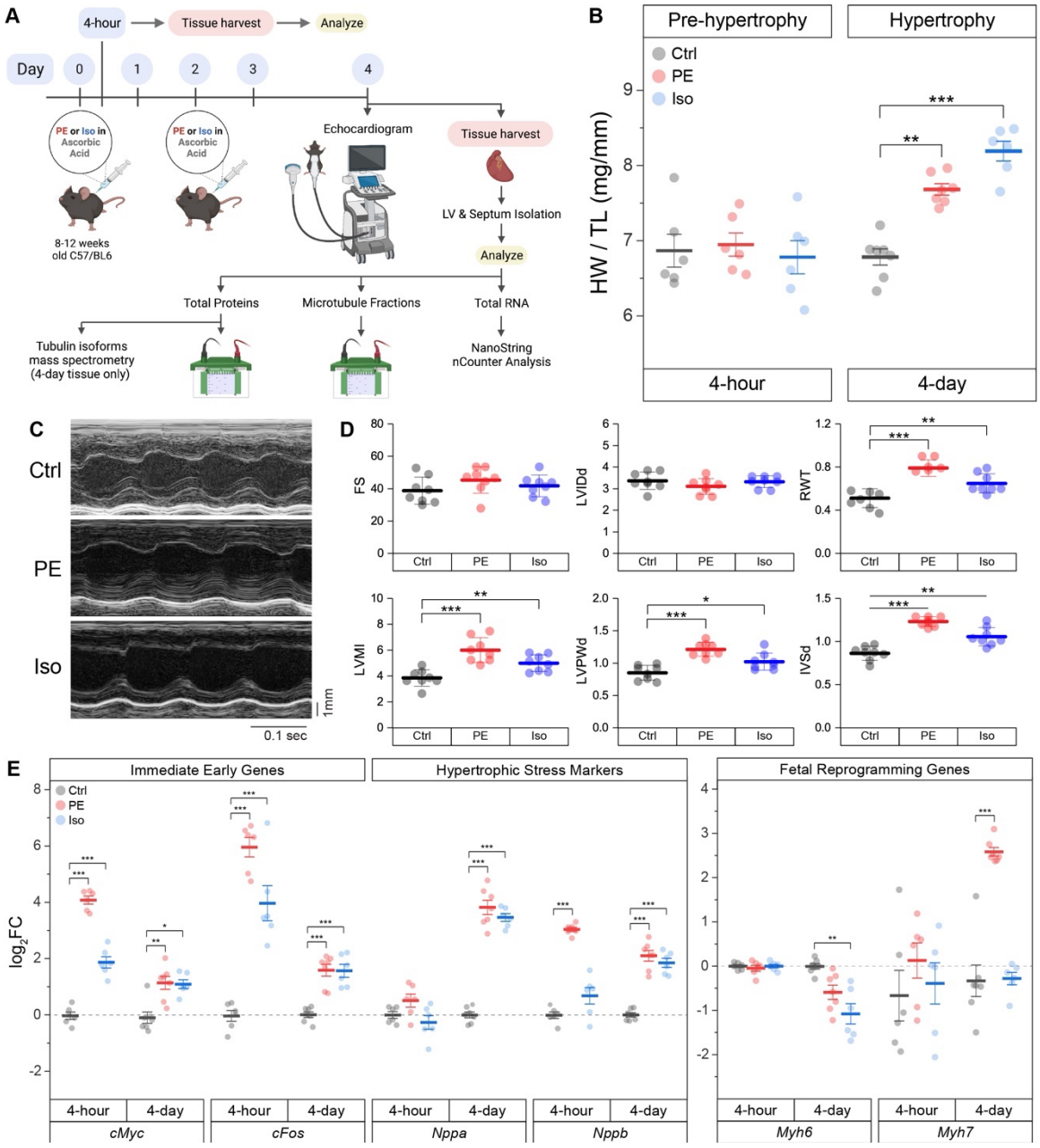

Figure 3. Acute α- or β- adrenergic stimulation induces cardiac hypertrophy.

(A) Graphical scheme of the experimental plan.

(B) Heart-weight / Tibia length (HW/TL) data of mice 4-hours (n=6) or 4-days (n = Ctrl:7, PE:7, Iso:6) following 10mg/kg/injection of phenylephrine (PE) or 5mg/kg/injection of isoproterenol (Iso).

(C) Representative echocardiographic M-mode images of 4-day mice hearts.

(D) Quantification of relevant echocardiographic parameters: FS = Fractional Shortening, LVIDd = Left-Ventricular Internal Diameter at end diastole, RWT = Relative Wall Thickness, LVMI = Left-Ventricular Mass Index, LVPWd = Left-Ventricular Posterior Wall thickness at end diastole, IVSd = InterVentricular Septal thickness at end diastole (n=8).

(E) Relative $\log_2$fold-change of nCounter mRNA counts of Immediate Early Genes (IEGs), hypertrophic stress markers, and genes of fetal reprogramming (n = 4h: 6, 4d: Ctrl:7, PE:7, Iso:6).

For all box plots, whiskers represent ± 1SEM and bolded-lines represent mean. For (B) and (D), * represents p-value from Welch-corrected two-tailed two-sample student's t-test < 0.025, ** represents p < 0.01, and *** represents p < 0.001.

For (E), * represents Bonferroni adjusted (for 45 genes) p-value < 0.025 (Bonferroni-corrected for two comparisons), ** represents adj_p < 0.01, and *** represents adj_p < 0.001 (see Methods for more statistical details).

A

```
TBA1A_MOUSE AREDMAALEKDYEEVGVDSVEGEGEEEGEEY---------- 451
TBA1B_MOUSE AREDMAALEKDYEEVGVDSVEGEGEEEGEEY---------- 451
TBA1C_MOUSE AREDMAALEKDYEEVGADSAEGD--DEGEEY---------- 449
TBA3_MOUSE  AREDLAALEKDYEEVGVDSVEAEAE-EGEEY---------- 450
TBA4A_MOUSE AREDMAALEKDYEEVGIDSYEDEDEGEE------------ 448
TBA8_MOUSE  AREDLAALEKDYEEVGTDSFEEENEGEEF----------- 449
TBB1_MOUSE  AESDIHDLVSEYQQFQDVRAGLEDSEEDVEEAEVEAEDKDH 451
TBB2A_MOUSE AESNMNDLVSEYQQYQDATADEQGEFEEEEGEDEA------ 445
TBB2B_MOUSE AESNMNDLVSEYQQYQDATADEQGEFEEEEGEDEA------ 445
TBB3_MOUSE  AESNMNDLVSEYQQYQDATAEEEGEMYEDDDEESEAQGPK- 450
TBB4A_MOUSE AESNMNDLVSEYQQYQDATAE-EGEFEEEAEEEVA------ 444
TBB4B_MOUSE AESNMNDLVSEYQQYQDATAEEEGEFEEEAEEEVA------ 445
TBB5_MOUSE  AESNMNDLVSEYQQYQDATAEEEEDFGEEAEEEA------- 444
TBB6_MOUSE  AESNMNDLVSEYQQYQDATVNDGEEAFEDEDEEEINE---- 447
```

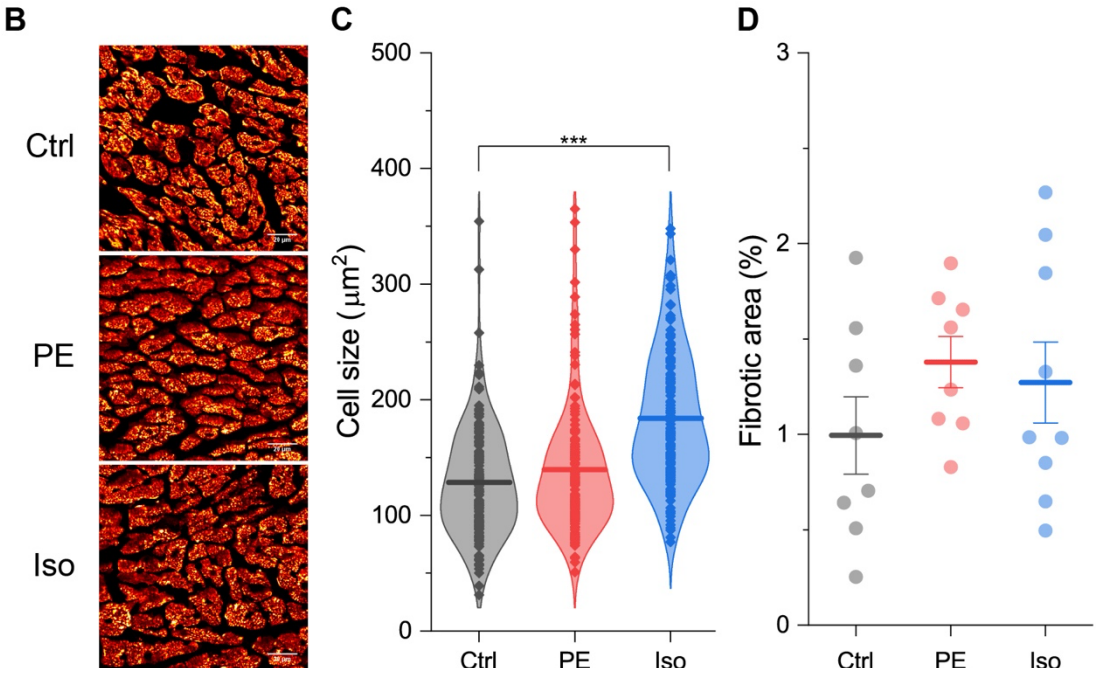

Figure 4. Tubulin isoform C-terminal amino acid sequences and 4-day cardiac histology.

(A) C-terminal amino-acid sequences of mouse a- and b- tubulin isoforms.

(B) Representative histological images of 4-day mice hearts.

(C) Cell-size quantifications from 4-day mice histology images (30 cells per image, 3 images per mouse, 3 mice per treatment); bolded line represents mean, * represents p-value from Welch-corrected two-tailed two-sample student's t-test < 0.025, ** represents $p < 0.01$, and *** represents $p < 0.001$.

(D) Fibrosis quantifications from 4-day mice Masson Trichome stained histology images; whisker represents ± 1SEM and bolded-line represents mean.

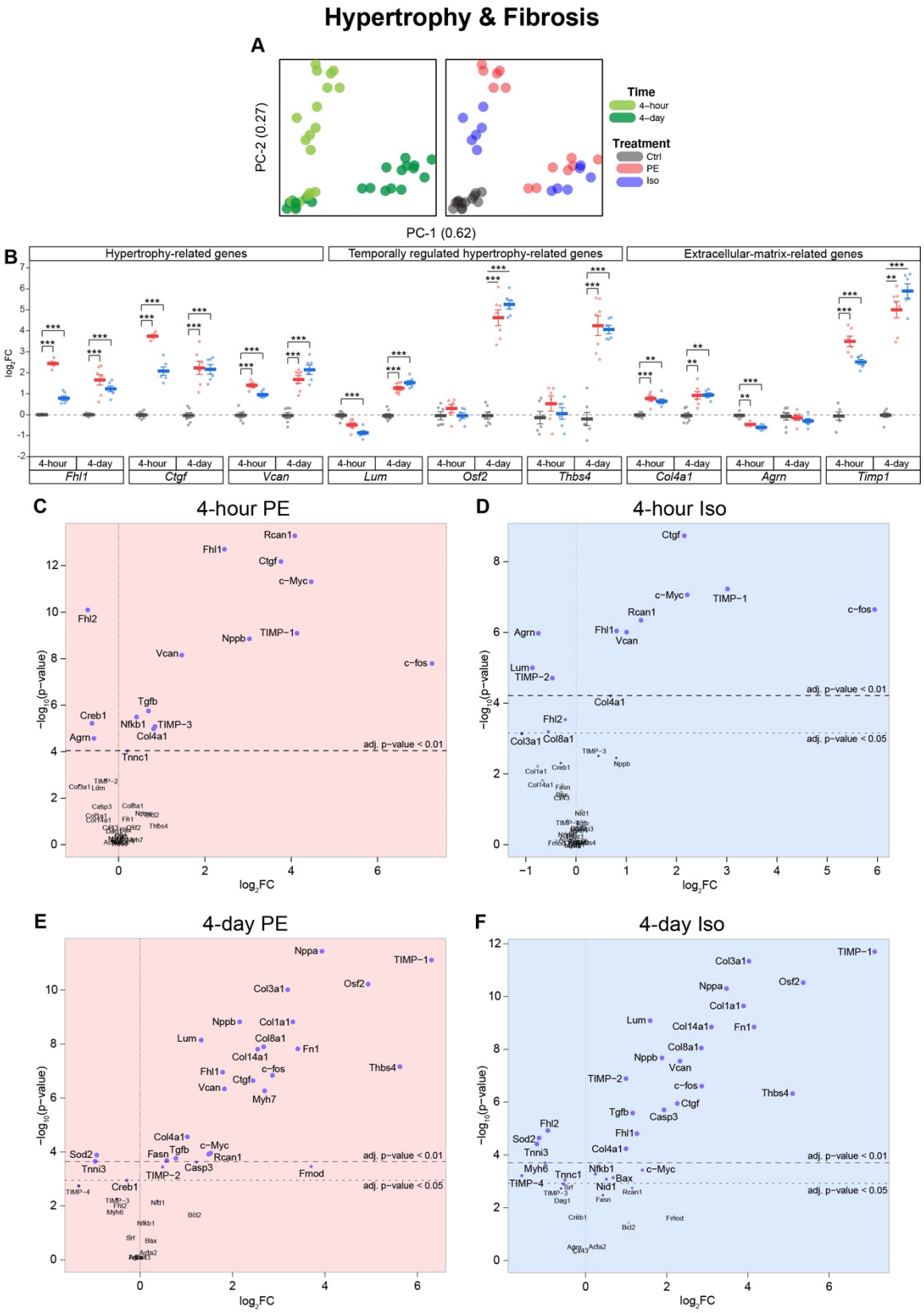
Hypertrophy & Fibrosis
A
PC-2 (0.27)
PC-1 (0.62)
Time
4–hour
4–day
Treatment
Ctrl
PE
Iso
B
Hypertrophy-related genes
Temporally regulated hypertrophy-related genes
Extracellular-matrix-related genes
log2FC
4-hour
4-day
Fhl1
Ctgf
Vcan
Lum
Osf2
Thbs4
Col4a1
Agrn
Timp1
C
4-hour PE
D
4-hour Iso
E
4-day PE
F
4-day Iso
−log10(p-value)
log2FC
adj. p-value < 0.01
adj. p-value < 0.05

Figure 5. Full data suite from hypertrophy and fibrosis panel

(A) Principal component analysis (PCA) of nCounter mRNA counts from 4-hour and 4-day mice heart tissues using the hypertrophy & fibrosis panel.

(B) Relative log_2fold-change of nCounter mRNA counts of hypertrophy-related genes, temporally regulated hypertrophy-related genes, and extracellular-matrix-related genes. (n = 4h: 6, 4d: Ctrl:7, PE:7, Iso:6).

Volcano plots of all mRNA counts from the hypertrophy & fibrosis panel for **(C)** 4-hour PE, **(D)** 4-hour Iso, **(E)** 4-day PE, & **(F)** 4-day Iso. (n = 4h:6, 4d: Ctrl:7, PE:7, Iso:6)

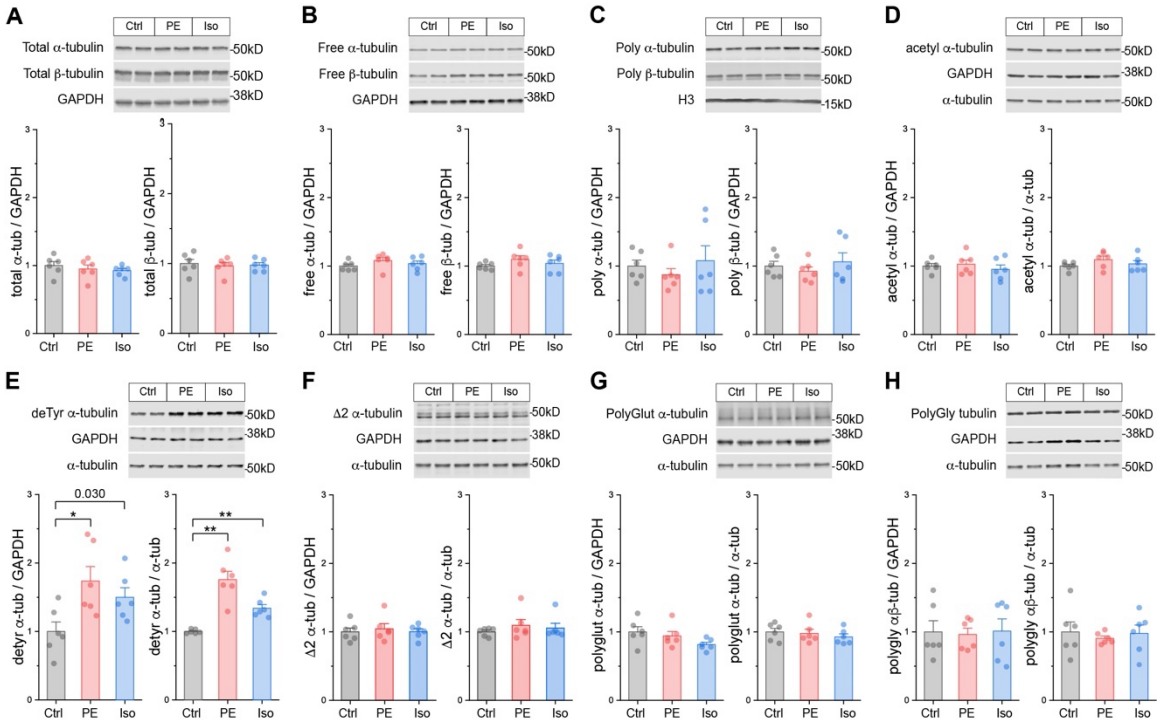

Figure 6. The microtubule network is rapidly detyrosinated upon hypertrophic stimulation.

Representative immunblots and relative fold-change of α-tubulin (left) and β-tubulin (right) in **(A)** total proteins, **(B)** free or **(C)** polymerized -tubulin fractions (n=6).

Representative immunoblots with technical duplicate lanes and relative fold-change using GAPDH (left) or α-tubulin (right) as loading controls for **(D)** acetylated α-tubulin, **(E)** detyrosinated α-tubulin, **(F)** Δ2 α-tubulin, **(G)** polyglutamylated α-tubulin, & **(H)** polyglycylated pan-tubulin (n=6).

For all bar plots, whiskers represent + 1SEM and bar represents mean. For all graphs, * represents p-value from Welch-corrected two-tailed two-sample t-test < 0.025

(Bonferroni-corrected for two comparisons), ** represents $p < 0.01$, and *** represents $p < 0.001$.

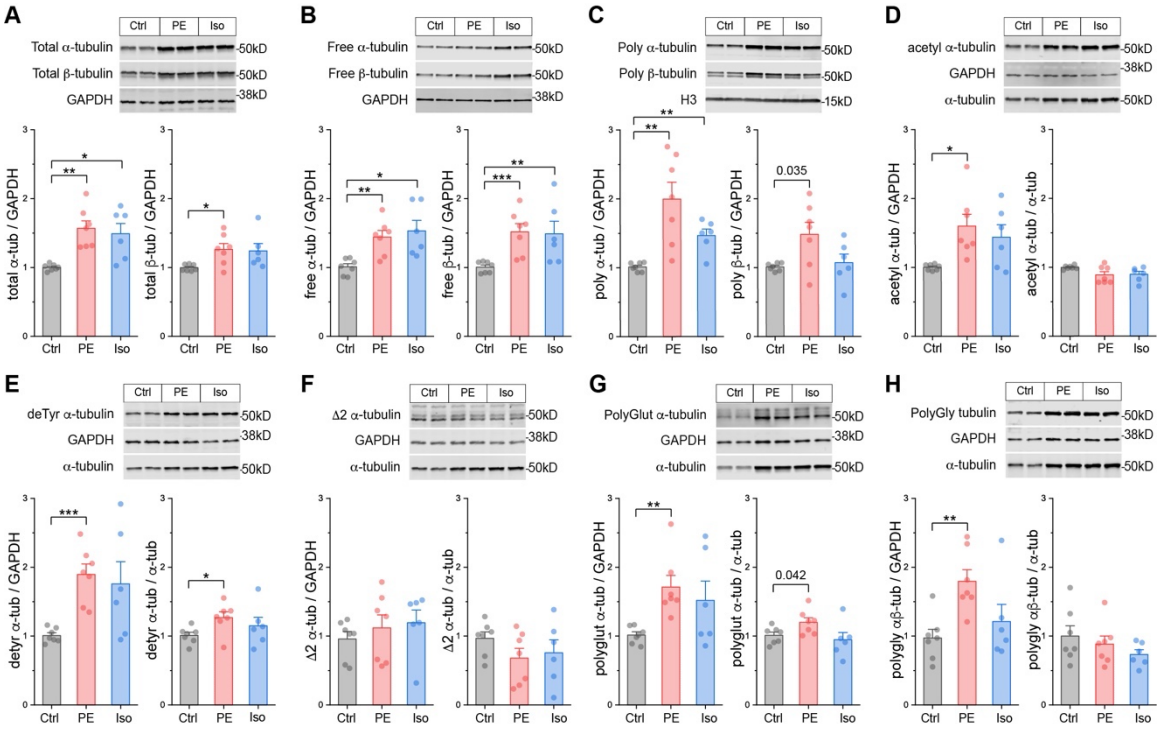

Figure 7. Total tubulin content increases & the microtubule network densifies during hypertrophy.

Representative immunoblots and relative fold-change of α-tubulin **(left)** and β-tubulin **(right)** in the **(A)** total proteins, **(B)** free, or **(C)** polymerized -tubulin fractions (n = Ctrl:7, PE:7, Iso:6).

Representative immuno- blots with technical duplicate lanes and relative fold-change using GAPDH **(left)** or α-tubulin **(right)** as loading controls for **(D)** acetylated α-tubulin, **(E)** detyrosinated α-tubulin, **(F)** Δ2 α-tubulin, **(G)** polyglutamylated α-tubulin, & **(H)** polyglycylated pan-tubulin (n = Ctrl:7, PE:7, Iso:6).

For all bar plots, whiskers represent + 1SEM and bar represents mean; * represents p-value from Welch-corrected two-tailed two-sample t-test < 0.025 (Bonferroni-corrected for two comparisons), ** represents $p < 0.01$, and *** represents $p < 0.001$.

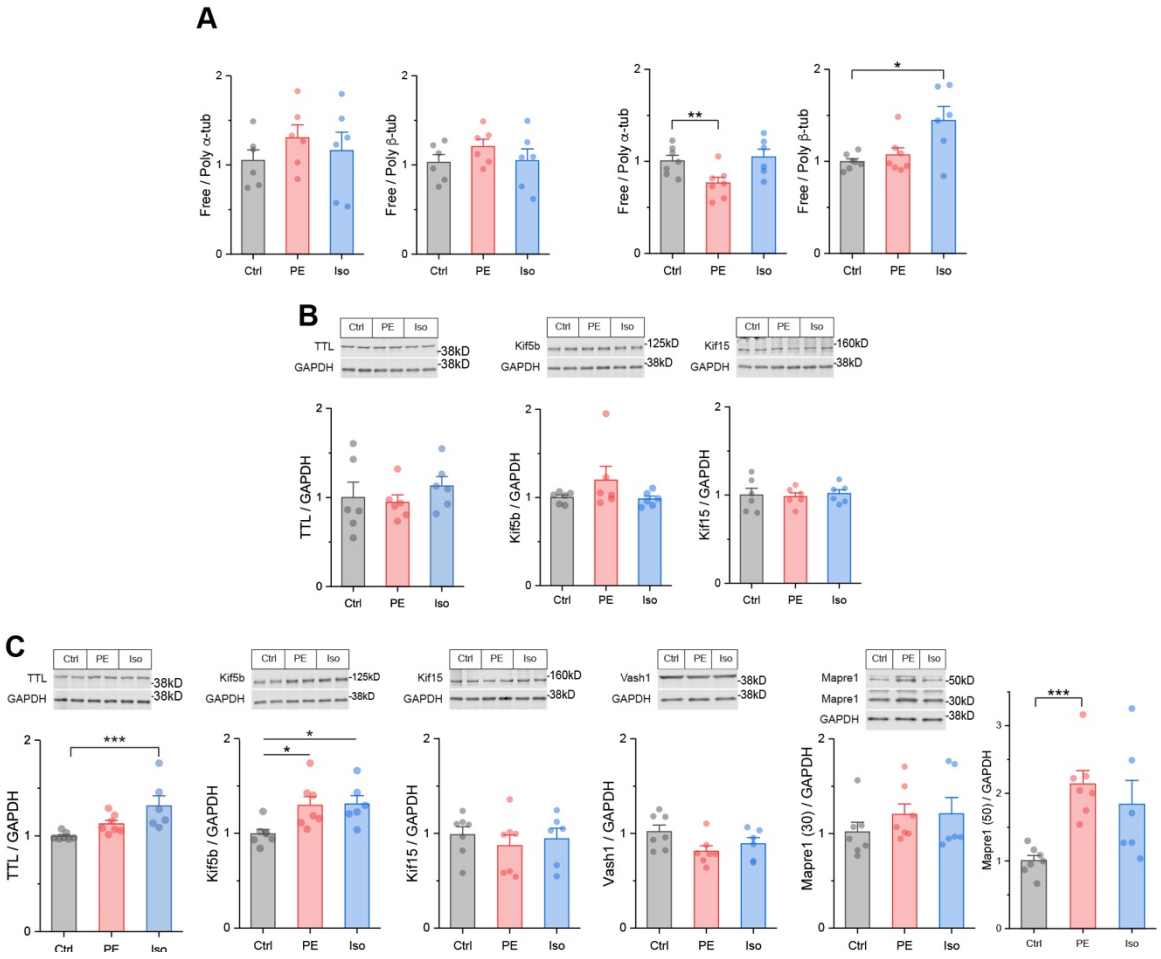

Figure 8. Additional protein level characterization of 4-hour and 4-day samples.

(A) Free/Poly quantifications for α and β -tubulins at 4-hour (left) and 4-day (right).

(B) Western blot analyses of TTL, Kif5b, and Kif15 at 4-hour. (n: Ctrl, PE, Iso = 6)

(C) Western blot analyses of TTL, Kif5b, Kif15, Vash1, and Mapre1 at 4-day. (n: Ctrl=7, PE=7, Iso=6). For Mapre1, we provided quantifications of two prominent bands at different molecular weights that were changed in the experimental groups: 30kDa band, which is the predicted molecular weight according to the amino acid sequence, and

50kDa band, which is also observed using the Anti-EB1 antibody produced in rabbit (Sigma: E3406) in certain cell types. For all graphs, * represents p-value from Welch-corrected two-tailed two-sample t-test < 0.025, ** represents $p < 0.01$, and *** represents $p < 0.001$.

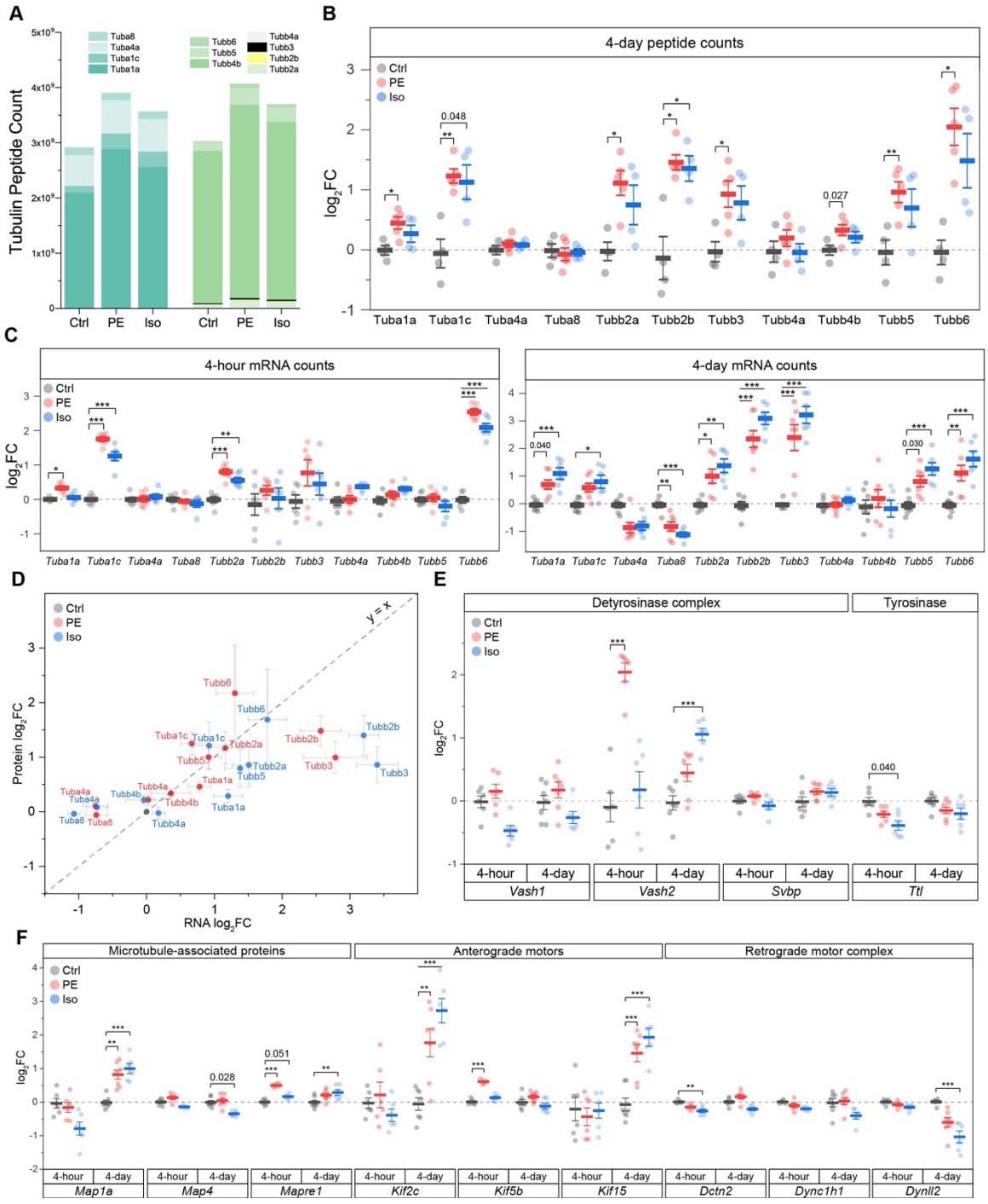

Figure 9. Differential expression of tubulin isoforms, modifying enzymes and MAPs during the onset and establishment of hypertrophy.

(A) MS counts of unique peptides of detectable αβ-tubulin isoforms at 4-day timepoint. For all following box plots, whiskers represent ± 1SEM and bolded line represents mean.

(B) Relative log_2fold-change of αβ-tubulin isoforms peptide counts at 4-days (n = Ctrl:4, PE:5, Iso:4); * represents p-value from Welch-corrected two-tailed two-sample t-test on non-log data < 0.025 (Bonferroni-corrected for two comparisons), ** represents p < 0.01, and *** represents p < 0.001.

(C) relative log_2fold-change of nCounter mRNA counts of detectable tubulin isoforms at 4-hour **(left)** (n=6) and 4-day timepoints **(right)** (n = Ctrl:7, PE:7, Iso:6); * represents Bonferroni adjusted (for 50 genes) p-value < 0.025, ** represents adj_p < 0.01, and *** represents adj_p < 0.001 (see Methods & Materials for more statistical details).

(D) Scatter-plot of log_2fold-change of mRNA on x-axis and log_2fold-change of protein on y-axis at 4-day timepoint; whiskers represent ± 1SEM and y = x represents a proportionate change between mRNA and peptide.

Relative log_2fold-change of nCounter mRNA counts of **(E)** detyrosinase complex and tyrosinase, & **(F)** MAPs, anterograde, & retrograde motors at 4-hour (n=6) and 4-day timepoints (n = Ctrl:7, PE:7, Iso:6); * represents Bonferroni adjusted (for 50 genes) p-value < 0.025, ** represents adj_p < 0.01, and *** represents adj_p < 0.001 (see Methods for more statistical details).

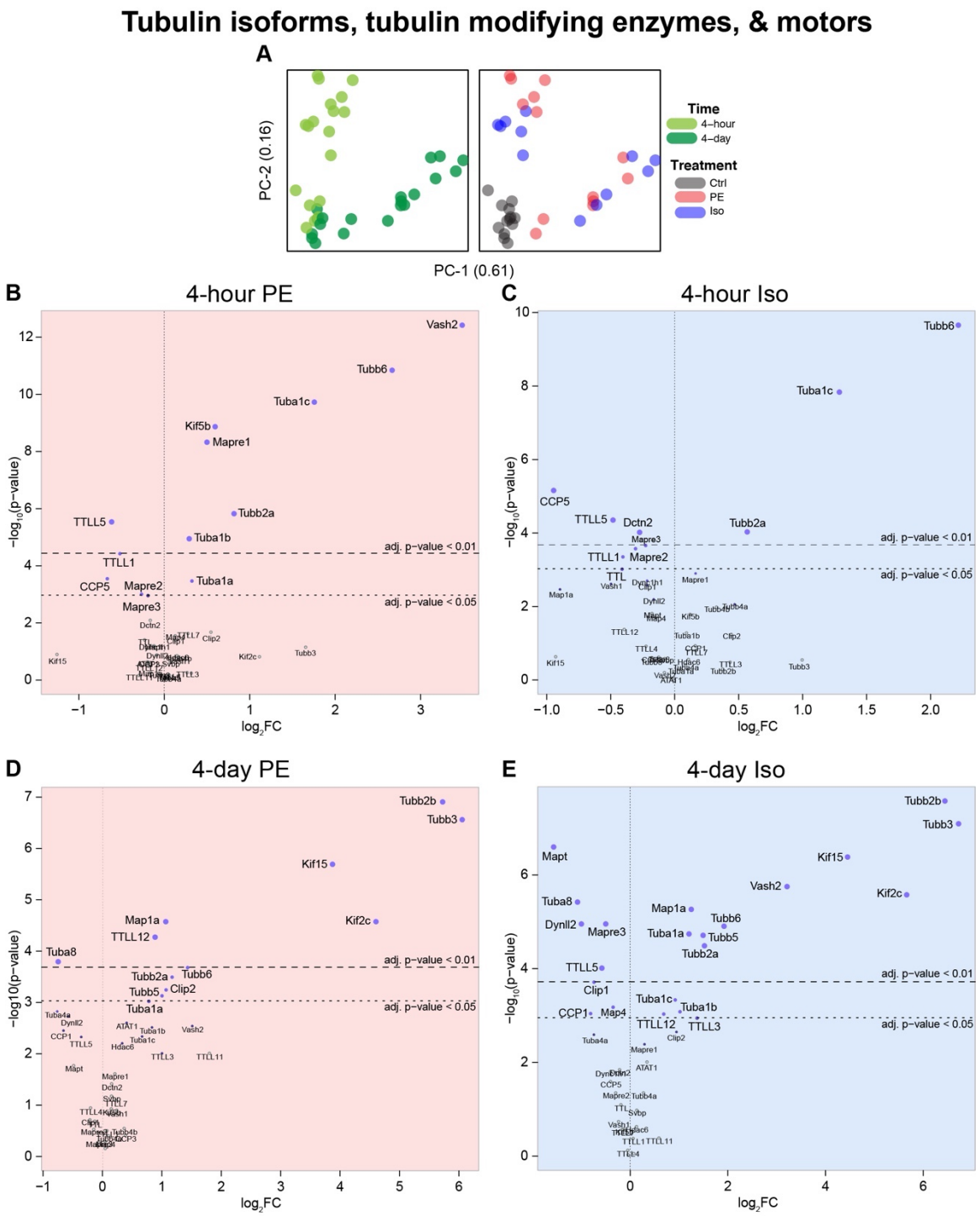

Figure 10. Full data suite from tubulin isoforms, tubulin modifying enzymes, and molecular motors panel.

(A) Principal component analysis (PCA) of nCounter mRNA counts from 4-hour and 4-day mice heart tissues using the tubulin panel.

Volcano plots of all mRNA counts from the tubulin panel for **(B)** 4-hour PE, **(C)** 4-hour Iso, **(D)** 4-day PE, & **(E)** 4-day Iso. (n = 4h:6, 4d: Ctrl:7, PE:7, Iso:6)

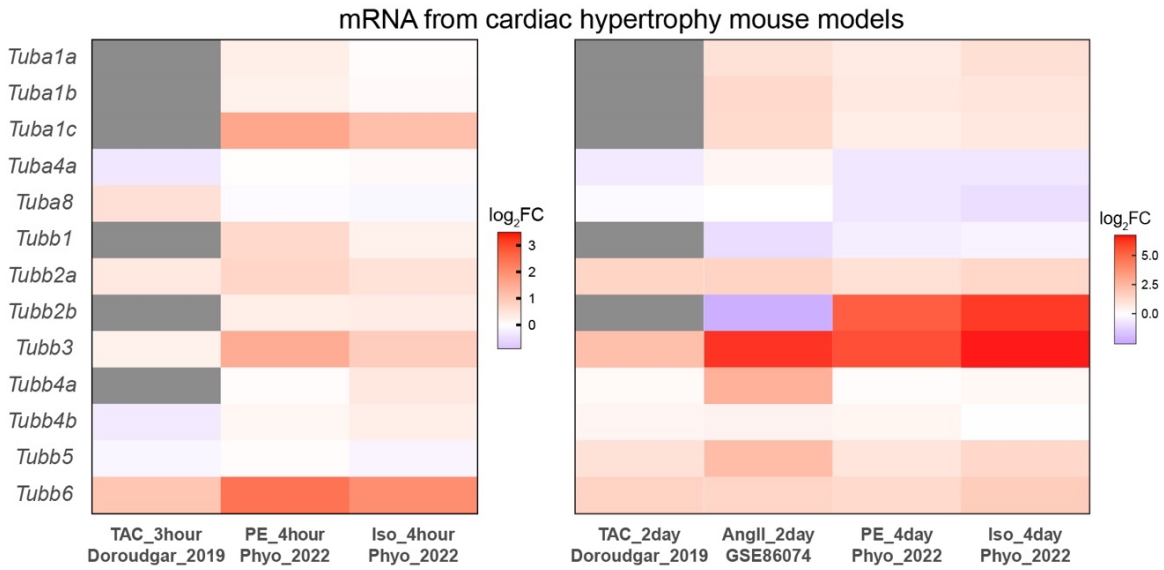

Figure 11. Previously published & current studies' mRNA data of mouse αβ-tubulin isoforms following different pathological stimulations (Bottermann et al., 2018, Doroudgar et al., 2019).

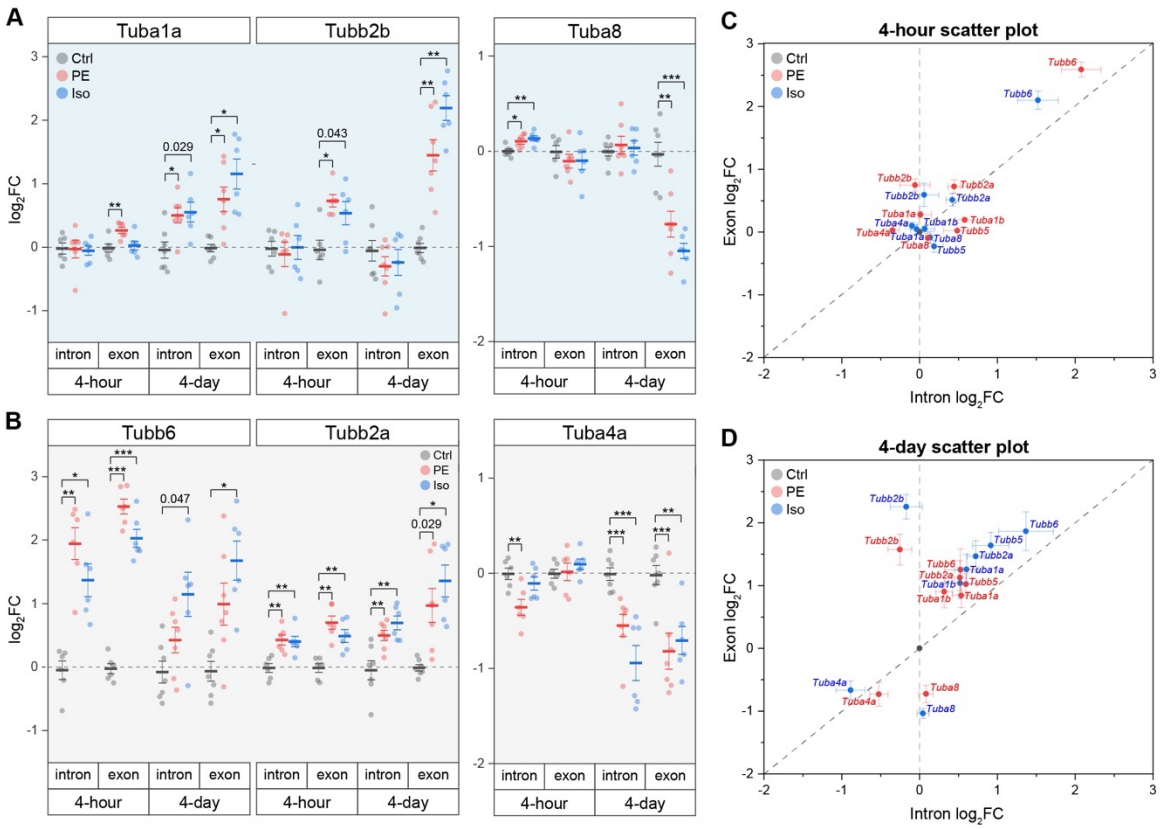

Figure 12. Tubulin isoforms are differentially regulated at the mRNA level through isoform-specific transcription and/or autoregulation during cardiac hypertrophy.

Relative log_2fold-change of mRNA counts of αβ-tubulin isoforms that are predominantly regulated through

(A) autoregulation, or **(B)** transcription (n = 4h: 6, 4d: Ctrl:7, PE:7, Iso:6); * represents p-value from Welch-corrected two-tailed two-sample t-test on non-log data < 0.025 (Bonferroni-corrected for two comparisons), ** represents p < 0.01, and *** represents p < 0.001.

Scatter-plots of relative log_2fold-change of intron on x-axis and exon on y-axis at **(C)** 4-hour and **(D)** 4-day timepoints; whiskers represent ± 1SEM.

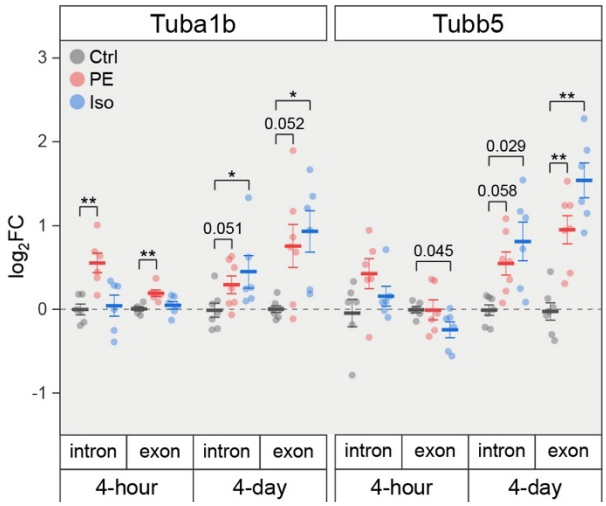

Figure 13. Unspliced and spliced mRNA counts of Tuba1b and Tubb5 (n = 4h:6, 4d: Ctrl:7, PE:7, Iso:6); * represents p-value from Welch-corrected two-tailed two-sample t-test on non-log data < 0.025 (Bonferroni-corrected for two comparisons), ** represents p < 0.01, and *** represents p < 0.001.

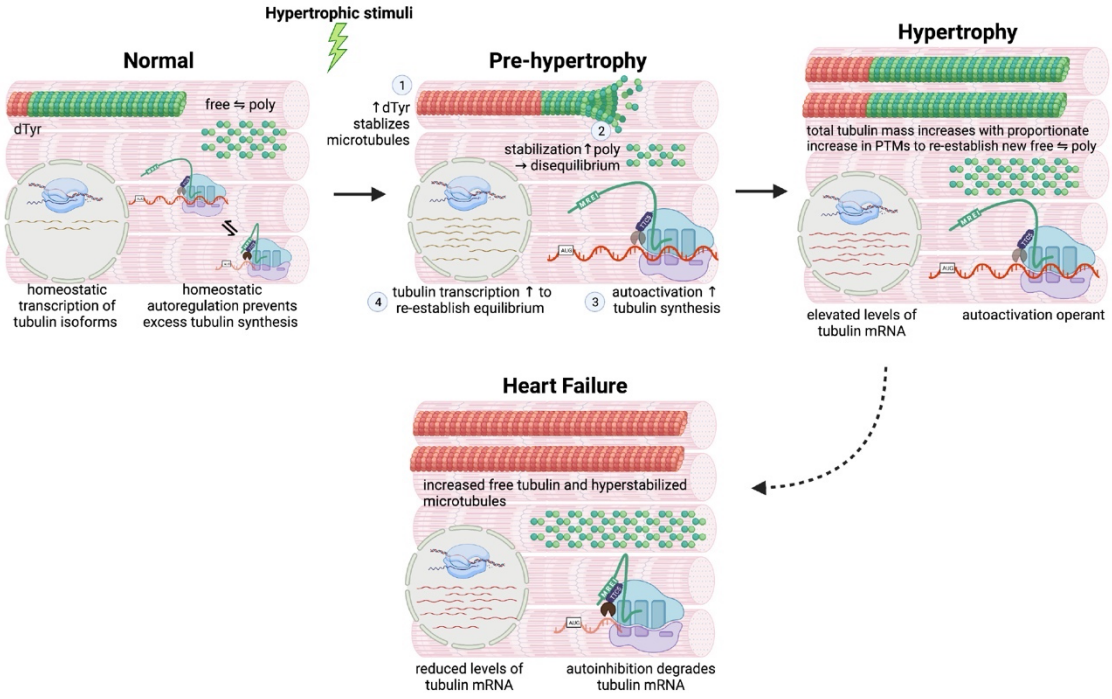

Figure 14. Proposed schematic model**.**

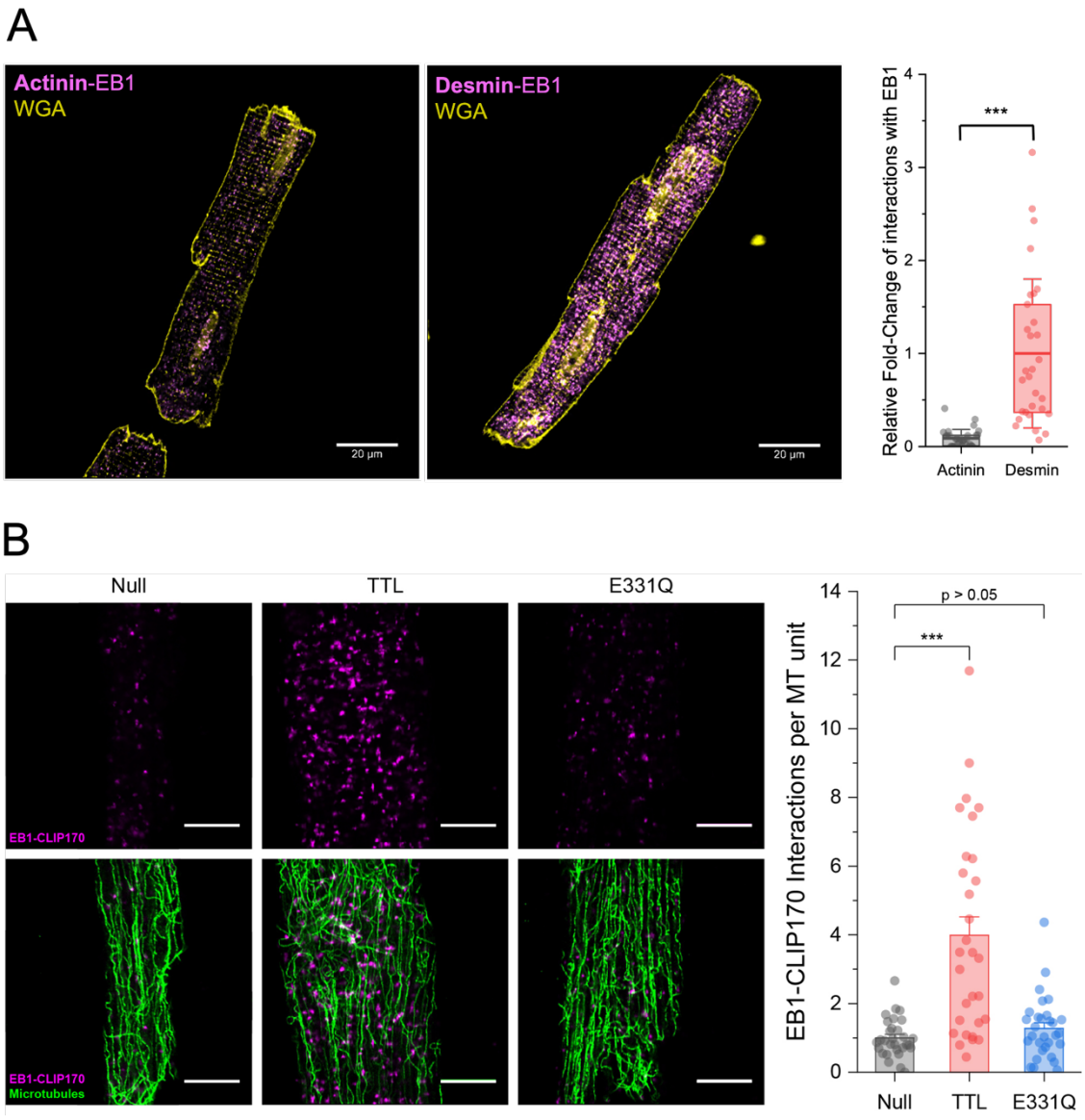

Figure 15. Unpublished results from how desmin and tubulin tyrosination influences microtubule stability.

(A) Representative images of α-actinin-EB1 (**left**) or desmin-EB1 (**right**) interactions in untreated rat cardiomyocytes, along with the quantifications (N = 3, n = 30). Box represents 25th and 75th percentiles, line represents mean, error bar represents ± 1 SD,

and *** represents p-value from Welch-corrected two-tailed two-sample t-test on non-log data < 0.01.

(B) Representative images of EB1-CLIP170 interactions on microtubules in Null, TTL, E331Q treated rat cardiomyocytes, along with the quantifications (N = 3, n = 30). Bar represents mean, error bar represents ± 1 SE, and *** represents p-value from one-way ANOVA test < 0.01.

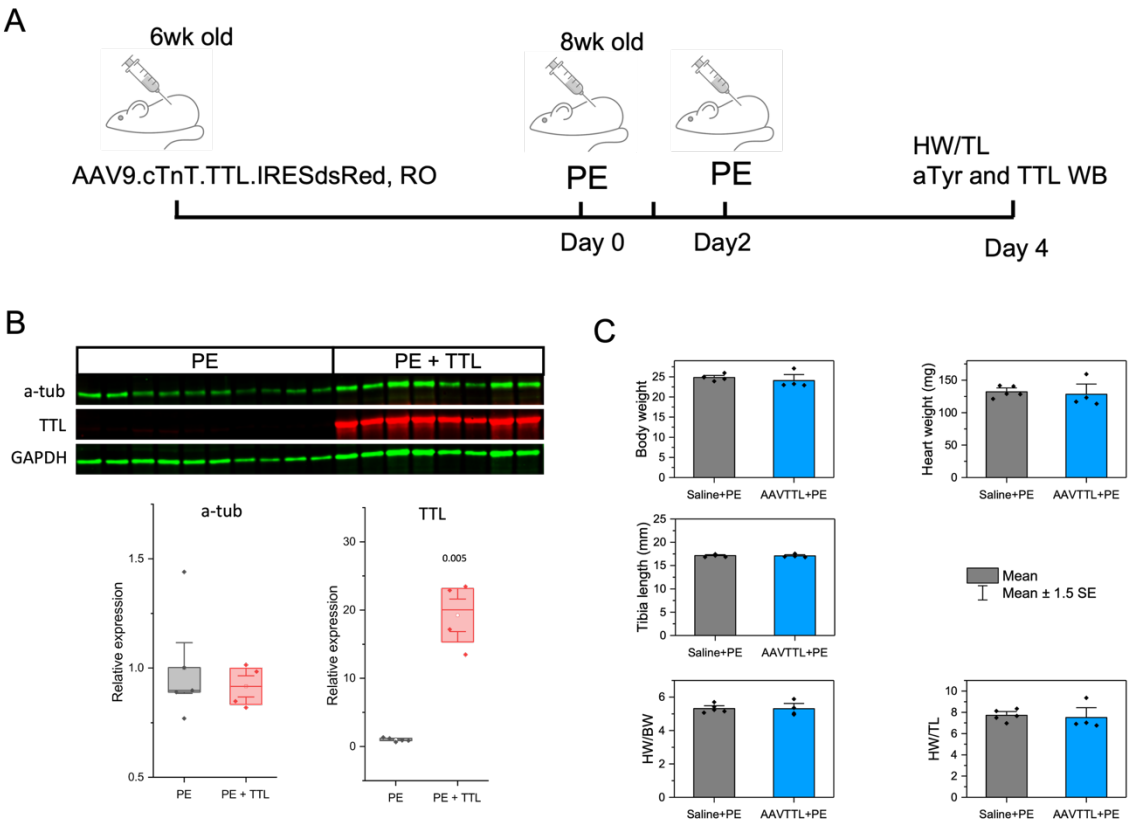

Figure 16. Unpublished results from pilot experiment to test the rescue effects of TTL overexpression in phenylephrine-induced hypertrophy.

(A) Schematic of the experiment

(B) Western-blot image, with duplicate technical lanes, and analysis of α-tubulin and TTL. Box represents 25th and 75th percentiles, line represents mean, and error bars represent mean ± 1 SE; p-values are from Welch-corrected two-tailed two-sample t-test.

(C) Body weight, heart weight, and tibia length measurements along with heart-weight-to-body weight and HW/TL ratios. Bar represents mean and error bars represent mean ± 1.5 SE

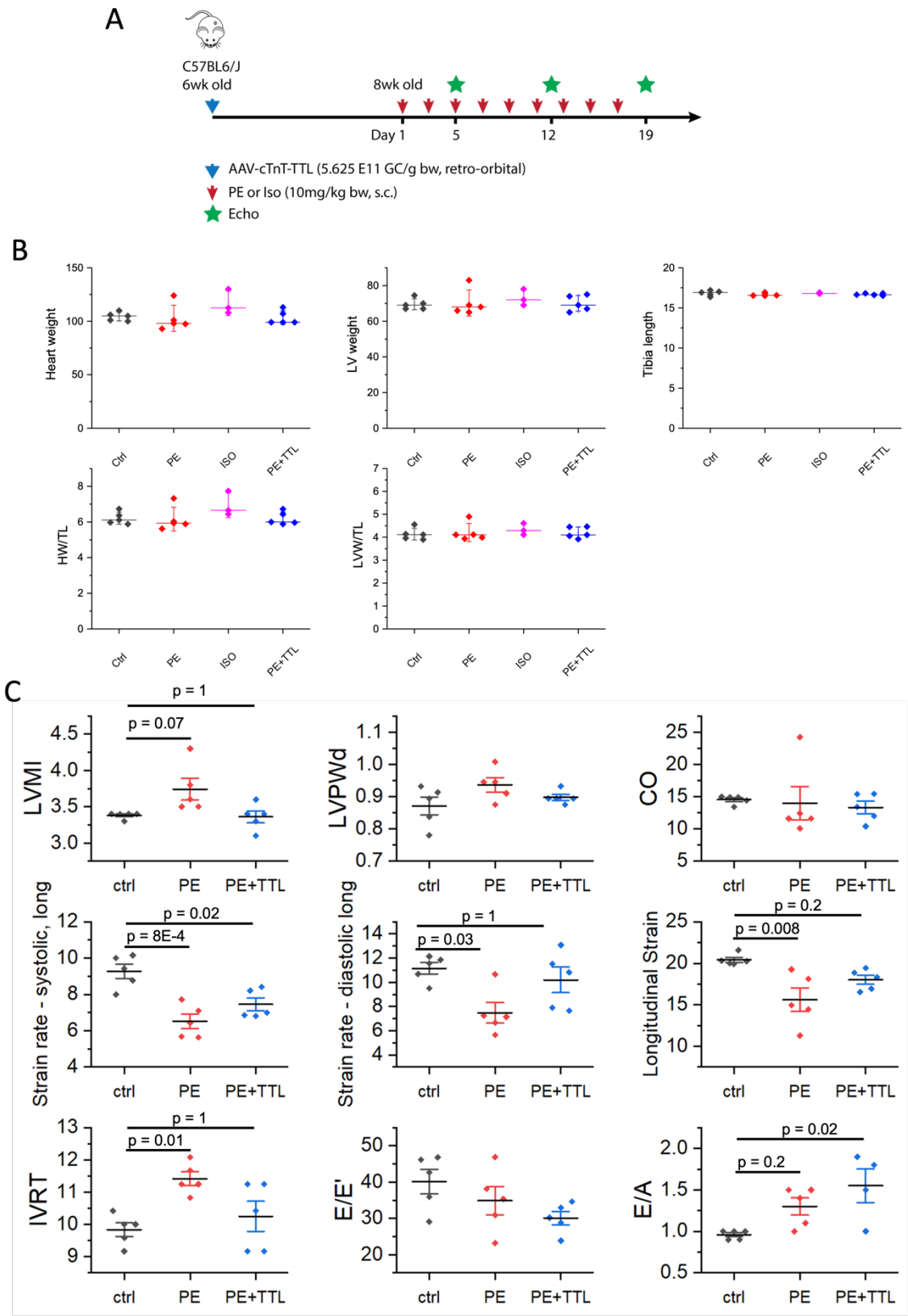
A
C57BL6/J
6wk old
8wk old
Day 1
5
12
19
AAV-cTnT-TTL (5.625 E11 GC/g bw, retro-orbital)
PE or Iso (10mg/kg bw, s.c.)
Echo
B
Heart weight
LV weight
Tibia length
HW/TL
LVW/TL
Ctrl
PE
ISO
PE+TTL
C
LVMI
LVPWd
CO
Strain rate - systolic, long
Strain rate - diastolic long
Longitudinal Strain
IVRT
E/E'
E/A
ctrl
PE
PE+TTL
p = 1
p = 0.07
p = 0.02
p = 8E-4
p = 0.03
p = 0.2
p = 0.008
p = 0.01
p = 0.02

Figure 17. Unpublished results from second pilot experiment to determine the extent of long-term phenylephrine or isoproterenol induced hypertrophy and the rescue effects of TTL overexpression in this phenylephrine-induced hypertrophy system.

(A) Schematic of the experiment

(B) Heart weight, left-ventricular weight, and tibia length measurements along with HW/TL and left-ventricle-weight-to-tibia-length ratios. Line represents mean and error bars represent mean ± 1.5 SE.

(C) Day 19 echocardiographic analysis of ascorbic acid, phenylephrine, and phenylephrine + TTL treated mice; p-values are from one-way ANOVA using treatment as the factor.

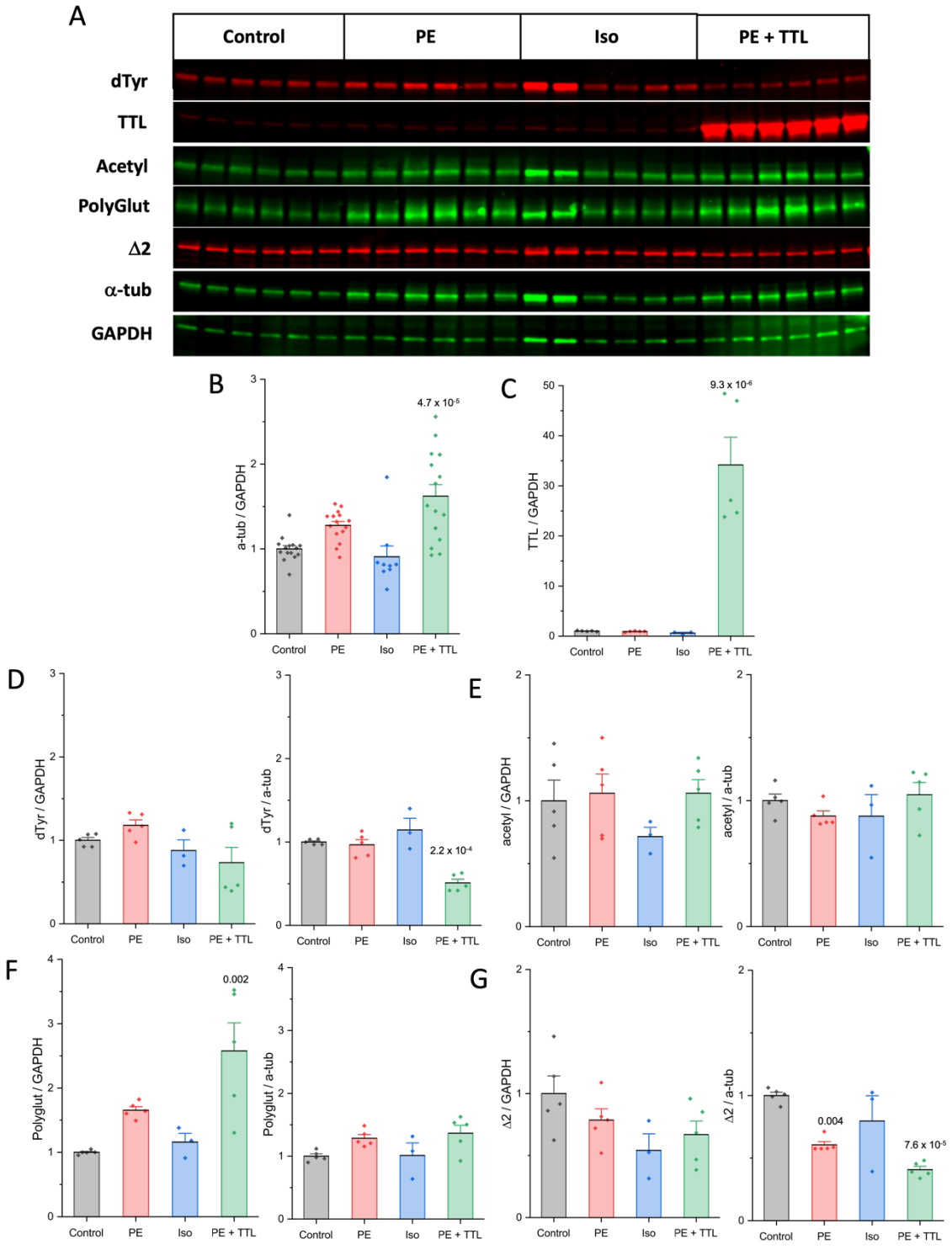

Figure 18. Unpublished western blot analysis of α-tubulin post-translational modifications during long-term phenylephrine and isoproterenol induced hypertrophies.

(A) Western blot images of α-tubulin and its post-translational modifications

Relative fold-change using GAPDH as loading controls for **(B)** α-tubulin, & **(C)** TTL (n = Ctrl, PE, PE+TTL = 5, Iso = 3). Since multiple western blots were ran to determine the levels of different post-translational modification with respect to α-tubulin, multiple total α-tubulin data points were obtained n = Ctrl, PE, PE+TTL = 5, Iso = 3 were obtained. The data in (B) represents all total α-tubulin data points.

Relative fold-change using GAPDH **(left)** or α-tubulin **(right)** as loading controls for **(D)** detyrosinated α-tubulin, **(E)** acetylated α-tubulin, **(F)** polyglutamylated α-tubulin, & **(G)** Δ2 α-tubulin (n = Ctrl, PE, PE+TTL = 5, Iso = 3).

For all bar plots, whiskers represent + 1SEM and bar represents mean; significant p-value from Welch-corrected two-tailed two-sample t-test are indicated on the bars.

B. Appendix B: Tables

Target	Vendor	Host Species	Clonal	Product No.	Concentration used (1:)
Total α-tubulin	Abcam	Mouse	Mono	ab7291	3000
Total α-tubulin	Abcam	Rabbit	Poly	ab4074	2000
Total β-tubulin	Abcam	Rabbit	Poly	ab6046	1500
Acetylated α-tubulin	Abcam	Mouse	Mono	ab24610	1000
Detyrosinated α-tubulin	Abcam	Rabbit	Poly	ab48389	1000
Polyglutamylated α-tubulin	Adipogen	Mouse	Mono	50-436-394	500
Δ2 α-tubulin	Moutin Lab	Rabbit	Poly		5000
Polyglycylated tubulin	EMD Millipore	Mouse	Mono	MABS276	700
Kif15	Proteintech	Rabbit	Poly	55407-1-AP	500
Vash1	Abcam	Rabbit	Mono	ab199732	1000
Mapre1 (EB1)	Sigma-Aldrich	Rabbit	Poly	E3406	WB: 500, PLA: 400
CLIP-170	Santa Cruz	Mouse	Mono	sc-28325	PLA: 100
Desmin	Agilent	Mouse	Mono	M076029-2	PLA: 500
α-actinin	Abcam	Mouse	Mono	ab9465	PLA: 1000
GAPDH	GenScript	Mouse	Mono	A01622-40	2000
H3	Abcam	Mouse	Mono	ab24834	3000
Anti-mouse	LI-COR	Donkey	Poly	925-32212	10000
Anti-rabbit	LI-COR	Donkey	Poly	925-68073	10000

Table 1: Primary and secondary antibodies used in this thesis.

Customer Identifier	Accession	Position	Target Sequence	Tm CP	Tm RP
CCP3	NM_178630.3	1047-1146	AGAGCCTGTTTACCCAAACTCCAAGGAAGATACTGTGGTTTATTTAGCTGAA GATGCTTACAAAGAGCCCTGTTTTGTGTATTCCCGAGTTGGGGGTAAC	79	80
CCP5	NM_001048192.2	919-1018	TCCGTTTCACAGGCAAAAGGATATTCTTCTTAAGCAGTAGGGTACACCCTGG AGAGACTCCATCTAGCTTTGTGTTCAATGGCTTTCTGGACTTCATCCT	80	79
CCP1	NM_001048008.2	399-498	CAGACTGTACTTAATATCCTAAGCATTCTCATTGAGCTGGTGTCATCGGGTG GGGGTCGAAGAGCGAGTTTCTTAGTTGCCAAAGGTGGTTCACAAATAC	78	82
ATAT1	NM_001142744.1	199-298	AAGGCGCAGCACCTCCCTGCACCCATCACCAGCGCTTTGAGGATGCAAAGC AACCGGCACGTTATTTACATACTGAAGGACACCTCAGCCCGACCGGCAG	83	82
Clip1	NM_019765.4	279-378	GCCCTCCATCCTCCGAGACCCAAGAGGAGTTTGTGGATGACTTTCGAGTTGG AGAACGTGTTTGGGTGAACGGGAATAAGCCCGGATTTATCCAGTTTCT	82	80
Clip2	NM_009990.3	1017-1116	CCTGCGGGAGAGTGTTCTTAACAGCTCAGTGAAGACGGGCAATGAGTCTGG TTCCAACCTCTCCGACAGTGGTTCTGTGAAGCGCGGTGACAAGGACCTC	82	82
Dctn2	NM_001190453.1	1631-1730	GCCCAGCCACATGCAGTTCCCGTCCAGTAAGTGCTTTGCCTGCTGTGGGAG AGGGACTGGATCCCGTCCTCTAACGTCTGTCTCTGGCCGAGTCTAACAC	82	82
Dync1h1	NM_030238.2	5945-6044	AGTCCGTCAAAGCCCTCGGCCATCAGCTGGGGCGGTTCGTCTTAGTTTTCAA CTGTGACGAAACCTTTGATTTCCAGGCGATGGGACGTATCTTTGTGGG	82	80
Dynll2	NM_026556.4	2373-2472	TTTGTTCATCTCTCATTTCTGGTGCAGTGACTGAGACCCTGCCACATCTATGC TCTGCATCCACGCCTCTTTTGGACATTAAAGGTCGATTGATGCACTT	79	79
GAPDH	NM_001001303.1	891-990	AGGTTGTCTCCTGCGACTTCAACAGCAACTCCCACTCTTCCACCTTCGATGCC GGGGCTGGCATTGCTCTCAATGACAACTTTGTCAAGCTCATTTCCTG	81	79
Hdac6	NM_010413.3	565-664	GATCTGAACCCTGAGACAAGAGTGCCAGTTGGTACTGGATTGGTGTTTGATG AACAACTAAATGACTTCCATTGCCTTTGGGATGACAGCTTCCCTGAAA	81	81
Kif15	NM_010620.1	515-614	TGGAGCTGGGAAGAGTTTCCTTTGTAAGTGCTCCTTTATTGAGGTCTACAAT GAGCAGATATATGACCTCCTGGACTCGGCGTCAGTCGGACTGTATTTG	78	82
Kif2c	NM_134471.3	916-1015	CAAGTGTCTCCTCCTGGTGCATGAACCCAAGTTAAAAGTGGACTTAACGAAG TACCTGGAGAACCAAGCTTTCTGCTTTGACTTTGCATTTGATGAGACA	82	79
Kif5b	NM_008448.3	1778-1877	TGGATCAGGAAGAGCTTCTGGCATCAACCAGAAGGGATCAAGATAATATGC AAGCTGAACTGAATCGCCTCCAAGCAGAAAATGATGCTTCTAAAGAAGA	86	84
Map1a	NM_001173506.1	197-296	TCAGCTCACAAACTCCTCATCTTGAGTGGACAAACTTTAGAACCCGAGGGAG ACCTTATCCTACAGAGTGGTACTTACTCATATCAAAACTTCGCCCAGG	82	81
Map4	NM_008633.4	3225-3324	GTCCAAAGCTAATATCAAGCACAAGCCTGGTGGAGGAGATGTCAAGATTGA AAGTCAGAAGTTGAACTTCAAGGAGAAGGCCCAAGCCAAAGTGGGATCC	85	86
Mapre1	NM_007896.3	161-260	TCAGTCACCAGTGATAACCTAAGTCGACATGACATGCTGGCTTGGATCAATG AATCTCTGCAGTTGAATCTGACAAAGATAGAACAGTTGTGTTCAGGGG	82	81
Mapre2	NM_001162941.1	3134-3233	AAAAATGTTCCCTGGCTAGTGTACTCCATTCTCTTTCCTAGTGGCTCGGGCCA GACTTCATCCATTTAGAGAGAAGCAGTACTTCCTGTTTGTGTGCCCA	80	78
Mapre3	NM_133350.1	169-268	TCCACTTCTGTGACCAGTGAGAATCTGAGTCGCCATGATATGCTTGCATGGG TCAATGACTCTCTGCACCTCAATTATACCAAGATTGAACAGCTCTGTT	83	80
Mapt	NM_001038609.2	1203-1302	CAGTCGAAGATTGGCTCCTTGGATAATATCACCCACGTCCCTGGAGGAGGG AATAAGAAGATTGAAACCCACAAGCTGACCTTCAGGGAGAATGCCAAAG	86	87
Rpl4	NM_024212.4	1323-1422	ATTCCAGAGAGCAAGTAGAGACCGCATATTTCAATAAATCAAACATGTGGTGACAAACCCT TGTGTGACTCTTAAATTGTGGATGTTTCCAAGCCCCTTG	78	78
Svbp	NM_001038998.2	557-656	CTGAGCTGGCCCAATGGAGCCTTACAGAACTAATCAGGACTTGTGGAGACC TCTGCACTGAACTTCCTATAAGTAACTTCCACCACACTGGTTTCTACTC	83	80
Tbp	NM_013684.3	71-170	GTGGCGGGTATCTGCTGGCGGTTTGGCTAGGTTTCTGCGGTCGCGTCATTTCTCCGCAG TGCCCAGCATCACTATTTCATGGTGTGTGAAGATAACCCA	83	79
TTL	NM_027192.2	1539-1638	GAGAGCCCAGCACTTCTCTGAAGGGCTGGGACCAGGGATTTGTTATGGCGT GATCTGATCCTTTGAGCGGTTTCTGGCCTTGGATGGTACTGGGAACAGA	82	82
TTLL1	NM_178869.4	895-994	GTGTCGCAGTCCACAAAAGAAGCGTACGTGATCTCAGTCTATATCAATAATC CGTTGCTCATCGGTGGAAGGAAGTTTGACCTTCGTCTGTATGTCCTGG	78	80
TTLL11	NM_028921.2	2499-2598	GCCTGCTGGTCAGAGCTTAGCATCATCGCATGTCTTTCCTTCTGCCCATTGCC TGAAACGAAGTTGAAATACGAAGAAGGTGGACACCTCCGATCATGTG	81	81
TTLL12	NM_183017.2	1459-1558	TGCTGCGCTCAGTGAGGCCGCTGAGGTTGTTTGCTTACGATGTGTTTTGGCT ACGCTTCTCCAATCGGCCCTTCGCCCTCGATGACCTAGACGACTATGA	81	82
TTLL13	NM_177765.3	977-1076	TATGATCTGCCAGCAGTACATCACCAAGCCCTTCCTTATTGATGGCTTCAAGT TTGACATGCGAATCTATGTTCTGATCACTTCCTGTGACCCTCTCCGG	81	79
TTLL3	NM_133923.6	676-775	AACGAAATGTTTCGGGAGTCGCAGCTGTTGGACTTGGATGGTTTCCTGGAAT TTGATGACCTAGATGGGATACATGCTTTGATGTCCCGCATGGTTCGAA	81	79
TTLL4	NM_001014974.1	3335-3434	GCCTATTACTTGACCCAGAAAATTCCTGACCAGGACTTCTATGCGTCCGTGCT GGACGTCTTGACACCAGATGATGTTCGGGTTTTGGTGGAGATGGAAG	82	82
TTLL5	NM_001081423.2	493-592	TCATGAAGTTCACCCGAGCAGCACTGACTATAATTTGATGTGGACAGGATCC CACCTAAAACCGTTCTTACTTCGAACCCTCTCTGAAGCACAAAAGGTT	83	81
TTLL7	NM_027594.1	291-390	TTCCTGTGACTTGGGGCCATATTCTACTTAGATGAACTCGGAACTTCCAGCTT TCCCGAGCGCTTGGCACTACAGGCAGGCTTCTTGCTTGCTTGGTATA	81	82
Tuba1a	NM_011653.2	1379-1478	GGGAGGAAGAAGGAGAGGAATACTAAATTAAATGTCACAAGGTGCTGCTTC CACAGGGATGTTTATTGTGTTCCAACACAGAAAGTTGTGGTCTGATCAG	86	77
Tuba1b	NM_011654.2	1456-1555	AGTTGCAGGCACTGATGCTTCTGTGCTGTTTCCATTCTGTGATCATGTCTTCT CCATGTTGTACCTCTTAAGTTTTCCATGATGTCTCAAAGTAAAAGCT	78	72
Tuba1c	NM_009448.4	447-546	GGACTCCTTGGTAGTCTGTTAGTGGGAGATCTTCGTCACCCTTTTTCACTTCC TCAGTTTTCGCGGACCACTTCAAGGACTAAATATGCGTGAGTGCATC	77	80
Tuba4a	NM_009447.3	1342-1441	GGAAAAAGATTATGAGGAAGTAGGCATCGACTCCTATGAGGACGAGGATGA GGGAGAAGAGTAGACCGCTACTTGGAGCCTGTTCACTGTGTTTATTGCA	85	83
Tuba8	NM_017379.1	1024-1123	CGGTGATGTGGTACCCAAGGACGTGAATGTCGCCATTGCTGCCATCAAGAC CAAGAGAACTATTCAGTTTGTTGACTGGTGTCCCACAGGTTTCAAGGTG	82	78
Tubb2a	NM_009450.1	1378-1477	GAGGAGGAAGAGGGTGAAGATGAGGCTTGAGAACTTCTCAGATACAATGTG CACCCTTAGTGAACTTCTGTTGTCCTCCAGCATGGTCTTTCTATTTGTA	87	75
Tubb2b	NM_023716.2	1439-1538	GAGGGCGAGGATGAGGCTTGAGTTCCCCAGGCCAAGCAGGTTAGGGAAAG CTGAGATGAAAGGAGGGGGTGGGGGGGCTTAATCTGTGAAAATACCTTGG	88	89
Tubb3	NM_023279.2	180-279	CATCAGCGTATACTACAATGAGGCCTCCTCTCACAAGTATGTGCCCAGGGCC ATTCTGGTGGACTTGGAACCTGGAACCATGGACAGTGTTCGGTCTGGC	84	83
Tubb4a	NM_009451.3	1820-1919	CCCCTCAACACATGTACACACACACACACACTCCACCTTCTTAGATCTTGAAA ATCCTTTCCTTTATGCCCTGTCCCTTCCCCAGCACTCCTGAACCATT	83	80
Tubb4b	NM_146116.1	747-846	CATGAGTGGGGTAACCACTTGCCTGCGATTCCCTGGCCAGCTAAATGCTGAC CTGCGGAAACTGGCTGTAAATATGGTGCCCTTCCCTCGCCTGCACTTC	85	84
Tubb5	NM_011655.4	2261-2360	ATTGGAAGTGTCTTCCCTGTATTGGTTCTCCTTTCTCGGAGAGATGGGGGTT GGGGGTGCGGCAAGGTCTTGGTCTTGGTCTCTGAACACTCCCAATTCC	79	82
Tubb6	NM_026473.2	1303-1402	CAGGACGCCACGGTCAATGATGGGGAAGAGGCATTTGAAGACGAGGATGA AGAAGAGATCAACGAATAGGGAGCCATAAGATGCTACAGTGAACGTCTGC	82	82
Vash1	NM_177354.4	1844-1943	GGAATTTACCTCACCAACAGTATGCCCACCCTGGAACGCTTTCCCATCAGCTT CAAGACCTATTTCTCAGGGAACTACTTCCGCCACATTGTGCTGGGGG	84	83
Vash2	NM_144879.2	917-1016	GGCATCTATCTCACCAATGGGCAGCCTTCCATTGAGCGGTTCCCTATCAGCT TTAAAACCTACTTCTCAGGAAACTACTTTCACCATGTCGTGCTGGGGA	81	79

Table 2: Mouse tubulin isoforms, tubulin modifying enzymes, and molecular motors panel design and information.

Customer Identifier	Accession	Position	Target Sequence	Tm CP	Tm RP
Acta2	NM_007392.2	46-145	GGAACCCTGAGACGCTGCTCCAGCTATGTGTGAAGAGGAAGACAGCACAGC CCTGGTGTGCGACAATGGCTCTGGGCTCTGTAAGGCCGGCTTCGCTGGT	82	82
Agm	NM_021604.3	4249-4348	CAGAGGGACTGCTGCTCTACAATGGCAATGCACGTGGCAAAGATTTCCTGG CTCTGGCTCTGTTGGATGGTCATGTACAGTTCAGGTTCGACACGGGCTC	82	82
Bax	NM_007527.3	736-835	CATAAATTATGACATTTTCCTGGGATGAATGGGGGAAGGGGAAAGGCATTTT TCTTACTTTTGTAATTATTGGGAGGGGTGGGAATGGTGGCCTGGGGAG	82	81
Bcl2	NM_009741.3	1845-1944	GGCCTTCTTTGAGTTCGGTGGGGTCATGTGTGTGGAGAGCGTCAACAGGGA GATGTCACCCCTGGTGGACAACATCGCCCTGTGGATGACTGAGTACCTG	85	87
Casp3	NM_009810.2	631-730	GAGGCTGACTTCCTGTATGCTTACTCTACAGCACCTGGTTACTATTCCTGGAG AAATTCAAAGGACGGGTCGTGGTTCATCCAGTCCCTTTGCAGCATGC	83	78
Ctgf	NM_010217.2	2241-2340	GGCTCAGGGTAAGGTCCGATTCCTACCAGGAAGTGCTTGCTGCTTCTTTGAT TATGACTGGTTTGGGGTGGGGGGCAGTTTATTTGTTGAGAGTGTGACC	82	81
Col14a1	NM_181277.3	785-884	GAGGTTCAACTTCAGGCTTGTGCGCAATTTCTTGGAAAACCTGGTCACAGCG TTCAACGTGGGCTCAGAAAAGACAAGAATCGGCTTGGCACAGTACAGT	80	82
Col1a1	NM_007742.3	216-315	CAATGGTGAGACGTGGAAACCCGAGGTATGCTTGATCTGTATCTGCCACAAT GGCACGGCTGTGTGCGATGACGTGCAATGCAATGAAGAACTGGACTGT	82	81
Col3a1	NM_009930.1	4371-4470	CAAGACAGTCTTTGAATATCAAACACGCAAGGCAATGAGACTACCCATCATA GATATCGCACCCTATGACATTGGGGGTCCTGATCAAGAATTTGGTGTG	82	82
Col4a1	NM_009931.2	4117-4216	CTCCAGGGATCACAGGTTCAAAGGGAGATATGGGACTGCCCGGAGTTCCAG GATTTCAAGGTCAGAAAGGGCTTCCTGGTCTGCAGGGAGTGAAAGGAGA	82	82
Col8a1	NM_007739.2	2936-3035	TCTGTAGTGCAGGGTCCATGGTAATCTCTAGTCCAAAGGATATTTCTCTGTGT TAGAGGCAATGCTTTGAGCTGCAGGACTACCTAGTCAGAATTGTGTG	79	83
Creb1	NM_001037726.1	2735-2834	TTCTGTCTGGACAGTTCACCAGATTCTCCAGAAGGCTTTCAAACGGCTAAAG TTTGATCTTTGTCCTGCTGAGCTTGCTGGGAAGGAGATAGCATAAAAG	80	81
Dag1	NM_010017.3	611-710	CCACCGTGGTTGGCATTCCAGACGGTACGGCTGTTGTCGGGCGCTCATTTC GAGTGAGCATTCCAACGGATTTAATTGCCTCCAGTGGGGAGATCATCAA	82	81
Fasn	NM_007988.3	6561-6660	TTCTCCTCTGTAAGCTGCGGGCGTGGTAATGCTGGCCAAACTAACTACGGCT TCGCCAACTCTACCATGGAGCGTATATGTGAACAGCGCAGGCACGATG	82	82
Fhl1	NM_010211.2	1991-2090	CGTTGTCTGCTCTTTGTCTGCATCCAGGAAGAGTGCAAAGTCCCTTTGCTTGT GATTCTTAGAACTTTCCCTCCAGAATTGCAGTTAGACTCTGGGGCTG	80	80
Fhl2	NM_010212.3	963-1062	CCATTAGTGGTCTGGGTGGCACAAAGTACATCTCTTTCGAGGAACGCCAATG GCACAACGACTGCTTTAACTGTAAGAAGTGCTCCCTGTCTCTGGTGGG	83	82
Fmod	NM_021355.3	1986-2085	GCTTTTAGTATCGAAGGGGCAAGCGTGGTTTTCAAAACATGAGAAAGAGCCT CTGCTCATCCTTTGGTCTAGTATGAAGGGTTGTTACGCAAATGGCAGA	80	80
Fn1	NM_010233.1	2628-2727	TCCAGACCCTACCGTGGACCAGGTTGATGATACTTCCATTGTTGTTCGGTGG AGTAGACCCCAGGCACCTATCACAGGGTATAGAATTGTCTATTCACCT	81	83
c-fos	NM_010234.2	1331-1430	AGCTGGTGCATTACAGAGAGGAGAAACACGTCTTCCCTCGAAGGTTCCCGT CGACCTAGGGAGGACCTTACCTGTTCGTGAAACACACCAGGCTGTGGGC	82	82
Gapdh	NM_001001303.1	891-990	AGGTTGTCTCCTGCGACTTCAACAGCAACTCCCACTCTTCCACCTTCGATGCC GGGGCTGGCATTGCTCTCAATGACAACTTTGTCAAGCTCATTTCCTG	81	79
Cx43	NM_010288.3	1451-1550	CTGGGGTGTTCATTTCGTTCCCGTGGAGGTGGTACTCAACAACCTCAGTAAT GAGGCGTAGAAAACAAAGACATTACAATATCTAGGTTCCTTGGGGGGT	81	83
Lum	NM_008524.2	871-970	CGACGGGCTGGTCAACTTGACCTTCATTTATCTTCAACACAACCAGCTCAAA GAGGATGCTGTCTCGGCTTCTCTGAAAGGTCTCAAATCACTAGAGTAC	80	82
c-Myc	NM_010849.4	631-730	CCCTCAACGTGAACTTCACCAACAGGAACTATGACCTCGACTACGACTCCGT ACAGCCCTATTTCATCTGCGACGAGGAAGAGAATTTCTATCACCAGCA	83	78
Myh6	NM_010856.2	26-125	ACTGTGGTGCCTCGTTCCAGCTGTGGTCCACATTCTTCAGGATTCTCTGAAAA GTTAACCAGAGTTTGAGTGACAGAATGACGGACGCCCAGATGGCTGA	82	82
Myh7	NM_080728.2	1133-1232	CCACGGATAGCGCCTTTGACGTGCTGGGCTTCACTCCAGAAGAGAAGAACT CCATTTACAAGCTGACAGGCGCCATCATGCACTTTGGAAACATGAAGTT	85	81
Nfkb1	NM_008689.2	2126-2225	GTCTTACACTTAGCCATCATCCACCTCCACGCTCAGCTTGTGAGGGATCTGCT GGAAGTCACATCTGGTTTGATCTCTGATGACATCATCAACATGAGAA	83	81
Nid1	NM_010917.2	735-834	AAAGCCAAGTACCTGCTGTGGTTGGTTTCAGCAAAGGTCTAGTAGGATTTCT ATGGAAGAGCAACGGAGCCTATAACATATTTGCCAATGACAGAGAATC	80	82
Nppa	NM_008725.2	691-790	CTATCACGATCGATGTTAAATGTAGATGAGTGGTCTAGTGGGGTCTTGCCTC TCCCACTCTGCATATTAAGGTAGATCCTCACCCTTTTCAGAAAGCAGT	80	80
Nppb	NM_008726.4	177-276	GCTTCTGCGGCATGGATCTCCTGAAGGTGCTGTCCCAGATGATTCTGTTTCT GCTTTTCCTTTATCTGTCACCGCTGGGAGGTCACTCCTATCCTCTGGG	83	81
Nppc	NM_010933.5	428-527	ACAAAGGCGGCAACAAGAAGGGCTTGTCCAAAGGCTGCTTTGGCCTCAAGC TGGACCGGATCGGCTCCATGAGCGGTCTGGGATGTTAGTGCAGCTACCC	84	85
Osf2	NM_015784.2	760-859	GACCTTTCATCATTTAGAGCAGCCGCCATCACCTCTGACCTCTTGGAGTCCCT TGGAAGAGATGGTCACTTCACGCTCTTTGCTCCCACCAATGAAGCTT	82	83
Rcan1	NM_001081549.1	1061-1160	ACACAAGGACACTGGGGACATCCTGAGAAAACTGATAGTTCTTGTAATTGCT CATTTCTAGGTTCTGTTTTTGGCAAGGACAGGTTGACTGGTGGCCCAG	82	79
Rpl4	NM_024212.4	308-407	CCAGGGTGCCTTTGGAAATATGTGTCGTGGGGGACGCATGTTTGCACCAAC CAAAACCTGGCGTCGTTGGCACCGCAGAGTGAATACAACCCAAAAACGA	84	86
Sod2	NM_013671.3	1496-1595	ATAGCTTTGCTCCTGCTTGAGGAGTGCTTATTATGAGAGGAAGGTAATGGTG CCTCTGGGTTTTCTATAGGCAGACATGCAAAAACAGCTAATCTTGTCT	82	80
Srf	NM_020493.2	3316-3415	AGCCAGCCTAAACCACCTGTATCCATTAAAGGAGCTTTTTCCGGGAGGGCAG TTGGGGTAGGGTGTCACTAAACCCTTGTTGCTGCCTTCAGTAGGAACA	83	82
Tbp	NM_013684.3	71-170	GTGGCGGGTATCTGCTGGCGGTTTGGCTAGGTTTCTGCGGTCGCGTCATTTT CTCCGCAGTGCCCAGCATCACTATTTCATGGTGTGTGAAGATAACCCA	83	79
Tgfb	NM_011577.1	1471-1570	GGAGTTGTACGGCAGTGGCTGAACCAAGGAGACGGAATACAGGGCTTTCG ATTCAGCGCTCACTGCTCTTGTGACAGCAAAGATAACAAACTCCACGTGG	82	78
Thbs4	NM_011582.3	1129-1228	CGTGGATGAGTGCAAATACCATCCCTGCTATCCAGGTGTGCGCTGTGTGAAT TTGGCTCCGGGTTTCAGATGTGACGCCTGTCCAGTAGGTTTCACAGGG	84	82
TIMP-1	NM_011593.2	437-536	AAGCCTCTGTGGATATGCCCACAAGTCCCAGAACCGCAGTGAAGAGTTTCTC ATCACGGGCCGCCTAAGGAACGGAAATTTGCACATCAGTGCCTGCAGC	83	83
TIMP-2	NM_011594.3	656-755	TTGCAGGAAAGGCAGAAGGAGATGGCAAGATGCACATTACCCTCTGTGACT TCATTGTGCCCTGGGACACGCTTAGCATCACCCAGAAGAAGAGCCTGAA	82	82
TIMP-3	NM_011595.2	2461-2560	GTCACTTCCGGAGGTGGTCACCTCATAGAATGAACATGATTGGTTACTGAGG GAGCCAGGCTCTGCCGTCCAAATGTAGGCCTTTTGTTGTGTTGTATTT	82	79
TIMP-4	NM_080639.3	326-425	GAAGGCCAAGGATATTCAGTATGTCTACACGCCATTTGACTCTTCCCTCTGTG GTGTGAAGCTAGAAACCAACAGTCACAAGCAGTATCTTTTGACTGGC	80	82
Tnnc1	NM_009393.2	58-157	CAAAGCTGCGGTAGAACAGTTGACAGAGGAGCAGAAGAATGAGTTCAAGG CTGCCTTTGATATCTTTGTCCTGGGCGCGGAGGATGGCTGCATCAGCACC	84	83
Tnni3	NM_009406.2	211-310	GAGCCTATGCCACCGAGCCACACGCCAAGAAAAAGTCTAAGATCTCCGCCT CCAGAAAACTTCAGTTGAAGACTCTGATGCTGCAGATTGCGAAGCAGGA	82	79
Vcan	NM_172955.1	1387-1486	AGTGTGGAGGAGGTCTACTTGGGGTGAGAACCCTGTATCGTTTTGAGAACC AGACATGCTTCCCTCTCCCTGATAGCAGATTTGATGCCTACTGCTTTAA	82	80

Table 3: Mouse hypertrophy and fibrosis panel design and information.

Customer Identifier	Accession	Position	Target Sequence	Tm CP	Tm RP
GAPDH	NM_001001303.1	891-990	AGGTTGTCTCCTGCGACTTCAACAGCAACTCCCACTCTTCCACCTTCGATGCC GGGGCTGGCATTGCTCTCAATGACAACTTTGTCAAGCTCATTTCCTG	81	79
Rpl4	NM_024212.4	308-407	CCAGGGTGCCTTTGGAAATATGTGTCGTGGGGGACGCATGTTTGCACCAAC CAAAACCTGGCGTCGTTGGCACCGCAGAGTGAATACAACCCAAAAACGA	84	86
Tbp	NM_013684.3	71-170	GTGGCGGGTATCTGCTGGCGGTTTGGCTAGGTTTCTGCGGTCGCGTCATTTT CTCCGCAGTGCCCAGCATCACTATTTCATGGTGTGTGAAGATAACCCA	83	79
Ttc5	NM_001080949.2	33-132	ATGATGGCTGATGAAGAGGAAGAAGCGAAGCACGTCTTGCAGAAATTGCAG GGACTGGTGGATCGGCTCTACTGTTTTCGAGACAGTTACTTTGAGACAC	82	83
Tuba1a	NM_011653.2	1379-1478	GGGAGGAAGAAGGAGAGGAATACTAAATTAAATGTCACAAGGTGCTGCTTC CACAGGGATGTTTATTGTGTTCCAACACAGAAAGTTGTGGTCTGATCAG	86	77
Tuba1b	NM_011654.2	1456-1555	AGTTGCAGGCACTGATGCTTCTGTGCTGTTTCCATTCTGTGATCATGTCTTCT CCATGTTGTACCTCTTAAGTTTTCCATGATGTCTCAAAGTAAAAGCT	78	72
Tuba1c_exon	NM_009448.4	240-339	CCACCTGGCCCTGGCGTGGACCCTGGGTGTCTCCTCCCCTTCCCACTTCCAG CTCCTTCTACGGAGTTTGATTTGAACTTTCGAACCCGCCAATCATCGG	89	77
Tuba1c	NM_009448.4	447-546	GGACTCCTTGGTAGTCTGTTAGTGGGAGATCTTCGTCACCCTTTTTCACTTCC TCAGTTTTCGCGGACCACTTCAAGGACTAAATATGCGTGAGTGCATC	77	80
Tuba4a	NM_009447.3	1342-1441	GGAAAAAGATTATGAGGAAGTAGGCATCGACTCCTATGAGGACGAGGATGA GGGAGAAGAGTAGACCGCTACTTGGAGCCTGTTCACTGTGTTTATTGCA	85	83
Tuba4a_ex_ex	XM_006496478.2	1997-2096	AAACTGGAGCTGGAAAACATGTGCCTCGGGCAGTCTTTGTGGACCTGGAGC CTACTGTAATCGATGAGATCCGAAATGGCCCATACCGTCAGCTCTTCCA	89	83
Tuba8	NM_017379.1	1024-1123	CGGTGATGTGGTACCCAAGGACGTGAATGTCGCCATTGCTGCCATCAAGAC CAAGAGAACTATTCAGTTTGTTGACTGGTGTCCCACAGGTTTCAAGGTG	82	78
Tuba8_2	XM_036166283.1	1450-1549	TGGAGAAGGATTATGAAGAAGTGGGGACTGATTCGTTTGAAGAAGAGAATG AGGGGGAGGAATTTTAAATATACACTTGCCCCATGACTATGCCTCTTTC	83	81
Tubb1_ex_ex	NM_001080971.2	282-381	GGAGAGGATCAGCGTTTACTACAACGAAGCCTACGGTAAGAAGTATGTGCC GCGAGCCGTCCTTGTGGACCTGGAACCCGGGACAATGGACAGCATCCGA	85	89
Tubb1	NM_001080971.2	481-580	GAGCTGATCGAAAATGTCATGGATGTGGTAAGGAGGGAGAGCGAGAGCTG CGACTGCCTACAGGGTTTCCAGATCGTGCATTCTCTGGGTGGAGGCACGG	90	87
Tubb2a	NM_009450.1	1378-1477	GAGGAGGAAGAGGGTGAAGATGAGGCTTGAGAACTTCTCAGATACAATGTG CACCCTTAGTGAACTTCTGTTGTCCTCCAGCATGGTCTTTCTATTTGTA	87	75
Tubb2a_exon	NM_009450.2	2-101	GGTCTTTTGCGCTCCTTAGCCCTCTGTCCACGCACTGCTCCGAGGGCAAGAG CCTCCACCCCTTCTACAACCAGCACCATGCGCGAGATCGTGCACATCC	87	89
Tubb2b	NM_023716.2	1439-1538	GAGGGCGAGGATGAGGCTTGAGTTCCCCAGGCCAAGCAGGTTAGGGAAAG CTGAGATGAAAGGAGGGGGTGGGGGGGCTTAATCTGTGAAAATACCTTGG	88	89
Tubb3 2	NM_023279.3	1348-1447	AGGAGGGGGAGATGTATGAAGATGATGACGAGGAATCGGAAGCCCAGGG GCCCAAGTGAAGTTGCTCGCAGCTGGGGTGTGGGGCCAAGTGGCAGCCAG	88	89
Tubb3_ex_ex	NM_023279.3	189-288	CGCATCAGCGTATACTACAATGAGGCCTCCTCTCACAAGTATGTGCCCAGGG CCATTCTGGTGGACTTGGAACCTGGAACCATGGACAGTGTTCGGTCTG	85	88
Tubb4a	NM_009451.3	1820-1919	CCCCTCAACACATGTACACACACACACACACTCCACCTTCTTAGATCTTGAAA ATCCTTTCCTTTATGCCCTGTCCCTTCCCCAGCACTCCTGAACCATT	83	80
Tubb4a_exon	NM_009451.4	33-132	GCCACAGCGGCCGGTCGACACCCGTCCATCAGACGCCACCAGCAGCGCCA CCACCATGCGGGAAATCGTGCACCTGCAAGCCGGTCAATGCGGTAACCAG	89	90
Tubb4b	NM_146116.1	747-846	CATGAGTGGGGTAACCACTTGCCTGCGATTCCCTGGCCAGCTAAATGCTGAC CTGCGGAAACTGGCTGTAAATATGGTGCCCTTCCCTCGCCTGCACTTC	85	84
Tubb4b_exon	NM_146116.2	1-100	GGCGGGTCATAAGAGGTATATAAATGTTGGCAGAGCGTCGGTTGTAGCACT CTGTGCGCCTGCTCCTCCCGAAGTGCTCCTCTTCTACAGCTGTTCCGCA	83	87
Tubb5	NM_011655.4	2261-2360	ATTGGAAGTGTCTTCCCTGTATTGGTTCTCCTTTCTCGGAGAGATGGGGGTT GGGGGTGCGGCAAGGTCTTGGTCTTGGTCTCTGAACACTCCCAATTCC	79	82
Tubb5_intron	Tubb5_int.1	253-352	TGTGAAGAGCTGGTCTTAAAAGGGGTTTTCTAACGGTTCGAGGACTGGAGG GATGCGGAAACGATCCGAGACAAAGCCGAGGCGAGGTTTTCCCCTTGCG	83	87
Tubb6	NM_026473.2	1303-1402	CAGGACGCCACGGTCAATGATGGGGAAGAGGCATTTGAAGACGAGGATGA AGAAGAGATCAACGAATAGGGAGCCATAAGATGCTACAGTGAACGTCTGC	82	82
Tuba1a_intron	Tub_14.1	1074-1173	GCTGGAAATAGAGCTTTCTCTGTTAAATAATGTAACAGCACAGGCTAGCACC AGGCACAGAGAACGTGGCAATGCAGAAATCAGACTTTGTCTAGCTTGT	81	85
Tuba1b_intron	Tub_15.1	445-544	TAGGGTGTGTCTCCAGTTGGATCCTTGTTTTGAGCTCAGGGTCTAACGCAGG ATCTCTACCATTTTAACTCAGCTATTACCGAGTTGCGGTCTCACCCGC	81	80
Tuba1c_intron	Tub_16.1	940-1039	TCTGTCTCCACTACCCAAGAGCTAGGGTTATTCACCTGGTTAACAATGTATTA GTTCAGTTTTCAAGAAAAAAATGGGTGAGGCTATCAAACCCTGGGCT	81	79
Tuba4a_intron	Tub_17.1	29-128	TGAGGAAAGTGGAGTGTCTCTTGAAGAATGTCTTGGCTGGGTTTTTGTGATC TTTGAAGCCTCTTGGTTTATTTGAAGCTGAAGATGGATGCTGGCAGAA	79	79
Tuba8_intron	Tub_18.1	311-410	TGGTGGTATCCTGGGAAGCTTTCAGCCGTATGTGAGGTTGAAGTTAGGAAC AAAGGTGAGTAAAGCTTTTGTTGGAAAGAAGTGAGGAAGAGATTTGAGC	83	80
Tubb1_intron	Tub_19.1	227-326	TGCTGAGACAACGAGCTAGACACACAGGAAAGACAGAAGTAGAGTTTTTAA AAGGTATTTTTACAGATCCATGTCATGGTGGGCTGGGTCAGATACGATC	85	80
Tubb2a_intron	Tub_20.1	390-489	TGAATGAAAAAAATGCAGTGTCATTGGGTTGACAGATGTTACAGAGGCGTGT CTTTGGGCCAACAGACGAGGGTGTTAGACAAATTCTCTTACAAGGGCT	80	83
Tubb2b_intron	Tub_21.1	316-415	CACAGGAGAATTGATTTTACTCGCTTGATCACCAGGCGAGCTGCGGGGGAG GGGAGGAAGAACGATTGCCAGACGGTCACTGAACGTGCTTTGAATTTAA	86	83
Tubb3_intron	Tub_22.1	233-332	GACCTTATGTAGTCTAGGGACAGGCAGGAGACTCAATGATACATCCTTAGCA GGGGTCACTGGGGGCTTGATTGAGGCTACTTGATAATTGATACAGTCT	85	85
Tubb4a_intron	Tub_23.1	308-407	CCCCAACTTCTCCCTTCTTGCTGGCTCATGCTTTGCTGTGGCTCTGAGTTCCC AGTTACCTCACAGACAGACAGTCAGCAACTGAAGAAGTGGCTTTAAG	82	85
Tubb4b_intron	Tub_24.1	100-199	TACCGGCGTACGCTGGGCCGAGACGTAGCGCCGGTGGCTGGTGTCGGTGG GGCGGACGGTGCGCGGCCCTTAGGGATTCGTCGCCCTGGCGCTCCTGAGA	89	89
Tubb6_intron	Tub_26.1	495-594	TTCATCGGGCGCCAAAACTGTAGACAGCTCTAAGAAATTAATGGGGAAATTA GCAAAATTCTAGACTCTGGATAATCCCAGTTTGGGAATAATAGCACCT	83	80

Table 4: Mouse tubulin isoforms exons and introns (autoregulation) panel design and information.

Customer Identifier	Accession	Position	Target Sequence	Tm CP	Tm RP
GAPDH	NM_001256799.1	387-486	GAACGGGAAGCTTGTCATCAATGGAAATCCCATCACCATCTTCCAGGAGCGA GATCCCTCCAAAATCAAGTGGGGCGATGCTGGCGCTGAGTACGTCGTG	85	86
RPL4	NM_000968.2	863-962	AGCCGCTTCCCTCAAGAGTAACTACAATCTTCCCATGCACAAGATGATTAATA CAGATCTTAGCAGAATCTTGAAAAGCCCAGAGATCCAAAGAGCCCTT	81	83
TBP	NM_001172085.1	588-687	ACAGTGAATCTTGGTTGTAAACTTGACCTAAAGACCATTGCACTTCGTGCCC GAAACGCCGAATATAATCCCAAGCGGTTTGCTGCGGTAATCATGAGGA	79	82
tuba1a_ex	NM_001270399.2	213-312	TGGTGGTATGTTTTGTGAGGTTTAGCTTAGCCCCAAATCCTCAAGCCCCGCC GCCGCCGCAGTGCGGGTGCAGGAACCGGGCCAGTACTGCGCCCAGGGC	80	93
tuba1a_in	Ar_tuba1a_in.1	761-860	CTGTTAAATAATGTAGCAGACAGTACAGGCTAGCACCAGGCACAGCAAATAC AGCAATGCAGCAATGCAGAAGGCAGACCTTGTCTAAACTCCTAGTATT	86	85
tuba1c_ex	NM_032704.5	2641-2740	CACTACACCTGGCCCCTAGATACGTTTTTTAATAACCTCCCAAATGATGCTGT TGGTCTGATGTGACCACATGTACAGTAGCAAAGGGTTAGATAACAGT	79	82
tuba1c_in	Ar_tuba1c_in.1	1348-1447	GGTAAGTCAGTGGCCGCTGACTGCCTGCTAAGCTTCAAGAAGGCAGTTTAG ACTGAGCAATGAAAGAAAAATTGCGGGCGCAAAATAGAAACGGCATTTA	86	82
tuba4a_ex	NM_006000.3	209-308	CCACCTTCTTCTGTGAAACTGGTGCTGGAAAACACGTACCCCGGGCAGTTTT TGTGGATCTGGAGCCTACGGTCATTGATGAGATCCGAAATGGCCCATA	86	83
tuba4a_in	Ar_tuba4a_in.1	834-933	TCACCGCAGGTTCCACTTCCTTTCTGGGTATTTGGAAACCGTCACCCCGCCAT TTCGGTGTGGGAAGAGCGCGCGGGCCCTGCCGGACTTTAGTGCTTTA	82	84
tuba8_ex	NM_001193414.2	405-504	CAGATGCTTGCTCTGGCCTGCAGGGCTTCCTGATTTTCCACAGTTTTGGTGG GGGCACTGGCTCCGGCTTCACTTCTCTGCTGATGGAACGCCTCTCCCT	81	92
tuba8_in	Ar_tuba8_in.1	441-540	ACATATATTATTGCCACCATGAGGTGGAGTTGAGGGGTGGGACAACTCTTG GGGGTCTAGGTTCTGGGCAGATCATCCTGAATCTTTCTCCATGTCCCTA	84	83
tubb_ex	NM_001293214.2	1581-1680	CCATTCTGGGTGACCCTGTATTTCTTTCTGGTGCCCATTCCATTTGTCCAGTTA ATACTTCCTCTTAAAAATCTCCAAGAAGCTGGGTCTCCAGATCCCA	75	79
tubb1_ex	NM_030773.4	993-1092	TGGCTGCCTGTGACCTCCGCCGTGGCCGCTACCTCACAGTGGCCTGCATTTT CCGGGGCAAGATGTCCACCAAGGAAGTGGACCAGCAACTGCTCTCCGT	91	91
tubb1_in	Ar_tubb1_in.1	1012-1111	GATAATACGGAAAGGGGCCCTCAAGAGAAAGTGTTAGGTTTAGATAGGGTT TTAGCTCTCACTCTGGAATCGTATGGTCTAGCGTTGAGAGTCCTGGCTG	84	82
tubb2a_ex	NM_001310315.2	1530-1629	GGAGGGCGAGGACGAGGCTTAAAAACTTCTCAGATCAATCGTGCATCCTTA GTGAACTTCTGTTGTCCTCAAGCATGGTCTTTCTACTTGTAAACTATGG	85	76
tubb2a_in	Ar_tubb2a_in.1	355-454	GAAAACATGCAGTGTCACTGGACTGGCAGATGTAACAGAGGCGTCCCTTTG GGTCGTACAGGCAAGGGTGTTAGATAAATTCCCTTGCTCGGGCACTGTC	87	85
tubb2b_ex	NM_178012.5	32-131	GTGACCCCGCAGTGGGTGTGTGAGGGGAGGACGGACAGACCCAGACGCC GCCGGACCAGGAGGACGCTGACGAGGCACCATGCGTGAGATCGTGCACAT C	93	92
tubb2b_in	Ar_tubb2b_in.1	30-129	GGGATTCATTTTACGCTGGGCAGTGGAGGCTGAAGAGGTGTGATTGCCAGA GGGAAAGCATGAAGAACATCCGCGGTGTGCCAACTTAGCTTTAATATAG	86	82
tubb3_ex	NM_006086.4	143-242	ATGGCATCGACCCCAGCGGCAACTACGTGGGCGACTCGGACTTGCAGCTGG AGCGGATCAGCGTCTACTACAACGAGGCCTCTTCTCACAAGTACGTGCC	91	88
tubb3_in	Ar_tubb3_in.1	316-415	CCTGGAGGGCTTAGTCAGGGGCTCTTTAGCAACTGGTGTGAAGTGATTTCCA TATCAAAGTGGTGATACACCCACCTGCCCACATGGACATGTGATTTAA	85	82
tubb4a_ex	NM_006087.4	1510-1609	AGAGCCCCGCTTTCCCTCCAAGGCTGACTCCCCGCTGACCCTAACAATACCT TTGGAGCTCGCTTTACCTCTGGCTACTTCATCTCCGACCCTGGCTCCC	92	85
tubb4a_in	Ar_tubb4a_in.1	623-722	TATCTGCAGTCTAGAATGTGAGTAGGATTTGGACTGGCCAAAGGGCATGGA AGGGAGGAAAGATGTTTAAGACGGAGGCAACAGCATATGTGAAGATAGT	86	86
TUBB4B_ex	NM_006088.5	381-480	TCAGAGTGGTGCTGGGAACAACTGGGCCAAGGGGCACTACACAGAAGGCG CGGAGCTGGTGGACTCGGTGCTGGATGTTGTGAGAAAGGAGGCTGAGAGC	93	92
tubb4b_in	Ar_tubb4b_in.1	268-367	GGGGTTTGTTAAGCTGTCAGGTTTGGCCCCTGACTTAATTCGTAGCAGGGCA GGCTGCCGTCTTTTGGCTTTGAAGGGTCCGTTTGCTCTACCTCCAGGG	81	83
tubb6_ex	NM_001303528.2	1446-1545	GGATGCCACCGCCAATGACGGGGAGGAAGCTTTTGAGGATGAGGAAGAGG AGATCGATGGATAGTCGGAATAGAGCCGCCCCAACTCAGATCCTACAACA	93	87
tubb6_in	Ar_tubb6_in.1	842-941	TTCCATGGAGCTAAAGTTGTAAAACTTCCTAACAGGAAAGAGGTGTCAGGGT GAGCTGGAAAATACAGTAGGCAGGAAGTCAGGGGACTTGATTTCTCAT	82	85
tubb_in	Ar_tubb_in.1	100-199	ATCTGTCATTTTGTCCCTTTCGTGAACCACCGTCGGGGCCAAAGACGTCTGC TGCCACCTGGTGGCGGGACCTGGAATGACAAGTCTCTGATCCCTGCTG	79	92

Table 5: Human tubulin isoforms exons and introns (autoregulation) panel design and information.